The influence of fluorine, boron, phosphorus and lithium on the viscosity of hydrous pegmatitic melts

Von der Naturwissenschaftlichen Fakultät der

Gottfried Wilhelm Leibniz Universität Hannover

zur Erlangung des Grades

Doktor der Naturwissenschaften

Dr. rer. nat.

genehmigte Dissertation

von

Dipl.-Geow. Alexander Bartels

geboren am 18. Mai 1982 in Frankfurt am Main

Referent: Prof. Dr. Francois Holtz

Korreferent: Prof. Dr. Harald Behrens

Tag der Promotion: 11.07.2012

Erklärung zur Dissertation

Gemäß §6(1) der Promotionsordnung der Naturwissenschaftlichen Fakultät der Gottfried Wilhelm Leibniz Universität Hannover für die Promotion zum Dr. rer. nat.

Hierdurch erkläre ich, dass ich meine Dissertation mit dem Titel „The influence of fluorine, boron, phosphorus and lithium on the viscosity of hydrous pegmatitic melts“ selbständig verfasst und die benutzten Hilfsmittel und Quellen sowie gegebenenfalls die zu Hilfeleistungen herangezogenen Institutionen vollständig angegeben habe. Die Dissertation wurde nicht schon als Masterarbeit, Diplomarbeit oder andere Prüfungsarbeit verwendet.

Hannover, 03.August 2012

Alexander Bartels

Table of contents

Part B The effect of fluorine, boron and phosphorus on the viscosity of pegmatite forming melts

Acknowledgment

First of all I have to thank the German Science Foundation who supported this research (Be 1720/24). Then, of course I want to thank all the people from the institute, especially Prof. Dr. Francois Holtz and Prof. Dr. Harald Behrens for the very good and friendly support and for the helpful discussions during my thesis but also during my study and diploma thesis. Then, I also want to thank Dr. Burkhart Schmidt and his team from the GZG who was responsible for the micropenetration experiments. Some special greetings are also going to my office mates. I have to say, it was a funny time. Then I want to thank some people, which are already somewhere in the world to work in the brought field of geosciences including Clemens Kirchner, Sarah Cichy, Jan Schüssler, Jan Stelling and many more, who helped me a lot in different ways during different periods of my thesis. I will also thank all the guys from the workshop and the preparation lab including Ullrich Kroll, Markus Köhler, Fabian Christ and Otto Dietrich for the time-spending work on the high pressure vessels and the preparation of samples and thin sections. Additionally I also have to thank Dr. Lothar Borchers from the Hannover Medical School for the help in recording the X-ray images of my samples. I also want to thank Jaayke Knipping, Lars Crede, Amrei Baasner and Nina Pukallus who participated to this study in the frame of their Bachelor theses.

And last but most important I want to thank my parents, my really good friends and my lovely wife who helped me a lot to just forget work sometimes.

Preface

Pegmatites are one of the most fascinating igneous rocks, which could be found in the upper continental crust. One reason is definitely the occurrence of high quality gemstones and collectibles in pegmatites, which are possibly the most valuable specimens when compared to their non-pegmatite related counterparts. Pegmatite bodies also gained in importance for the mining industry due to the enrichment of a broad spectrum of rare elements which have multiple high technology applications, like lithium, tantalum, niobium or beryllium. Even the simplest pegmatites are of interest for mining of feldspar and mica, which are used in the ceramic industry. Pegmatitic rocks occur as sheets or fracture fillings within different host rocks in the upper continental crust. Most pegmatites are granitic in composition and developed from a granitic parental magma due to a high grade of fractionation and the gradual enrichment of incompatible and light elements. The formation and especially the internal evolution of pegmatitic rocks have been debated in the scientific community since decades. Different models were suggested by numerous scientists to explain natural features observed in pegmatitic rocks like extremely coarse but variable grain size, giant crystal size or the occurrence of crystals with skeletal, graphic, or other strongly directional growth-habits. However, it is difficult to find a general model including all features observed in pegmatites because the crystallization is strongly dependent on cooling history of the melt, which might be dramatically different from one to another pegmatite system. One key property governing dynamics in partially melted systems is the melt viscosity and the knowledge about pegmatite melt viscosity could give new approaches for explanations of pegmatite formation and internal evolution. Thereby especially the observance of fluxing elements like water (H_2O), fluorine (F), boron (B), phosphorus (P) and

lithium (Li) are of importance because the concentration of these elements could reach weight percent levels in highly enriched pegmatites and could effectively influence the viscosity of the melt. In this work, I present the results of an experimental study on melt viscosities, which allows discussing the individual influences of F, B, P, Li and K in hydrous pegmatitic melts. Additionally the occurrence of liquid immiscibility and its role during the internal evolution of pegmatitic systems is discussed. The presented viscosity dataset and the occurrence of liquid immiscibility will provide new explanations for the complex story of pegmatite formation and the origin of their exceptional fabrics.

Zusammenfassung

In dieser Studie wurde die Viskosität von pegmatitischen Schmelzen untersucht. Durch hochgradige Fraktionierungsprozesse weisen diese Schmelzen oft deutlich erhöhte Konzentrationen von Fluor (F), Bor (B), Phosphor (P) und Lithium (Li) auf. Um den kombinierten Einfluss dieser Komponenten auf die Viskosität von wasserhaltigen Schmelzen zu bestimmen, wurden Viskositätexperimente mit zwei synthetischen Schmelzen (PEG0 und PEG2), die unterschiedlich hohe Konzentrationen dieser Stoffe enthalten, durchgeführt. Für die Untersuchung der individuellen Einflüsse eines jeden Elements auf die Viskosität, wurde eine Ausgangsschmelze synthetisiert, welche die gleichen molaren Anteile von SiO_2, Al_2O_3, Na_2O und K_2O aufweist, wie die PEG2 Zusammensetzung. Anschließend wurden dieser Ausgangsschmelze jeweils die Elemente F, B, P und Li hinzugefügt und die Auswirkung dieser Komponenten auf die Viskosität der Schmelze bestimmt. Um die unterschiedlichen Effekte der Alkalien auf die Viskosität zu bestimmen wurde zusätzlich eine Schmelze synthetisiert, in der der molare Anteil von K_2O durch Li_2O ersetzt wurde. Die Durchführung der Experimente zur Bestimmung niedriger Viskositäten von wasserhaltigen Schmelzen bei Temperaturen von 873 K – 1530 K und Drücken von 200 bis 650 MPa, erfolgte in intern beheizten Gasdruckanlagen mittels der „falling sphere“ Methode. Im Bereich hoher Viskositäten, erfolgte die Bestimmung der Viskosität mit Hilfe der Mikropenetrations-Technik bei Umgebungsdruck und Temperaturen von 586 bis 1124 K. Die experimentellen Daten zeigen, dass die Viskosität von Schmelzen, die neben Wasser (~9 wt%) auch hohe Konzentrationen der Elemente F, B, P und Li enthalten, bei 1073 K in einem Bereich von 3 – 60 Pa*s liegt und damit extrem niedrig ist. Die Untersuchungen der individuellen Einflüsse von F, B, P und Li auf die Viskosität zeigen, dass diese extremen

Viskositäten auf den additiven Einfluss der Komponenten H_2O, Li und F zurückgeführt werden können. Die Elemente B und P haben in wasserhaltigen Systemen hingegen keinen Einfluss auf die Viskosität. Des Weiteren konnte gezeigt werden, dass der Einbau von Li gegenüber K in die silikatische Schmelze zwar nur geringe Auswirkungen auf die Viskosität hat, andere rheologische Eigenschaften der Schmelze wie z. B. die Fragilität oder die Glasübergangstemperatur hingegen signifikant ändert. Der Vergleich der erhaltenen Daten mit aktuellen Viskositätsmodellen zeigt, dass diese für die Modellierung der Viskosität von pegmatitischen Systemen nur bedingt geeignet sind, da sie Komponenten wie B, P und Li nicht oder nur zum Teil berücksichtigen und sie für hohe Konzentrationen dieser Elemente in Schmelzen nicht kalibriert sind.

In einer zusätzlichen Studie wurden Kristallisations- und dynamische Kristallisationsexperimente mit der pegmatitischen Schmelze PEG2 bei 973 K und 200 MPa durchgeführt. In Proben mit einem initialen Wassergehalt von ~0.5 Gew% wurde dabei die Entmischung einer zweiten Schmelze beobachten. Diese Schmelze bildete sich entlang einer schnell wachsenden Kristallisationsfront in dynamischen Kristallisationsexperimenten sowie in Koexistenz mit silikatischer Schmelze und Feldspat-Kristallen während Kristallisationsexperimenten. Die Analyse der entmischten Schmelze zeigt in beiden Typen von Experimenten eine nahezu identische Zusammensetzung von ~27 Gew% Al_2O_3, ~11 Gew% Na_2O, 49 Gew% F und ~22 Gew% P_2O_5. Die Bildung einer solchen Schmelze liefert neue Erklärungen für Transport-, Kristallisations- und Fraktionierungsprozesse während der Kristallisation von pegmatitischen Systemen.

Schlagwörter: Viskosität, Pegmatit, Fluor, Bor, Phosphor, Lithium

Abstract

Viscosity experiments were conducted to investigate the viscosities of hydrous synthetic pegmatitic melts, containing high concentration of fluxing elements like fluorine (F), boron (B), phosphorus (P) and lithium (Li). To determine the combined effects of these fluxes, experiments were carried out with two different pegmatitic melt compositions, PEG0 and PEG2 containing 1.04, 4.06, 2.30 and 1.68 and 1.68, 5.46, 2.75 and 2.46 wt% of Li_2O, F, B_2O_3 and P_2O_5, respectively. To determine the individual influences of these components on melt viscosity, a starting glass composition (PEG3-base) with the same molar proportion of SiO_2, Al_2O_3, Na_2O and K_2O (~75.50, ~13.17, ~8.32 and ~3.01 mol%, respectively) as the PEG2 composition was synthesized and doped with different amounts of either F (up to 4.81 wt%), B_2O_3 (0.93 wt%), P_2O_5 (up to 2.98 wt%) or Li_2O (1.36 wt%). To determine the role of Li_2O in comparison to other alkalis within a pegmatitic melt, an additional melt composition was synthesized, where the K_2O content of the PEG3-base composition was exchanged with Li_2O.

The viscosity of hydrous melts containing 0.08 to 9.04 wt% H_2O was determined in internally heated gas pressure vessels using the falling sphere method in the temperature range 873 - 1530 K at 200 MPa to 650 MPa pressure. In the high viscosity range, the viscosity was determined between 586 and 1124 K at ambient pressure using the micropenetration technique. The experimental data reveal that the viscosity of water-rich (~9 wt% H_2O) melts containing high concentration of fluxes is in the range of 3 – 60 Pa·s at 1073 K, which is extremely low when compared to a normal granite. The investigation of the individual influences of F, B, P and Li on melt viscosity demonstrates, that very low viscosities could reasonably explained by the combined effects of H_2O, F and Li, whereas P and B do not play a major role in lowering the

viscosity of water-rich pegmatitic melts. Additionally it has been shown, that the incorporation of Li in exchange for K did not lead to a decrease in viscosity, but significantly changes other rheological properties like fragility or glass transition temperature of the melt. The comparison of the dataset from this study with the predictions of available multicompositional viscosity models shows, that these models need to be improved and calibrated for higher concentrations of F, B, P and Li, to predict accurately the viscosity of flux-rich water bearing melts.

In an additional study the PEG2 composition was used to conduct crystallization and dynamic-crystallization experiments at 973 K and 200MPa. In samples with an initial water content of approximately 0.5 wt%, an immiscible melt phase segregated from the pegmatitic starting composition. This low density melt segregates from a boundary layer developed through rapid crystallization of feldspar in dynamic-crystallization experiments but also in normal crystallization experiments coexisting with aluminosilicate melt and feldspar crystals. Electron microprobe analyses show that the segregated melts in both types of experiments are almost similar in composition and contain 26.96 wt% Al_2O_3, 10.91 wt% Na_2O, 48.91 wt% F and 21.60 wt% P_2O_5. The segregation of an immiscible melt phase, which is highly enriched in F and P_2O_5 and effectively fractionates Na_2O from K_2O, gives new explanations for transport and crystallization processes within pegmatitic systems.

keywords: viscosity, pegmatite, fluorine, boron, phosphorus, lithium

Part A

Viscosity of flux-rich pegmatitic melts

The viscosity of a melt is crucial to understand transport and crystallization processes. Since natural silicate melts at depth can incorporate significant amounts of volatiles, one important goal is to determine the effect of volatiles on the viscosity of silicate systems. Especially for pegmatitic systems not only the role of water but also the combined effects of F, B, P and Li on the viscosity of melt are of importance. These elements are commonly traces in silicate melts but due to high grade of fractionation they could reach weight percent levels in pegmatites and therefore significantly influence the viscosity of the melt. The first part of this work investigates the melt viscosity of synthetic pegmatitic melts which are highly enriched in H_2O but also other fluxes like F, P, B and Li. This dataset is crucial needed to verify if high enrichment of these elements is influencing melt properties and if available models could be used to well predict pegmatite melt viscosities.

A modified version of this part is published in *Contrib. Mineral. Petrol.* 162, 51-60 (2011) Viscosity of flux-rich pegmatitic melts. Bartels, A., Vetere, F., Holtz, F., Behrens, H., Linnen, R.L.

A.1. Abstract

Viscosity experiments were conducted with two flux-rich pegmatitic melts PEG0 and PEG2. The Li_2O, F, B_2O_3 and P_2O_5 contents of these melts were 1.04, 4.06, 2.30 and 1.68 and 1.68, 5.46, 2.75 and 2.46 wt% respectively. The water contents varied from dry to 9.04 wt% H_2O. The viscosity was determined in internally heated gas pressure vessels using the falling sphere method in the temperature range 873 - 1373 K at 200 MPa and 320 MPa pressure. At 1073 K, the viscosity of water-rich (~9 wt% H_2O) melts is in the range of 3 – 60 Pa·s, depending on the melt composition. Extrapolations to lower temperature assuming an Arrhenian behaviour indicate that highly fluxed pegmatite melts may reach viscosities of ~30 Pa·s at 773 K. However, this value is a minimum estimation considering the strongly non-Arrhenian behavior of hydrous silicate melts. The experimentally determined melt viscosities are lower than the prediction of current models taking compositional parameters into account. Thus, these models need to be improved to predict accurately the viscosity of flux-rich water bearing melts. The data also indicate that Li influences significantly the melt viscosity. Decreasing the molar Al/(Na+K+Li) ratio results in a strong viscosity decrease and highly fluxed melts with low Al/(Na+K+Li) ratios (~0.8) have a rheological behaviour which is very close to that of supercritical fluids.

A.2. Introduction

According to London (2008) a pegmatite is an essentially igneous rock, commonly of granitic composition, that is distinguished from other igneous rocks by its extremely coarse but variable grain size, or by an abundance of crystals with skeletal, graphic, or other strongly directional growth-habits. Pegmatites occur as sharply bounded homogeneous to zoned bodies within igneous or metamorphic host-rocks. A general consensus is that pegmatites derive from the residual melt and volatile phases at the end of the crystallization of magmatic

systems (Fersmann 1931). Pegmatitic residual liquids are characterized by high concentrations in volatile constituents, including H_2O, B, F, Li and P, which are partly known to lower melt viscosity. One debated feature of granitic pegmatites is the role of water and additional volatiles in forming the typical pegmatitic features, e.g., giant crystal sizes, extreme degrees of fractionation, chemically and texturally heterogeneous zones, high-grade mineralization, etc. As dissolved components, volatiles considerably modify the physico-chemical properties of the melt (viscosity, element diffusivity, temperatures of liquidus and solidus), whereas as exsolved components (e.g., aqueous fluid), they can react with the crystals and the residual melt, and can be an efficient transport medium for elements that preferentially partition into the aqueous fluid phase. The formation of pegmatite bodies has been debated since decades (e.g. Jahns 1953; Jahns and Burnham 1969; Černý 1991). In recent years, there is a general consensus that large pegmatite bodies crystallize mainly from hydrous silicate melts (London 2008; Simmons and Webber 2008; Sirbescu and Nabelek 2003). The concept of crystallization from melts in boundary layers, advocated by London (1992, 1999, 2005), can explain the concentrations of some rare minerals of economic interest in pegmatites. Such boundary layer which leads to the concentration of incompatible elements can occur at the crystallization front of minerals if the rate of crystal growth is faster than the element diffusion in the melt (London 1992; Webber et al. 1997; London 2005). Due to the high concentration of fluxing elements like H_2O, B, F, Li and P the viscosity of such a flux-enriched boundary melt should be very low when compared to the bulk melt (London 2009). At low viscosities the diffusivity, and especially that of the network-forming cations like Si or Al, is expected to depend on melt viscosity (e.g., Dingwell and Webb 1990). Therefore, data on the viscosity of pegmatitic melts are crucially needed to test the boundary layer crystallization process. In particular, viscosity data would allow us to estimate crystallization rates in pegmatitic systems. Previous results (Veksler and Thomas 2002; Sirbescu and

Nabelek 2003) have shown that highly fluxed extremely mobile silicate melts of low density can exist in the crust at temperatures far below the normal granite solidus, overlapping with temperatures characteristic of hydrothermal processes and low grade metamorphism. Thomas and Webster (2000) and London (2005) estimated the viscosities of pegmatite melts at 773 to 973 K to be 10 Pa·s or lower.

The individual effects of volatiles on the viscosity of silicate melts has been determined in silicate melts with various compositions, but the combined effect of these elements on the rheology of a pegmatite melt is poorly understood. Water was studied in detail for several granitic or leucogranitic compositions (e.g. Scaillet et al. 1996; Schulze et al. 1996; Zhang et al. 2003; Whittington et al. 2004), and the effect of B_2O_3 and F has also been determined for some model granitic compositions (Dingwell et al. 1992). The combined effect of H_2O and F on granitic melts was studied by Baker and Vaillancourt (1995) and Giordano et al (2004). At the investigated conditions Baker and Vaillancourt (1995) concluded that F has the same effect as water. Giordano et al. (2004) confirmed that water and fluorine both have a similar effect on viscosity and can be considered to be additive, but at high combined concentrations, the addition of more of either component has little further effect on viscosity. However, the viscosity of a highly fluxed melt representative of pegmatites has yet to be quantitatively determined. Here, we present the results of a first experimental study on the viscosity of dry to water-rich pegmatitic melts. The data are compared with the prediction of general viscosity models of Hui and Zhang (2007) and Giordano et al. (2008) and the implications for pegmatitic processes are discussed.

A.3. Experimental methods

A.3.1. Starting material

Two different pegmatitic starting glasses (PEG0 and PEG2) were prepared from a mixture of SiO_2, Al_2O_3, Na_2CO_3, K_2CO_3, AlF_3 and H_3BO_3. For PEG0 Li and P were added as Li_3PO_4, whereas for PEG2 these elements were added as Li_2CO_3 and $(NH_4)H_2PO_4$.

The mixture for PEG0 was melted at 1473 K for two hours. The glass was then ground in an agate mortar, re-melted at 1473 K and re-ground to ensure homogeneity. The composition of the glass PEG0 was measured by solution ICP-MS after acid dissolution of glass, electron microprobe (anhydrous glass) and B was measured by Instrumental Neutron Activation Analysis (INAA).

PEG2 was melted in a chamber furnace at 1673 K and ambient pressure for 40 min. The major elements composition of this glass was analysed by electron microprobe. Measured concentration profiles showed a homogenous glass composition. The Lithium concentration was determined by inductively coupled plasma optical emission spectrometry (ICP-OES). Additionally, Al-, Na- and K-contents were measured with this method to check the analytical data obtained with microprobe dataset (Tab. A.1). F and B were analysed commercially by Actlabs/Canada using ISE (Ion Selective Electrode) for F and PGNAA (Promp Gamma Activation Analysis) for B.

The glass compositions PEG0 and PEG2 are given in table A.1. The molar ratios Al/(Na+K+Li) (=$A.S.I._{Li}$) are 0.81 and 0.92 respectively. The ratios Al/(Na+K) (=A.S.I.) are 0.97 and 1.26 respectively.

Table A.1 Analyses of the starting glasses PEG0 and PEG2

oxides	PEG0 [wt %]	PEG2 [wt %]
SiO_2	64.07 (0.74)[a]	59.73 (0.13)[a]
Al_2O_3	17.70 (0.33)[a]	19.56 (0.07)[a]
		19.75 (0.13)[d]
Na_2O	8.18 (0.42)[a]	6.81 (0.15)[a]
		7.25 (0.10)[d]
K_2O	4.50 (0.08)[a]	4.01 (0.17)[a]
		3.82 (0.02)[d]
F	4.06 (0.41)[a]	5.46 (0.01)[c]
P_2O_5	1.68 (0.03)[c]	2.46 (0.21)[a]
Li_2O	1.04 (0.01)[c]	1.68 (0.01)[d]
B_2O_3	2.30 (0.23)[c]	2.75 (0.01)[c]
2F = O	-1.71	-2.3
total	101.82	100.16
A.S.I.	0.97	1.26
$A.S.I._{Li}$	0.81	0.92

1σ standard deviation is given in parentheses

A.S.I. molar ratio of Al/(Na+K); $A.S.I._{Li}$ molar ratio of Al/(Na+K+Li)

[a] mean of 10 electron microprobe analyses

[b] measured by ICP-MS

[c] measured by Actlabs using INAA, PGNAA or ISE

[d] measured by ICP-OES-analysis

A.3.2. Sample preparation for viscosity experiments

The melt viscosity at high pressure was measured with the falling sphere method (e.g., Shaw 1963) using the following experimental steps:

A.3.2.1. Synthesis of dry and hydrous glass cylinders

Cylinders of PEG2 with different amounts of water, ranging from dry to 9.04 wt%, were synthesised whereas for PEG0 only cylinders with around 8.5 wt% water were prepared (Tab. A.2). In doing so the synthesized dry glasses PEG0 and PEG2 were crushed by grinding in an agate mortar. Platinum capsules (i.d. 6mm, o.d. 6.4mm, length ~30mm) were filled with these powders, together with distilled water. The filling was done in several steps and the powders

were compacted using a steel piston between these steps, which produced large glass cylinders ~6 mm in diameter and 25 – 30 mm in length. A stepwise filling ensures a homogeneous distribution of the water inside the glass cylinder during the experiment.

The dry and water-bearing glass cylinders were synthesized in an internally heated gas pressure vessel (IHPV) for 16 to 20 hours at 1273-1473 K, 200 MPa and a quenching rate of 200K/min initiated by switching off the heating power of the furnace. The water contents of 9.04 and 8.5 wt% are close to the water solubility in the melts at these synthesis conditions.

The obtained glass bodies were roughly cylindrical, optically homogeneous and microscopically free of crystals and bubbles except for PEG2-4 in which several microbubbles were observed. The absence of crystals was verified using backscattered electron images recorded with the electron microprobe. However, the glasses with more than 4 wt% H_2O were not transparent but "milky", which is attributed to the formation of micro-bubbles. Such an effect can occur even during rapid quench for very high water contents of the melts when approaching the critical temperature of the silicate-H_2O system, as observed for instance for haplobasaltic melts (Benne and Behrens 2003).

A.3.2.2. Sample preparation for falling sphere experiment

The preparation of the falling sphere experiments were conducted following the procedure described in detail by Schulze et al. (1996), implying two step experiments: (1) synthesis of a water-bearing glass containing a Pt horizon (immobile marker) and noble metal spheres;(2) conducting the falling sphere viscosity experiments. In the experiments of this study Pt and Pd spheres with radii ranging from 54 to 100.5 μm were used (Tab. A.2). In some cases (PEG0-1 and PEG2-4) two spheres within one experiment were used. Due to the density variation between Pt and Pd (21.45 g/cm^3 and 12.02 g/cm^3) the different settling distance of the spheres allows calculating two viscosity values for these experiments. To produce the

spheres, a 0.025 mm thick Pt or Pd wire was melted with a sudden D.C. current. The melt droplets were quenched in distilled water. The water was filtered and the diameter of the hand-picked spheres was measured using a microscope with an attached Leica DFC290 camera system and a Leica Application Suite V3.0.0 program. The radii of the selected spheres are given in table A.2. After welding shut the capsules, the samples were pre-pressurised in a vertical autoclave to ensure a higher stability of the experimental setup before loading into the IHPV. The first experimental run in the IHPV at 923 K (for high water contents) to 1273 K (for dry samples) and 200 MPa for a few minutes established a well defined starting position of the spheres in the glass cylinder. Because of the observed microbubbles in sample PEG2-4 we evacuated the capsule following the method described by Boettcher et al. (1989) before welding shut to minimize the initial gas phase within the samples. During the experimental run we additionally increased the pressure up to 320 MPa for the water-rich samples to minimize the risk of bubble nucleation. The samples were cooled down with a rapid quench device (samples PEG2-3 and PEG2-4) or with a normal quench device (all samples of PEG0; PEG2-1 and PEG2-2) described by Berndt et al. (2002). After removing the glass cylinder from the capsule, pictures of transparent samples were taken with a Zeiss AxioCam ICc3 camera attached to a binocular microscope and processed with the AxioVision Rel.4.6 program. To improve the visibility of the glass bodies the samples were placed in water. To measure the sphere positions in non-transparent samples we had to use an X-ray apparatus (SIEMENS HELIODENT DS X-ray camera with 60 kV voltage and a current of 7 mA, AQUA DENTUS films M2 comfort or KODAK INSIGHT IP-21 films and an exposure time of 0.16 seconds). Using these images the exact position of the sphere relative to the insert Pt-horizon was evaluated with CoralDRAW X3. To compare both methods some transparent samples were also x-rayed. The measured difference for the sphere positions is < 2%.

Table A.2 Experimental conditions and results

sample	H_2O [wt%]	H_2O* [wt%]	T [K]	ρ_m [g/cm^3]	mat.	r [µm]	d [m]	t [s]	log η [h in Pa·s]
PEG0-1a	8.46	n.d.	873	2.11	Pd	55	0.0059	961	1.01 (0.04)
PEG0-1a	8.46	n.d.	873	2.11	Pt	54	0.0102	961	1.05 (0.04)
PEG0-2a	8.51	n.d.	973	2.09	Pd	82.5	0.0071	383	0.88 (0.05)
PEG0-3a	8.69	n.d.	1073	2.06	Pd	82.5	0.0166	391	0.52 (0.05)
PEG2-1a	0.07		1173	2.35	Pt	92	0.0004	86458	4.91 (0.05)
PEG2-1c			1243	2.34	Pt	92	0.0049	172863	4.06 (0.04)
PEG2-1b			1273	2.34	Pt	92	0.0034	86468	3.92 (0.04)
PEG2-1d		0.09	1378	2.33	Pt	92	0.0054	28877	3.25 (0.04)
PEG2-2d		0.46	973	2.35	Pt	80	0.0012	345660	4.85 (0.03)
PEG2-2b			1073	2.34	Pt	80	0.0022	86471	4.00 (0.04)
PEG2-2a	0.5		1173	2.33	Pt	80	0.0061	43284	3.25 (0.04)
PEG2-2c			1273	2.32	Pt	80	0.0026	7297	2.85 (0.03)
PEG2-3e			975	2.23	Pt	85	0.0061	64871	3.48 (0.03)
PEG2-3a	3.89		1073	2.21	Pt	85	0.0054	10885	2.76 (0.03)
PEG2-3b			1073	2.21	Pt	85	0.01	21685	2.79 (0.03)
PEG2-3c			1173	2.19	Pt	85	0.004	1900	2.13 (0.03)
PEG2-3d			1173	2.19	Pt	85	0.004	1900	2.13 (0.03)
PEG2-3f		3.29**	1273	2.18	Pt	85	0.001	415	2.07 (0.07)
PEG2-4b		n.d.	973	2.09	Pt	77	0.0053	3600	2.22 (0.03)
PEG2-4a	9.04		1073	2.07	Pt	77	0.0052	1003	1.66 (0.03)
PEG2-4a			1073	2.07	Pd	100.5	0.0032	1003	1.80 (0.03)

Characters in the sample name refer to base composition (PEG0 or PEG2), the synthesized sample (1,2,3,4) and the order of subsequent experiments with the same sample (a,b,c..). Images used for viscosity calculation are given in the Appendix.

All experiments were done at 200MPa except for PEG2-4a and PEG2-4b, which were run at 320 MPa.

Melt densities were calculated after the modified model of Ochs and Lange (1999).

H_2O contents measured by KFT and IR, H_2O* = water content after experiments; ** leak during quench

Maximal uncertainties: water content ± 0.08 wt%, T 5 K, P ± 3 MPa, sphere radius ± 2 µm; distance ± 2 %; time ± 57 seconds; viscosity ± 15%

mat. = sphere material; n.d. = not determined; *r* = sphere radius; *d* = falling distance; t = experimental duration

A.3.2.3. Falling sphere experiments and viscosity determination

Viscosity experiments were performed by sealing the glass cylinder in a platinum capsule, holding it at a given temperature and pressure for a certain time. After quenching the experiment, the positions of the spheres were determined using the methods described above. The effective settling distance was calculated using the platinum horizon as a reference, considered to be static, and the positions of the spheres before and after the experiment. If

possible, the same sample was used for several viscosity runs at different P-T-conditions. After each experiment the capsule material was removed, the settling distance was measured, the cylinder was turned upside-down (only if the sphere was close to the platinum marker) and sealed again in a platinum capsule. Because of the multiple uses of the glass cylinders the Pt-horizon becomes progressively diffuse. Nevertheless the position of the marker could be estimated from the shape of the samples as well, using images recorded before and after the experiment.

A.3.3. High pressure equipment

All viscosity experiments of the third step were conducted in the temperature range of 873 to 1373 K at 200 to 320 MPa in an internally heated pressure vessel (IHPV) with Ar as pressure medium. The heating rate was 80 K/min and experiments were terminated by rapid quench with a cooling rate of ~150 K/s (Berndt et al., 2002; Benne and Behrens, 2003) or normal quench with a cooling rate of ~200K/min, and the experimental duration varied from 345660 seconds (PEG2-2d) to 383 seconds (PEG0-2a) (Tab. A.2). Temperatures were measured by using Ni-CrNi and Pt-$Pt_{90}Rh_{10}$ thermocouples. Due to the experimental setup a maximum temperature gradient of approximately 5K can be detected across the sample and is included in the error calculation of the viscosity. Quenching was close to isobaric. All capsules were weighted before and after the experiments to ensure that no leaks occurred during the experiments.

A.4. Analytical techniques

The composition of starting glasses was measured using a Cameca SX-100 electron microprobe with 15 keV accelerating voltage, 4 nA beam current and a beam diameter of 20

μm. The counting time ranged from 4 to 20 seconds. The respective standards were albite (Na), wollastonite (Si), corundum (Al), orthoclase (K), SrF_2 (F) and apatite (P).

The Li-content in the starting glasses, as well as Al-, Na- and K-contents in PEG2, were measured by inductively coupled plasma optical spectroscopy (ICP-OES) using a 1.2 kW plasma power, 15 l/min plasma flow, 1.5 l/min auxiliary flow and 0.9 l/min nebuliser flow. The emission lines used were 236.705, 237.312 and 394.401nm for Al, 766.491 and 769.897nm for K, 323.263, 460.289, 610.365 and 670.783nm for Li and 330.237, 568.821 and 589.592nm for Na. The uncertainties of the analyses were determined to be (±1σ). The standard deviations were ±0.13 wt% for Al, ±0.02 wt% for K, ±0.01 and ±0.05 wt% for Li and ±0.10 wt% for Na.

The water contents of all synthesized glass bodies were determined by pyrolysis and subsequent Karl-Fischer titration (KFT, Behrens et al. 1996). An increment of 0.10 wt% was added to the values measured by KFT to account for incomplete dehydration during analysis (Leschik et al. 2004). For sample PEG2-4 both ends of the cylinder were analyzed by KFT to check for homogeneous distribution of the water within the cylinder. The resulting values do not significantly differ from each other and are 9.00 ± 0.08 and 9.08 ± 0.08 wt%. In addition, the water contents of samples of PEG2-1, PEG2-2 and PEG2-3 were measured by KFT before and after the viscosity experiments. The maximum variation is within the analytical error and therefore negligible. The water content of the post-viscosity sample PEG2-3f was lower by 0.6 wt% compared to the starting material, which is attributed to a water loss during quenching at the end of the last viscosity experiment with this sample. This is confirmed by a change in total weight of the sample.

The stability of the glasses with respect to water loss at room temperature was tested for two glasses of PEG0 containing 9.9 and 8.6 wt% H_2O. The water loss was only 1.3 and 0.6 wt%, respectively, after 16 days exposure to air. Thus, water loss is not a severe problem for the

pegmatites used in our study, at least at room temperature. However, the water-rich glasses clearly started to loose water at temperatures in the range 353 – 373 K (formation of bubbles occurring after placing glasses in a drying furnace for a few hours). Thus we avoided any annealing of the samples to prevent any alteration including water loss.

For water-poor glasses (PEG2-1 and PEG2-2, Tab. A.2), additional analyses were performed using IR spectroscopy. Water concentrations were calculated by the Beer-Lambert law using the peak height of the OH stretching vibration band at 3550 cm^{-1} after subtraction of a linear baseline. MIR absorption spectra were recorded using a Bruker IFS88 FTIR spectrometer combined with an IR-ScopeII microscope (Institute of Mineralogy, Hannover). The operating conditions were: globar light source, KBr beamsplitter, and MCT narrow range detector. The glasses were prepared as both-side polished thin sections with a thickness of ~60 - 200 μm. For each spectrum 50 to 100 scans were collected with a spectral resolution of 2 cm^{-1}. The spot size was about 50 x 50 μm. For every sample three spectra were collected in different parts of the glass piece to check for homogeneity of volatile distribution. The thickness of the polished pieces of glass was measured with a digital micrometer Mitutyo (precision ± 2 μm, Behrens, 2009). The density of the PEG2 glasses was determined using the Archimedean method with water as immersion liquid. Based on 8 samples with water contents in the range 0 – 9 wt%, the density – water content relationship was established to be density (in g/cm^3) = 2.395 – 0.0127 x wt% H_2O. The absorption coefficient for the band at 3550 cm^{-1} was determined for standard samples containing 0.89 ± 0.06 to 1.97 ± 0.06 wt% H_2O (determined by KFT). A small effect of water content on the absorption coefficient was observed, as found by Leschik et al. (2004) for rhyolitic glasses. The highest values were obtained for the glasses with water contents around 1 wt% (86 to 93 $L \cdot mol^{-1} \cdot cm^{-1}$). Slightly lower values were determined for glasses containing around 2 wt% H_2O (80 to 82 $L \cdot mol^{-1} \cdot cm^{-1}$). However, this variation is within error and we used an average absorption coefficient of 86 ± 7 $L \cdot mol^{-1} \cdot cm^{-1}$

for quantification of water contents of water-poor pegmatitic glasses. This absorption coefficient for the 3550 cm^{-1} band is identical within error to that determined for rhyolitic glasses (80 ± 4 $L \cdot mol^{-1} \cdot cm^{-1}$) by Leschik et al., 2004).

A.5. Experimental Results

The run duration, sphere radius, settling distance, calculated melt density and temperature of the experiments is given in table A.2. The resulting viscosity (Tab. A.2) was calculated using the following modified Stokes law:

$$\eta = \frac{2 \cdot t \cdot g \cdot \Delta\rho \cdot r^2 \cdot C_F}{9 \cdot d} \qquad [A.1]$$

where d is the settling distance, t is the run duration, $\Delta\rho$ is the density difference between the sphere and the melt, g is the acceleration due to gravity (9.81 m/s^2), r is the radius of the sphere and C_F is the Faxen correction (Faxen 1923) to account for the effect of viscous drag by the capsule wall on the settling sphere. The Faxen correction is given by the equation:

$$C_F = 1 - 2.104\left(\frac{r}{R}\right) + 2.09\left(\frac{r}{R}\right)^3 - 0.95\left(\frac{r}{R}\right)^5 \qquad [A.2]$$

where r is the radius of the sphere and R is the inner radius of the capsule. For all experiments we calculated a time correction due to the sinking of the sphere during heating and cooling. This was done assuming a constant heating ramp of 80 K/min and a constant cooling rate of 120 K/min and using the following equation (method is described in detail by Vetere et al., 2006)

$$t_{effective} = \int \exp\left[\frac{-E_a}{R}\left(\frac{1}{T(t)} - \frac{1}{T_{target}}\right)\right] \cdot dt \qquad [A.3]$$

E_a is the activation energy for viscous flow and R is the universal gas constant. A preliminary value of the activation energy was determined using viscosity data without time correction, i.e. using the experimental dwell at the target temperature for each water content and assuming an Arrhenian behaviour of log viscosity and reciprocal temperature over the investigated temperature range. The calculated values of $t_{effective}$ are given in table A.2. The melt densities at given P and T calculated after Ochs and Lange (1999) are listed in table A.2. Thereby we had to extend the model by including the components F, Li_2O, B_2O_3 and P_2O_5. The partial molar volumes for these elements were taken from Knoche et al. (1995).

Taking into account the uncertainties in run duration, sphere radius, falling distance, melt density and temperature the estimated total error of viscosity is always ≤ 10% except for samples PEG2-1a, PEG0-3a and PEG2-3f. In these cases either a very short falling distance (0.35 mm for PEG2-1a) was measured or a short run duration (391 seconds for PEG0-3a and 415 seconds for PEG2-3f) had to be used.

To check the reproducibility of the viscosity data, the experiments PEG2-3a and PEG2-3c were repeated under the same P-T-conditions (PEG2-3b and PEG2-3d). The difference between the viscosities from both experiments is < 8% and therefore within the calculated error of viscosity determination.

The calculated viscosity for experiment PEG2-3f should be considered as a rough estimation because a leak was observed after the last experiment. The KFT analysis after the experiment showed a water content which is lower by ~ 0.6 wt% H_2O compared to the starting glass.

A.5.1. Temperature dependence of viscosity

Figure A.1 shows a plot of viscosity (expressed as log η) against temperature (expressed as $10^4/T$ (K^{-1}). For PEG0 the viscosities range from 11.14 Pa·s at 873 K to 3.29 Pa·s at 1073 K. The values at 873 K refer to two different spheres (Pd and Pt) which were used in the same experiment. Both viscosity data differ only by 8%, confirming the reliability of the experimental technique.

For PEG2 the viscosities range from 81658 Pa·s for a dry melt at 1173 K to 42.3 Pa·s for water saturated conditions at 1073 K. The viscosity decrease with increasing temperature is more pronounced for samples with low water content (PEG2-1 compared to PEG2-2 or PEG2-3).

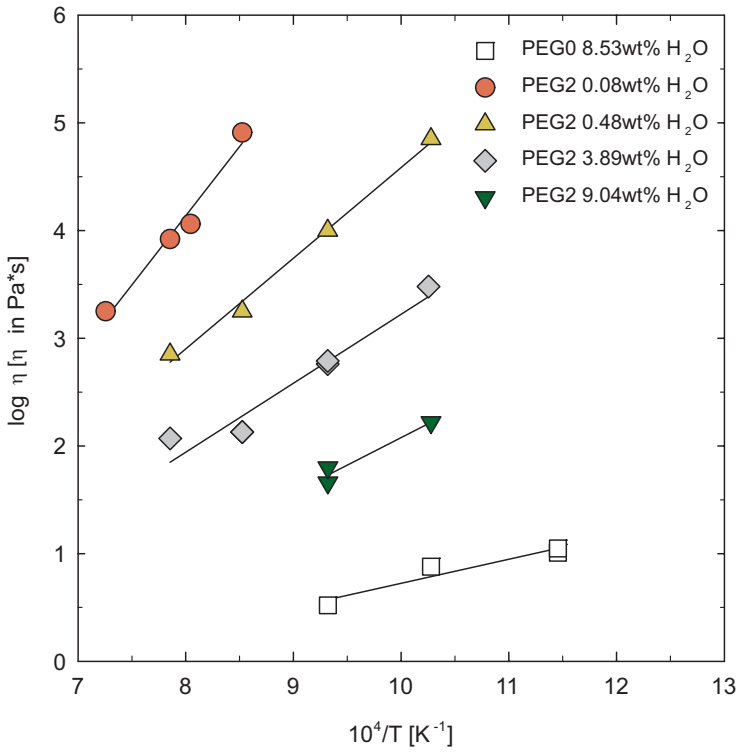

Figure A.1 Effect of temperature on melt viscosity for two pegmatitic melts. *Error bars* are smaller than symbols

Within the restricted temperature range of this study the viscosity data can be considered to be a linear function of reciprocal temperature and therefore represented by the following Arrhenian equation:

$$\log \eta = \log \eta_0 + \frac{E_a}{2.303 \cdot R \cdot T} \qquad [A.4]$$

where log η_0 is the pre-exponential factor, E_a the activation energy (kJ/mol) of the viscous flow, 2.303 is the conversion factor of ln to log, R the gas constant and T the temperature (K). The values for log η_0 as well as for E_a are calculated for each composition by using first order regression lines. The value of log η_0 is given by the y-axis intercept of the regression line and E_a is calculated from the slope of the regression line. The results are given in table A.3.

Especially at low water contents, E_a shows a strong dependence on the water concentration in the melt. It decreases from 246 ± 27 kJ/mol for the anhydrous sample PEG2-1 to 161 ± 9 kJ/mol for sample PEG2-2, which contains 0.48 wt% H_2O. The further addition of H_2O decreases the activation energy down to 98 ± 24 kJ/mol for sample PEG2-4 with 9.04 wt% H_2O. The errors for the activation energy were calculated taking into account the uncertainty of the regression lines.

Table A.3 Activation energies and pre-exponential coefficients for viscosity

sample	wt% H_2O	T range [K]	E_a [kJ/mol]	log η_0 [η in Pa·s]
PEG0	8.46 – 8.69	873 - 1073	43 (8)	-1.55 (0.47)
PEG2-1	0.07 – 0.09	1173-1378	246 (27)	-6.20 (1.11)
PEG2-2	0.46 – 0.50	973 -1273	161 (9)	-3.82 (0.43)
PEG2-3*	~3.89	975 - 1173	122 (16)	-3.16 (0.76)
PEG2-4	~9.04	973 - 1073	98 (24)	-3.03 (1.22)

* The last experiment of this series was not considered in the Arrhenius equation because its departure from the other data and the post-experimenal water determination indicated a water loss. 1σ standard deviation is given in parentheses.

A.5.2. H_2O dependence of viscosity for PEG2

Experiments with different water contents were conducted for the PEG2 composition (Tab. A.2). Figure A.2 shows the viscosity dependence of this melt composition on water content over the temperature range of 973 to 1273 K, at 200 MPa. Because of the very long run durations we were not able to conduct experiments without water at temperatures below 1173 K. At 1173 K and 1273 K the viscosity of the melt strongly decreases with the addition of H_2O. For example by adding only 0.41 wt% H_2O to the melt the viscosity decreases by a factor of more than 45 (1.66 log units from $10^{4.92}$ to $10^{3.26}$ Pa·s) at 1173 K. This decrease of the melt viscosity with the addition of water is greatest at low than at high water contents which is typical for all hydrous silicate melts.

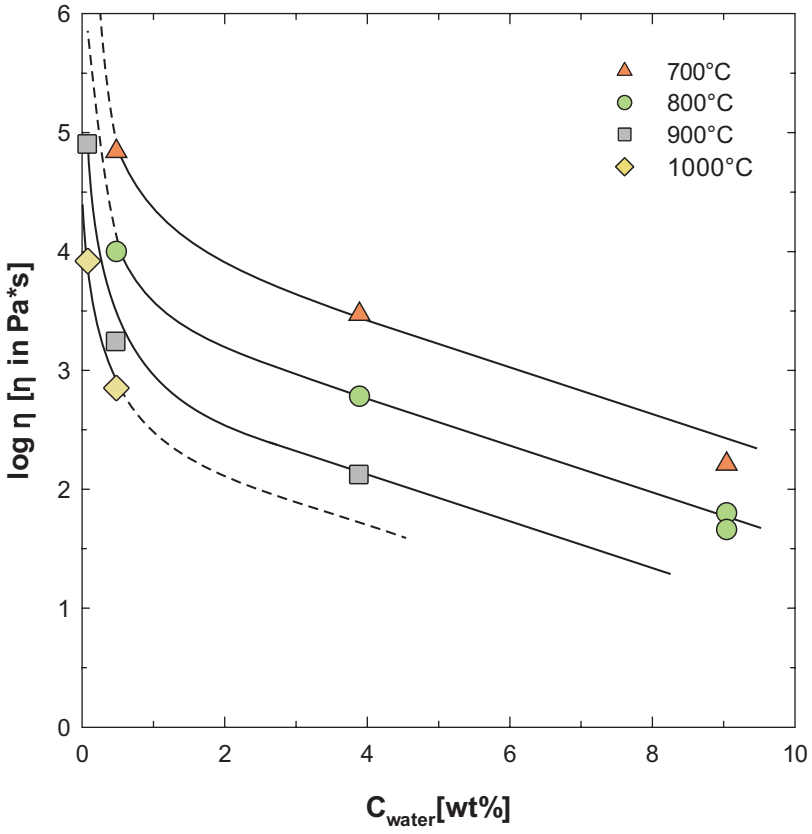

Figure A.2 The effect of water on melt viscosity of PEG2 at different temperatures. *Error bars* are smaller than symbols

At 1173 K and 200 MPa the further addition of 3.4 wt% H_2O only decreases the viscosity by 1.1 log unit. However, even at water contents above 4 wt% H_2O the viscosity significantly

decreases upon further hydration, e.g. by 1 log unit when increasing the water content from 5 to 9 wt% H_2O at 973 and 1073 K (Fig. A.2).

A.6. Discussion

A.6.1. Effect of melt composition

The pegmatitic melt PEG0 containing 8.55 wt% H_2O has a much lower viscosity and activation energy than PEG2 containing 9.04 wt% H_2O over the investigated temperature range. This might be surprising because the melt composition PEG2 contains higher concentration of elements like F, P, Li and B which are partly known to lower melt viscosity (Baker and Vaillancourt 1995; Dingwell et al. 1996; Giordano et al. 2004). On the other hand, the alumina content is higher in PEG2 than in PEG0 (Table A.1). Thus, the ratio between alkalis and network-forming cations (Al and Si), $A.S.I._{Li}$, is lower in PEG0 (0.81) than in PEG2 (0.92), and therefore PEG0 is more "peralkaline" which may explain the lower melt viscosity.

By extrapolating the data to temperatures of 1673 K, the viscosity of the anhydrous melt PEG2-1 is more than 4 log units lower when compared to measurements of Schulze et al. (1996) for a synthetic haplogranitic melt composition. This difference is also observed for the water-rich melts. The viscosities of the pegmatitic melts PEG2-4 and PEG0 (9.04 and 8.55 wt% H_2O, respectively) are lower by more than 2.5 log units when compared to that of a haplogranitic melt containing 8.21wt% H_2O (Schulze et al., 1996) at 1073 K (Fig. A.3). The viscosity difference between haplogranitic melts and pegmatitic melts may be explained by different factors. First, it has been shown that the replacement of alkalis by Li in aluminosilicate melts leads to a viscosity decrease (Boiret and Urbain, 1987). Second, taking the Li content into account, both melts PEG0 and PEG2 are clearly peralkaline ($A.S.I._{Li}$ of PEG0 and PEG2 are 0.81 and 0.92, respectively), and it has been shown that peralkaline

haplogranitic melts have very low viscosities compared to their metaluminous or peraluminous counterparts, both for anhydrous (Hess et al. 1995) and hydrous conditions (Dingwell et al. 1998). However, it has to be mentioned that the melts investigated by Hess et al. (1995) and Dingwell et al. (1998) were much more peralkaline when compared to the melts of this study. Third, the pegmatitic melts investigated in this study also contain high concentrations of F, P and B. Previous works have shown that the effect of F is the same as that of water, at least for silica-rich melts, and that the effect of both could be additive (Baker and Vaillancourt, 1995; Giordano et al., 2004). Clearly, the addition of 4.06 wt% F (PEG0) to a rhyolitic composition with A.S.I. ~1 is not sufficient to explain a viscosity variation of ~4 log units (at 1073 K; Fig. A.3; compare data obtained by Schulze et al., 1996 and data obtained for PEG0).

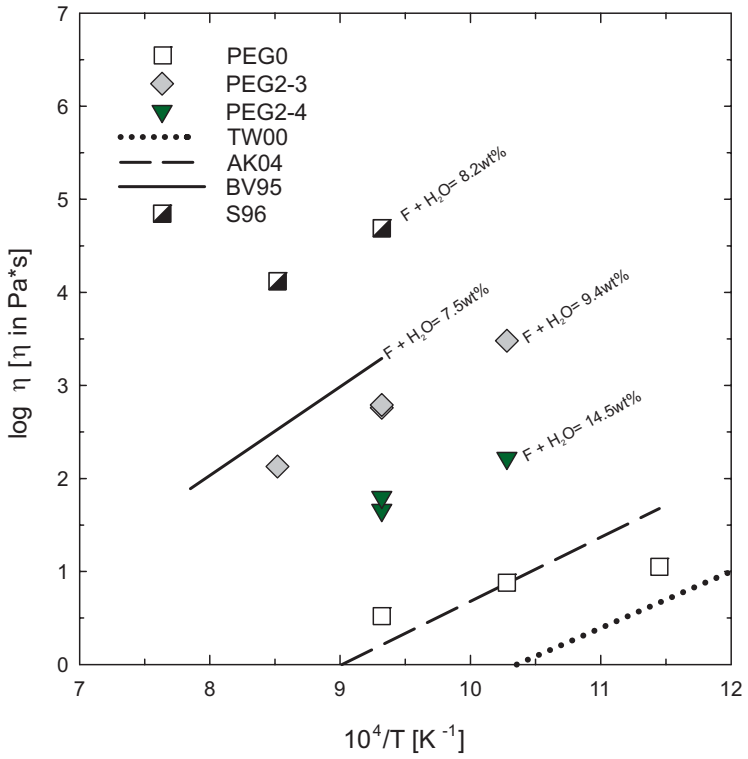

Figure A.3 Viscosity of water rich melt compositions in comparison with different models. TW00: pegmatite, Thomas and Webster 2000; AK04: supercritical fluids with 86 wt% dissolved solid, Audétat and Keppler 2004; BV95: rhyolite, Baker and Vaillancourt 1995; S96: haplogranite, Schulze et al. 1996

Thus, we attribute the low viscosity of the investigated pegmatitic melts to the combined effects of the different fluxing elements (Li, F, B and P) and the peralkaline composition (taking Li into account).

A.6.2. Comparison with recent models

Two recently developed non-Arrhenian models taking compositional variations into account are available to calculate silicate melt viscosities: the model of Hui and Zhang (2007) and the model of Giordano et al. (2008).

Using the model of Hui and Zhang (2007) for the pegmatitic melts investigated in this study leads to a dramatic overestimation of the viscosity. This might be due to the fact that this model does not include elements like F, Li or B. Even if F is assumed to have the same effect than water (Baker and Vaillancourt 1995), the calculated viscosities are overestimated by several log units. For example at 1073 K the model calculates viscosities of $10^{4.29}$ and $10^{6.67}$ Pa·s for PEG0 and PEG2 containing 8.55 and 9.04wt% H_2O, respectively, whereas the experimental data are $10^{0.52}$ and $10^{1.74}$ Pa·s, respectively. The deviation of the calculated values from experimental data becomes more critical at lower temperature. At 973 K, the calculated viscosity of PEG2 with 9.04 wt% H_2O is $10^{16.1}$ Pa·s whereas the measured value is $10^{2.23}$ Pa·s. However, it has to be noted that Hui and Zhang (2007) mention that their model should only be used for viscosities below 10^{15} Pa·s. and that it should not be extrapolated to H_2O contents above 5 wt% for melts other than rhyolite. Thus, taking these restrictions into account, the model of Hui and Zhang (2007) can not be applied to the melts investigated in this study.

The model of Giordano et al. (2008) does not include Li and B but, in contrast to the model of Hui and Zhang (2007), P and F are taken into account. Therefore it might be more appropriate to calculate viscosities of pegmatitic melts. For the nearly dry melt composition PEG2-1 the

experimental data set is in good agreement with the calculated values (Fig. A.4). For a PEG2 melt containing 0.48 wt% H_2O, the experimental value at 973 K is lower by almost 1.6 log units when compared to the modelled value.

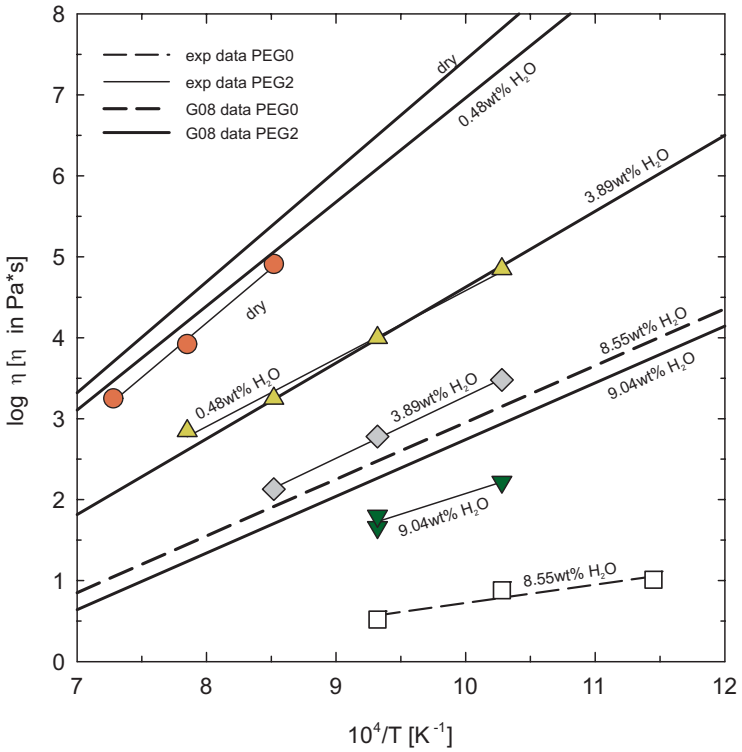

Figure A.4 Comparison between the measured viscosities from this study and calculated viscosities after Giordano et al. (2008), referred to as G08. Symbols see Fig. A.1.

This overestimation of viscosity can be observed for all water-bearing samples but the deviation is particularly strong for low water contents. The difference between the modelled and experimental data for PEG2-4 which contains 9.04wt% H_2O is only 0.7 log units at 973 K ($10^{2.94}$ Pa·s for modelled data and $10^{2.22}$ Pa·s for PEG2-4b). For PEG0, even at high water contents (8.55wt% H_2O), the modelled data differ by almost 2.3 log units when compared to the experimental data at 973K ($10^{3.15}$ Pa·s for modelled data and $10^{0.88}$ Pa·s for PEG0-2a). This comparison demonstrates that even the model of Giordano et al. (2008) which includes P and F is not well calibrated for highly evolved melt compositions like pegmatites.

In addition to general (multicompositional) models, specific models for given compositions may be tested. Baker and Vaillancourt (1995) proposed different equations for peralkaline to peraluminous rhyolitic melt compositions with 1.5 wt% F and 6 wt% H_2O. At 973 K and using the equation for peralkaline compositions, the calculated viscosity for PEG2-4 containing 9.04 wt% H_2O and 5.46 wt% F is higher by almost 2 log units (Fig. A.3). If the experimental results for PEG2-3 containing 3.89 wt% H_2O and 5.46 wt% F (total F + H_2O of 9.35 wt%) (Fig. A.3) are compared to the model of Baker and Vaillancourt (1995), the calculated viscosity is 0.7 log units higher than the experimentally determined value at 973 K. Thus, the interpolation of our experimental data to a composition PEG2 containing a total amount of F + H_2O of 7.5wt% using the trend lines in figure A.2 lead to viscosity values which are very close to those predicted by the equation of Baker and Vaillancourt (1995).

Thomas and Webster (2000) derived an Arrhenian equation to account for the viscosity of highly evolved late-stage pegmatitic melts with H_2O + F = 17.3 wt% and the accuracy of this equation can be tested with our dataset. By using their equation the viscosity is only about 0.23 Pa·s at 1073 K. Using figure A.2 for extrapolation of the calculated viscosity data we can estimate a viscosity of around 15 Pa·s for PEG2 melts containing H_2O + F = 17.3 wt%, which is more than 1.5 orders of magnitude higher than predicted by Thomas and Webster (2000). The difference may be due to the different base composition of the pegmatites used in both studies. Although the role of changing composition (e.g. $A.S.I._{Li}$) is not taken into account by Thomas and Webster (2000), this equation established on the basis of the analysis of melt inclusions is consistent with the extremely low viscosities of pegmatite melts determined in this study and also predicted by London (2005).

Finally, our results can be compared to the viscosity determinations of supercritical fluids performed at very high pressure (1000 - 2000 MPa) by Audetat and Keppler (2004) as well as to the model of Whittington et al. (2009). Audetat and Keppler (2004) used the falling sphere

method to determine the viscosity of fluids containing 10 to 80 wt% of dissolved solids (albite, leucite and pectolite). According to Audetat and Keppler (2004), the calculated viscosity of a fluid with 86 wt% dissolved solid fraction is very close to that of the PEG0 melt containing 12.6 wt% H_2O+F (Fig. A.3), although it needs to be mentioned that this is an extrapolation out of the experimental range of Audetat and Keppler (2004). Thus, at least for depolymerised compositions (low $A.S.I._{Li}$), the rheological behaviour of highly fluxed melts seems to be very close to that of supercritical fluids. When comparing our data with the model of Whittington et al. (2009), the experimentally determined viscosities are lower than predicted for a haplogranitic composition, which might be expected considering the role of additional volatiles and $A.S.I._{Li}$.

A.7. Conclusion

This study demonstrates the extremely low viscosities of volatile-rich pegmatitic melts. Most of the investigated experimental temperatures are unrealistically high for natural pegmatites but an extrapolation to lower temperatures using an Arrhenian approach leads to melt viscosities in the range $10^{1.5}$ to $10^{3.5}$ Pa·s at 773 K for H_2O+F concentrations in the range 12 - 15 wt%. Further investigations in the high viscosity range are necessary to model the non-Arrhenian behaviour of pegmatite melts. However, based on our available general knowledge on the deviation from Arrhenian behaviour in granitic melts (e.g. Whittington et al., 2009), the viscosities given above (Arrhenian approach) may be underestimated by ~ 1 to 2 log units (10-15 wt% H_2O + F; 773 K). In this case, the viscosity of pegmatite melts at 773 K would not be very different from that of residual water-saturated granitic melts at 973-1023 K (Scaillet et al. 1996). Assuming that crystal growth is mainly controlled by the diffusivity of network forming cations, this observation indicates that the large crystal size observed in pegmatite systems can not be explained by extremely low diffusivities in low-temperature

pegmatite melts. If such large crystals crystallize from an aluminosilicate melt, additional factors such as nucleation and undercooling must play a significant role.

It is also demonstrated that the melt composition (A.S.I.) and specially the Li concentration influence significantly the viscosity of pegmatitic melts. Changes in residual melt compositions resulting from fractionation processes or from loss of volatiles or Li to the wall rock of pegmatite bodies can influence significantly the melt viscosity during crystallization and consequently the diffusivities of metals in pegmatites.

Part B

The effect of fluorine, boron and phosphorus on the viscosity of pegmatite forming melts

The first part of this work showed that the viscosity of volatile-rich melts, from which pegmatites crystallize, is extremely low and that available models are not able to predict accurately the viscosity of these melt compositions. The main reason for the low viscosity values is related to the high concentrations of additional fluxes like F, B, P and Li but it remains unclear to which extend the individual elements are causing a decrease in viscosity. Therefore the second part will focus on the individual influences of F, B and P on the behavior of highly fractionated melts. The dataset also delivers new suggestions for improvements for the available viscosity models.

A modified version of this part is submitted to *Chem. Geol.*, The effect of fluorine, boron and phosphorus on the viscosity of pegmatite forming melts. Bartels, A., Behrens, H., Holtz, F., Schmidt, B.C., Fechtelkord, M., Knipping, J., Crede, L., Baasner, A., Pukallus, N.

B.1. Abstract

The individual influences of F, B and P on viscosity of hydrous pegmatite forming melts have been determined experimentally. A starting glass composition (68.01 wt% SiO_2, 20.14 wt% Al_2O_3, 7.73 wt% Na_2O and 4.26 wt% K_2O, Al/(Na+K) = 1.16) was doped with different amounts of F (up to 4.81 wt%), B_2O_3 (0.93 wt%) and P_2O_5 (up to 2.98 wt%). The viscosity of melts containing 0.08 to 6.15 wt% H_2O was determined in the high and low viscosity range using the micropenetration technique and the falling sphere method, respectively. Falling sphere experiments were carried out at 200 to 650 MPa and 1173 to 1530 K. Micropenetration measurements were performed in the temperature range of 586 to 1124 K at ambient pressure. For all compositions a large decrease of viscosity upon hydration was observed, consistent with previous findings. The results also confirm that the viscosity decreases with the addition of F at all investigated temperatures. This decrease is more pronounced at low temperature and at low water content. According to our data, P and B do not play a major role on viscous flow in water-rich systems. However, the depolymerising effect of H_2O and F is not sufficient to explain very low viscosities of complex highly fractionated melts containing H_2O, F, B, P and Li (Bartels et al., 2011). Thus, although we confirm that F is clearly a fluxing agent, Li must play a crucial role in lowering the viscosity of natural pegmatite forming melts and combined effects between different constituents need to be taken under consideration.

B.2. Introduction

According to London (2008), a pegmatite is an essentially igneous rock, commonly of granitic composition that is distinguished from other igneous rocks by its extremely coarse but variable grain size, or by an abundance of crystals with skeletal, graphic, or other strongly directional growth-habits. Pegmatites occur as sharply bounded homogeneous to zoned bodies within igneous or metamorphic host-rocks. Although there is no general model to explain all

features observed in pegmatites, most of the recent studies agree on the hypothesis that pegmatites derive from the crystallisation of a residual melt which is highly enriched in fluxes, volatiles and rare elements (e.g., London, 1987; London, 2008; Simmons and Webber, 2008; Nabelek et al., 2010).

In contrast to common silicate melts the residual liquids from which pegmatites crystallize, are characterized by elevated concentrations of additional volatile constituents, including mainly H_2O, F and B. In addition, elements such as P and Li can also be present in high concentrations. Bartels et al. (2011) showed that the viscosity of melts which are enriched in these elements is much lower than predicted by available viscosity models (Hui and Zhang, 2007; Giordano et al., 2008) and concluded that these volatiles play an important role on the behaviour of pegmatite forming melts. Furthermore, as detailed below, it has been shown by different authors that these elements individually play a crucial role in lowering melt viscosities at least in anhydrous systems.

It is well known that the addition of water results in a strong decrease of the melt viscosity (e.g., Shaw, 1963; Schulze et al., 1996; Hess and Dingwell, 1996; Richet et al., 1996; Scaillet et al., 1996; Whittington et al., 2000, 2001; Romano et al., 2001, 2003; Liebske et al., 2003; Zhang et al., 2003; Giordano et al., 2004). Viscosity measurements on anhydrous haplogranitic melt compositions with different amounts of F, B and P (Dingwell et al., 1993) allow us to estimate the individual effect of these elements. Dingwell et al. (1993) concluded that the effect of phosphorus on haplogranitic melt viscosity is much lower than that of boron or fluorine, and that phosphorus will not significantly influence melt viscosity at least at the investigated experimental conditions. On the other hand, boron must be considered as a fluxing agent in B-rich granitic and pegmatitic systems (Dingwell et al. 1992).

So far only a few studies are available to understand the combined effect of water and elements like F, B, P and Li and to verify whether the effects of these elements on dry silicate

melt viscosity are also transferable to hydrous systems. The combined effect of H_2O and F on granitic melts was studied by Baker and Vaillancourt (1995) and Giordano et al. (2004). For the investigated conditions Baker and Vaillancourt (1995) concluded that, on a molar basis, fluorine has the same effect as water. Giordano et al. (2004) confirmed that water and fluorine can have additive effects on viscosity within a hydrous system, but at low combined concentrations, the effect of F compared to water is smaller. However, the individual influences of B and P in hydrous melts are not quantitatively determined yet. In this study we present the results of an experimental study on melt viscosity that allows us to discuss the individual influences of F, B and P in hydrous highly fractionated melts in the low and high temperature range.

B.3. Experimental methods

B.3.1. Starting materials

The composition of the starting glass (PEG3-base) was chosen to be representative of a highly fractionated melt, from which a pegmatite would crystallize. The molar concentrations of SiO_2, Al_2O_3, Na_2O and K_2O (~ 75.50 mol%, 13.17 mol%, 8.32 mol% and 3.01 mol%) were comparable to a composition previously investigated by Bartels et al. (2011) (composition PEG2). The PEG3-base glass composition was synthesized from a mixture of SiO_2, Al_2O_3, K_2CO_3 and Na_2CO_3 powder. This mixture was homogenized in an agate ball mill and fused for three hours at 1873 K in a platinum crucible placed in a 1 atm chamber furnace. To ensure homogeneity, the resulting glass was crushed and melted again for 4 hours at 1873 K.

Different amounts of F, B and P were added to the PEG3-base composition. For the fluorine-bearing starting glasses, a composition with a lower Al_2O_3 concentration than the PEG3-base composition was synthesized (two times melting at 1873 K, see above). In a second step, AlF_3 and Al_2O_3 were added to the glass powder in different proportions. Thus, two glasses with

similar molar proportions of SiO_2, Al_2O_3, Na_2O and K_2O but different F contents of 1.68 wt% (PEG3-F2) and 4.81 wt% (PEG3-F5) were synthesized. The nominal F-contents of the glasses were ~2.00 and ~6.00 wt%. Although fusion time was reduced to two hours the batches lost 0.32 and 1.19 wt% F, respectively.

For the boron- and phosphorus-bearing glasses, PEG3-B, PEG3-P2 and PEG3-P3, the PEG3-base compositions was doped with either H_3BO_3 or $NH_4H_2PO_4$ and homogenized in an agate ball mill. Afterwards the doped glass powders were fused twice at 1873 K for 3 hours in the case of the boron-bearing melt and for 2 hours in the case of the phosphorus-bearing melts.

The glass compositions were analysed by electron microprobe (at least 15 analyses on two or three glass pieces). The compositions of PEG3-base, PEG3-F2, PEG3-F5, PEG3-B, PEG3-P2 and PEG3-P3 together with the PEG2 composition from Bartels et al. (2011) are given in Table B.1. All glasses were found to be homogeneous (see standard deviations in Table B.1). The aluminium saturation index (A.S.I.: molar ratio Al/(Na + K)) varies between 1.11 and 1.19. The PEG2 composition has an A.S.I. of 1.23. However, when Li is taken into account, the composition PEG2 is peralkaline (Al/(Na + K + Li) = 0.92).

Table B.1 Composition of the starting glasses.

Oxides	PEG2 [wt%]		PEG3-base [wt%]		PEG3-F2 [wt%]		PEG3-F5 [wt%]		PEG3-P2 [wt%]		PEG3-P3 [wt%]		PEG3-B [wt%]	
SiO_2	59.73	(0.13)	68.01	(0.72)	66.02	(0.42)	64.79	(0.51)	66.57	(0.90)	65.55	(1.00)	67.42	(0.43)
Al_2O_3	19.75	(0.13)	20.14	(0.25)	20.01	(0.38)	19.45	(0.22)	19.38	(0.25)	19.51	(0.35)	19.66	(0.30)
Na_2O	7.25	(0.1)	7.73	(0.20)	8.11	(0.24)	7.93	(0.14)	7.35	(0.37)	7.37	(0.42)	7.47	(0.48)
K_2O	3.82	(0.02)	4.26	(0.05)	4.16	(0.07)	4.11	(0.08)	4.10	(0.07)	4.00	(0.07)	4.11	(0.06)
F	5.46	(0.01)			1.68	(0.25)	4.81	(0.28)						
P_2O_5	2.46	(0.21)							2.20	(0.32)	2.98	(0.11)		
Li_2O	1.68	(0.01)												
B_2O_3	2.75	(0.01)											0.93	(0.05)
2F = O	-2.3				-0.71		-2.03							
total	100.6		100.14		99.27		99.06		99.60		99.41		99.59	
A.S.I.	1.23		1.16		1.12		1.11		1.17		1.19		1.17	
A.S.I.Li	0.91													

Values are mean of at least 15 electron microprobe analyses

1σ standard deviation is given in parentheses

A.S.I. molar ratio of Al/(Na+K); $A.S.I._{Li}$ molar ratio of Al/(Na+K+Li)

Additionally PEG2 from Bartels et al., 2011 is shown.

B.3.2. Falling sphere method

The melt viscosity at high pressure and temperature was measured with the falling sphere method (e.g. Shaw 1963; Schulze et al., 1996; Holtz et al., 1999; Vetere et al., 2006) using the procedure described by Bartels et al. (2011). For each composition, glass cylinders with water contents ranging from 1 to 6 wt% were synthesized in an internally heated pressure vessel (IHPV) at 1373 K, 300 MPa and run durations from 17-22 h, except for PEG3-P2 with only one cylinder containing ~ 6 wt% water. All glasses were optically homogeneous and microscopically free of crystals and bubbles except for PEG3-base-1 and PEG3-base-3 in which some crystals were observed. These crystals were too small for microprobe analyses and were most likely aluminosilicates because of the excess of aluminium in the PEG3-base composition. In any case, the amount of crystals was so low (< 3 vol%) that it should not have affected the viscosity determination.

The falling sphere setup is composed by a large glass cylinder with a Pt-horizon as immobile marker on bottom and one or two noble metal spheres on top. The distance of the sphere(s) with respect to the marker is measured before and after the viscosity experiment to determine the settling distance for given heating time. Pt spheres with radii ranging from 83.5 to 150 μm and Pd spheres with radii ranging from 188 to 194 μm were used (Tab. B.1.A (appendix)). In samples PEG3-F5-1 and PEG3-B-6 two spheres were placed on top of the cylinder in distance of approx. 2 mm. This allows determining two viscosity values in a single experiment. The falling sphere experiments were performed in an IHPV in the temperature range of 1173 to 1530 K at pressures between 200 and 650 MPa. The heating rate was always 80 K/min. The experimental duration varied from 96 hours (PEG3-F5-1c) to 15 minutes (PEG3-base-6c and PEG3-F5-6b, uncorrected values) (Tab. B.1.A). Except for experiment PEG3-B-6d, the variation of temperature along the samples was less than 10 K. The measured variation in T within an experiment was included in the error calculation of the viscosity (Tab. B.2a). In the

case of sample PEG3-B-6d a temperature variation of approximately 20 K was observed, leading to a very high relative error for viscosity calculation of around 21%.

B.3.3. Micropenetration technique

The melt viscosity at low temperatures was measured using the micropenetration technique. Water-bearing samples were synthesized in an IHPV at the GZG (Geowissenschaftliches Zentrum der Universität Göttingen) at a temperature of 1473 K and pressures between 150 and 200 MPa. Heating was accomplished within 30 to 60 minutes and the experimental duration varied from 69 to 75 h. Dry glass cylinders were prepared at similar P- and T-conditions with run durations of 22 h. The water contents ranged from dry to approximately 4 wt%. After synthesis the samples were cut into 1mm thick slices and polished on both sides.

The micropenetration technique involves determining the rate of which a sapphire sphere (diameter of 1mm) under a fixed load moves into the sample surface (e.g. Webb et al., 2004). These measurements were conducted in a vertical dilatometer (Netzsch TMA 402) at the GZG. The sample is placed in a ceramic holder. The sapphire sphere is held in the middle of the sample by a ceramic rod which is connected to a weight pan. The metal connection of the ceramic rod and the weight pan acts as the core of a calibrated linear voltage displacement transducer (LVDT). After the whole setup is inserted into an electro furnace and brought to experimental temperature, a weight is placed onto the weight pan and the movement of the sphere into the sample is recorded by the LVDT. The temperature is measured by $Pt/Pt_{90}Rh_{10}$ thermocouples, which were calibrated against the melting temperatures of bismuth, zinc, aluminium and silver.

B.4. Analytical methods

B.4.1. Microprobe

The composition of starting glasses was measured using a Cameca SX-100 electron microprobe with 15 keV acceleration voltages, 4 nA beam current and a beam diameter of 20 µm. The counting time ranged from 4 to 30 s and the respective standards were albite (Na), wollastonite (Si), corundum (Al), orthoclase (K), SrF_2 (F) and apatite (P). The boron content was analysed by Actlabs/Canada by ICP-MS on samples fused with sodium peroxide.

Additional microprobe analyses of all phosphorous- and fluorine-bearing glasses were conducted after experiments to ensure that no compositional change occurred during experiments (in particular for samples PEG3-F2-6, PEG3-F5-3 and PEG3-P3-6 where a leakage was observed after the last experiment). The measured difference in composition is within the analytical error and the leakages probably occurred during the quench of experiments.

B.4.2. Karl-Fischer-Titration

The water contents of all synthesized hydrous glasses and the falling sphere samples after the final viscosity experiments were determined by pyrolysis and subsequent Karl-Fischer-Titration (KFT) (Behrens et al., 1996). An increment of 0.10 wt% was added to the measured values to account for an incomplete dehydration of the samples during the analysis (Leschik et al., 2004). To check for homogeneous distribution of H_2O, especially within the water-poor samples (PEG3-base-1, PEG3-F2-1, PEG3-F5-1, PEG3-B-1 and PEG3-P3-1), two analyses from both ends of the PEG3-B-1 cylinder were performed. The measured values do not significantly differ from each other and are within error of determination.

The difference between the pre- and post-experimental water contents in the falling sphere experiments was always within the error of analysis and therefore negligible (see Table B.2a).

The mean value of both measurements was used for calculating the molar values of H_2O (Table B.2a) and for modelling of viscosities.

For sample PEG3-F5-3 the water content was close to that in the starting glass, whereas for samples PEG3-F2-6 and PEG3-P3-6 a drop in water concentration was observed. Water contents of 3.99 and 3.76 wt%, were determined, which is lower by 1 and 2 wt%, respectively, compared to the starting glasses. Infrared (IR) spectra confirm these low water concentrations and show an inhomogeneous water distribution within the glasses, indicating water loss by leakage during experiment. The viscosity data of these two experiments are included in the following figures but were not used for the viscosity calculation models (see B.6.1.).

B.4.3. Infrared (IR) spectroscopy

IR spectroscopy was used to test the homogeneity of glasses, to identify possible water loss after falling sphere experiments and to determine the fraction of OH and molecular H_2O within the samples. Water concentrations were calculated by the Beer-Lambert-law using the peak heights of the H_2O and OH combination bands at 5200 cm^{-1} and 4500 cm^{-1} after subtraction of tangential baselines. Near infrared (NIR) spectra were recorded using a Bruker IFS88 FTIR spectrometer equipped with Mercury-Cadmium-Tellurium (MCT) narrow range detector, a tungsten lamp, a KBr beamsplitter and a Bruker IRscope II microscope.

The glass samples were prepared as two-sided polished thin sections with a thickness of around 300 µm. The thickness was measured using a digital Mitutoyo micrometer (precision ± 2 µm). For each spectrum 100 scans were collected with a spectral resolution of 2 cm^{-1}. The spot size was about 50 x 50 µm. For every sample, three to six spectra were collected starting at the rim of the sample to check for homogeneous distribution of the water. The densities of

the samples were determined by the Archimedean method with water and a droplet of tenside (Tween 80) per liter as immersion liquid.

For every composition the absorption coefficients ε of H_2O and OH were determined using samples with water contents from ~0.5 wt% to ~6 wt% water (determined by KFT). Assuming that no other hydrous species are present in the glass beside OH and H_2O ($C_{H_2O_t} = C_{H_2O} + C_{OH}$, where $C_{H_2O_t}$ refers to the total water content and C_{H_2O} and C_{OH} to water dissolved as molecular H_2O and OH groups, respectively) and that the ε values do not vary with water content, the ε values can be determined using plots of absorbances normalized by density ρ, thickness d and water content (Behrens et al., 1996):

$$\left[\frac{1802 \cdot A_{5200}}{d \cdot \rho \cdot c_{H_2O_t}}\right] = \varepsilon_{H_2O} - \frac{\varepsilon_{H_2O}}{\varepsilon_{OH}} \cdot \left[\frac{1802 \cdot A_{4500}}{d \cdot \rho \cdot c_{H_2O_t}}\right] \qquad [B.1]$$

where A_{5200} and A_{4500} are the absorbances of the bands at 4500 cm^{-1} and 5200 cm^{-1}, respectively, and ε_{H_2O} and ε_{OH} are the corresponding linear molar absorption coefficients. The molar absorption coefficients were determined by linear regression as the intercepts of the straight line with both axes (Fig. B.1). Whereas the composition PEG3-base has a similar ratio of $\varepsilon_{H_2O}/\varepsilon_{OH}$ of 1.1 as found in rhyolite and dacite (Withers and Behrens, 1999; Ohlhorst et al., 2001) when using the same spectra evaluation (i.e. tangential baselines), the ratio is larger for the F and B doped glasses indicating an increased excitation probability for H_2O compared to OH. The determined coefficients were used to calculate water contents of water-poor samples as well as of samples for which KFT measurements were not successful (for example due to explosion caused by rapid dehydration of samples during the KFT measurement (e.g. PEG3-base-4 (Table B.2a and B.2b, italic numbers)).

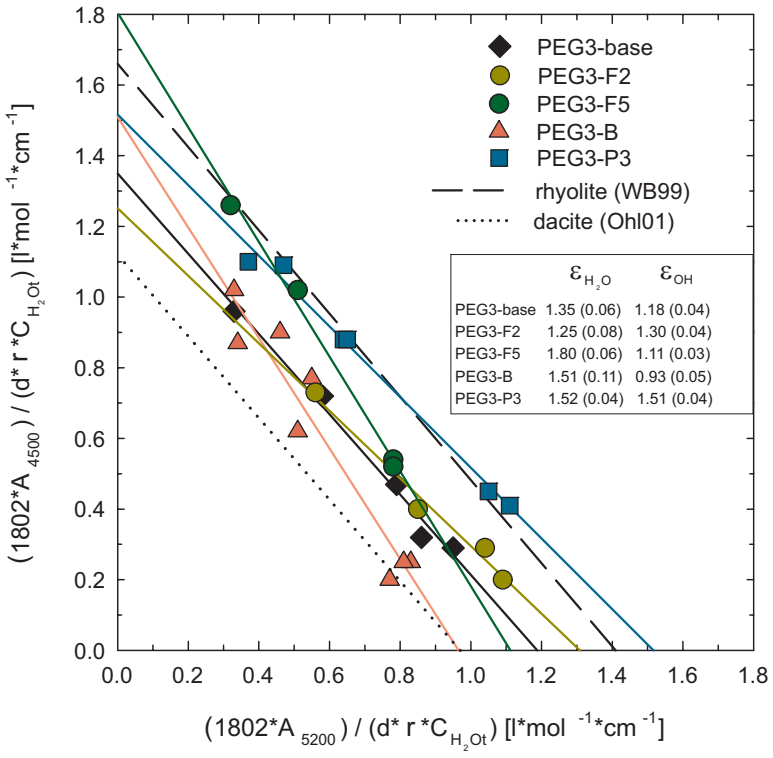

Figure B.1 Normalized absorbances of H_2O- and OH-bands for the investigated melt compositions. The dashed line represents rhyolitic data from Withers and Behrens, 1999 (WB99). The dotted line represents dacitic data from Ohlhorst et al., 2001 (Ohl01). Error bars are not shown for better clarity, max. error was ± 0.13 (l· mol^{-1}·cm^{-1})

Absorption coefficients ε_{OH} and ε_{H_2O} are given by the intercepts of the linear regression lines with the *x*- and *y*-axes, respectively. Values are given in (l·mol^{-1}·cm^{-1}). Errors take the uncertainty of the regression lines into account.

B.4.4. ^{11}B MAS NMR experiments

Magic angle spinning nuclear magnetic resonance (MAS NMR) analysis were performed at the Institute for Geology, Mineralogy and Geophysics at the Ruhr-Universität Bochum. All NMR spectra were recorded on a Bruker ASX 400 NMR spectrometer at room temperature. ^{11}B MAS NMR measurements were carried out at 128.38 MHz using a standard Bruker 4 mm MAS probe with sample spinning at 12.5 kHz. Solid $NaBH_4$ has been used as secondary reference standard (δ_{iso} = -42.0 ppm). For the ^{11}B MAS NMR experiments, short single pulse duration of 0.6 µs has been used to ensure homogenous excitation of the central and all

satellite transitions. A recycle delay of 1 s has been used, and 6000 scans have been accumulated. The ^{11}B MAS NMR spectra were fitted with quadrupolar lineshapes including convolution using the DmFit 2010 program (Massiot et al., 2002). Tolerances were estimated by varying the parameters in the fit function observing χ^2 until a distinct change of χ^2 took place.

B.5. Viscosity calculation

B.5.1. Falling sphere experiments

The viscosity values for falling-sphere experiments (Tab. B.2a) were calculated using the following modified Stokes law:

$$\eta = \frac{2 \cdot t \cdot g \cdot \Delta\rho \cdot r^2 \cdot C_F}{9 \cdot d} \qquad [B.2]$$

where d is the settling distance, t is the run duration, $\Delta\rho$ is the density difference between the sphere and the melt, g is the acceleration due to gravity (9.81 m/s^2), r is the radius of the sphere and C_F is the Faxen correction (Faxen, 1923) to account for the effect of viscous drag by the capsule wall on the settling sphere. The run duration, sphere radius, settling distance, calculated melt density (after Ochs and Lange, 1999) and temperature of the experiments is given in Table B.1.A. The Faxen correction is given by the equation:

$$C_F = 1 - 2.104\left(\frac{r}{R}\right) + 2.09\left(\frac{r}{R}\right)^3 - 0.95\left(\frac{r}{R}\right)^5 \qquad [B.3]$$

where r is the radius of the sphere and R is the inner radius of the capsule. For experiments where the dwell on target temperature was less than 2 hours a time correction was used to

account for sinking of the sphere during heating and cooling. This was done assuming a constant heating ramp of 80 K/min and a constant cooling rate of 120 K/min and using the following equation (Vetere et al., 2006):

$$t_{effective} = \int \exp\left[\frac{-E_a}{R}\left(\frac{1}{T(t)} - \frac{1}{T_{target}}\right)\right] \cdot dt \qquad [B.4]$$

E_a is the activation energy for viscous flow and R is the universal gas constant. A preliminary value of the activation energy was determined using viscosity data without time correction, i.e. using the experimental dwell at the target temperature and assuming an Arrhenian behaviour over the investigated temperature range. The values of t for experiments with run durations of less than 2 h given in Table B.1.A are already corrected using equation B.4.

The densities of melts at given P and T were calculated after Ochs and Lange (1999) and are listed in Table B.1.A. The model of Ochs and Lange (1999) had to be extended for the components F, B_2O_3 and P_2O_5 and the partial molar volumes for these elements were taken from Knoche et al. (1995).

Taking into account the uncertainties of temperature, falling distance, sphere radius, run duration and melt density the calculated total error of viscosity is always less than ± 15 %, except for sample PEG3-B-6d, for which the high temperature gradient was observed during experiment, the relative error is ± 21 %.

B.5.2. Micropenetration

The temperature, water content and viscosity of conducted micropenetration experiments are given in Table B.2b. The absolute shear viscosity of micropenetration experiments is determined by the following equation:

$$\eta = \frac{0.1875 \cdot F \cdot t}{\sqrt{r} \cdot \sqrt{l^3}} \qquad [B.5]$$

(Pocklington, 1940), where η is the viscosity, F the applied force given by the weight and the gravitational force, t the experimental duration, r the radius of the sphere and l the penetration depth. The uncertainty of the micropenetration apparatus was determined from measurements of a standard glass from the Deutsche Glastechnische Gesellschaft e.V. (DGG) to be 0.06 log units.

B.6. Experimental results

Table B.2a Experimental conditions and results for falling sphere experiments

experiment	H_2O [wt%]	H_2O^* [wt%]	[mol%]	F_2O_{-1} [mol%]	T [K]	P [Mpa]	*Log η* [η in Pa*s]
PEG3-base-1a	1.28 (0.08)		4.45		1479 (6)	200	4.03 (0.04)
PEG3-base-1b			4.45		1529 (6)	300	3.63 (0.04)
PEG3-base-1c		***1.19 (0.02)***	4.45		1430 (6)	200	4.21 (0.04)
PEG3-base-3a	2.63 (0.07)		9.10		1383 (10)	200	3.48 (0.07)
PEG3-base-3b			9.10		1474 (1)	300	2.95 (0.02)
PEG3-base-3c		n.d.	9.10		1269 (4)	300	4.23 (0.04)
PEG3-base-6a	6.14 (0.07)		19.54		1383 (5)	300	2.44 (0.03)
PEG3-base-6b			19.54		1278 (5)	300	2.77 (0.03)
PEG3-base-6c		6.15 (0.08)	19.54		1474 (1)	300	2.03 (0.04)
PEG3-F2-1a	1.16 (0.06)		4.12	2.80	1383 (10)	200	4.25 (0.06)
PEG3-F2-1b			4.12	2.80	1275 (2)	200	4.90 (0.03)
PEG3-F2-1c			4.12	2.80	1481 (8)	200	3.69 (0.05)
PEG3-F2-1d			4.12	2.80	1403 (10)	500	4.00 (0.06)
PEG3-F2-1e		1.18 (0.06)	4.12	2.80	1383 (10)	600	4.35 (0.07)
PEG3-F2-3a	3.07 (0.07)		10.32	2.62	1283 (10)	200	3.69 (0.07)
PEG3-F2-3b			10.32	2.62	1383 (10)	300	3.26 (0.06)
PEG3-F2-3c		n.d.	10.32	2.62	1481 (7)	300	2.59 (0.04)
PEG3-F2-6a	5.01 (0.07)		16.08	2.45	1372 (2)	300	2.33 (0.03)
PEG3-F2-6b			16.08	2.45	1278 (5)	300	2.75 (0.03)
PEG3-F2-6c		3.99 (0.08)[1)]	16.08	2.45	1176 (3)	300	3.15 (0.03)
PEG3-F5-1a	1.40 (0.06)		4.56	7.73	1271 (2)	200	4.10 (0.03)
PEG3-F5-1a			4.56	7.73	1271 (2)	200	4.15 (0.02)
PEG3-F5-1b			4.56	7.73	1373 (5)	200	3.48 (0.04)
PEG3-F5-1b			4.56	7.73	1373 (5)	200	3.56 (0.03)
PEG3-F5-1c			4.56	7.73	1223 (5)	200	4.41 (0.04)
PEG3-F5-1c			4.56	7.73	1223 (5)	200	4.43 (0.04)
PEG3-F5-1d			4.56	7.73	1473 (1)	200	3.08 (0.03)
PEG3-F5-1d		1.29 (0.08)	4.56	7.73	1473 (1)	200	3.09 (0.02)
PEG3-F5-3a	2.92 (0.07)		9.51	7.33	1265 (10)	200	3.24 (0.06)
PEG3-F5-3b		***2.65 (0.15)[1)]***	9.51	7.33	1178 (10)	200	3.72 (0.07)
PEG3-F5-6a	5.70 (0.06)		17.43	6.69	1179 (2)	200	2.91 (0.03)
PEG3-F5-6b			17.43	6.69	1368 (5)	300	2.06 (0.03)
PEG3-F5-6c		n.d.	17.43	6.69	1268 (10)	300	2.37 (0.06)
PEG3-B-1a	1.18 (0.06)		4.20		1375 (2)	200	4.58 (0.02)
PEG3-B-1b			4.20		1476 (3)	200	4.06 (0.02)
PEG3-B-1c			4.20		1426 (3)	200	4.29 (0.02)
PEG3-B-1d			4.20		1530 (6)	200	3.75 (0.03)
PEG3-B-1e		1.14 (0.10)	4.20		1403 (10)	500	4.41 (0.06)
PEG3-B-3a	3.28 (0.07)		10.68		1378 (2)	300	3.52 (0.02)
PEG3-B-3b			10.68		1269 (4)	300	3.98 (0.03)

continued

PEG3-B-3c			10.68	1478	(5)	300	2.95 (0.03)
PEG3-B-3d		2.92 (0.06)	10.68	1175	(2)	300	4.53 (0.03)
PEG3-B-6a	5.90 (0.07)		19.05	1378	(5)	300	2.49 (0.04)
PEG3-B-6a			19.05	1378	(5)	300	2.51 (0.03)
PEG3-B-6b			19.05	1276	(3)	300	2.92 (0.03)
PEG3-B-6b			19.05	1276	(3)	300	3.01 (0.02)
PEG3-B-6c			19.05	1173	(2)	300	3.56 (0.03)
PEG3-B-6c			19.05	1173	(2)	300	3.65 (0.02)
PEG3-B-6d			19.05	1343	(20)	300	2.81 (0.11)
PEG3-B-6d		5.94 (0.11)	19.05	1343	(20)	300	2.82 (0.1)
PEG3-P2-1a	1.38 (0.07)		4.48	1376	(3)	200	4.52 (0.02)
PEG3-P2-1b			4.48	1483	(10)	200	3.94 (0.05)
PEG3-P2-1c		0.98 (0.06)	4.48	1529	(6)	200	3.68 (0.03)
PEG3-P3-1a	0.97 (0.06)		3.47	1474	(1)	200	4.07 (0.02)
PEG3-P3-1b			3.47	1375	(2)	200	4.62 (0.02)
PEG3-P3-1c			3.47	1426	(3)	200	4.40 (0.02)
PEG3-P3-1d			3.47	1528	(5)	200	3.87 (0.03)
PEG3-P3-1e			3.47	1403	(10)	500	4.38 (0.06)
PEG3-P3-1f		0.90 (0.06)	3.47	1378	(5)	650	4.55 (0.04)
PEG3-P3-3a	2.63 (0.09)		9.13	1375	(2)	300	3.34 (0.02)
PEG3-P3-3b			9.13	1480	(8)	300	2.90 (0.05)
PEG3-P3-3c			9.13	1275	(2)	300	3.96 (0.02)
PEG3-P3-3d		2.54 (0.07)	9.13	1433	(10)	300	3.13 (0.05)
PEG3-P3-6a	5.81 (0.08)		18.96	1375	(2)	300	2.47 (0.03)
PEG3-P3-6b		3.76 (0.10)[1)]	18.96	1273	(2)	300	2.92 (0.03)

H_2O contents measured by KFT and IR (*italic*); H_2O* = water content after

experiments; mean value of both measurements was taken for calculation in mol% (calculation based on oxide components)

[1)] leak during experiment; n.d. = not determined

The error on T takes into account the temperature gradient along the sample and the temperature fluctuation over time.

Characters in the sample name refer to base composition (e.g. PEG3-base), the synthesized sample (1,2,3,4) and the order of subsequent experiments with the same sample (a,b,c,...).

Maximal uncertainties: T ± 10 K; P ± 3 MPa; density ± 0.01 g/cm^3; sphere radius ± 2 µm; distance ± 2 %; time ± 68 seconds; viscosity ± 15%

Table B.2b Experimental conditions and results for micropenetration experiments

experiment	H_2O [wt%]	[mol%]	F_2O_{-1} [mol%]	T [K]	*Log η* [η in Pa*s]
m PEG3-base-1a	1.08 (0.06)	3.89		901	10.25 (0.06)
m PEG3-base-1b	1.08 (0.06)	3.89		875	10.73 (0.06)
m PEG3-base-1c	1.08 (0.06)	3.89		849	11.11 (0.06)
m PEG3-base-1d	1.08 (0.06)	3.89		927	9.99 (0.06)
m PEG3-base-3a	3.10 (0.06)	10.60		777	9.94 (0.06)
m PEG3-base-3b	3.10 (0.06)	10.60		725	10.96 (0.06)
m PEG3-base-3c	3.10 (0.06)	10.60		694	11.76 (0.06)
m PEG3-base-4a	***4.05*** (0.06)	13.53		715	10.40 (0.06)
m PEG3-base-4b	***4.05*** (0.06)	13.53		689	11.10 (0.06)
m PEG3-base-4c	***4.05*** (0.06)	13.53		663	11.71 (0.06)
m PEG3-F2-0.5a	0.50 (0.06)	1.79	2.87	872	10.60 (0.06)
m PEG3-F2-0.5b	0.50 (0.06)	1.79	2.87	842	11.28 (0.06)
m PEG3-F2-0.5c	0.50 (0.06)	1.79	2.87	822	11.58 (0.06)
m PEG3-F2-0.5d	0.50 (0.06)	1.79	2.87	902	10.08 (0.06)
m PEG3-F2-0.5e	0.50 (0.06)	1.79	2.87	802	11.82 (0.06)
m PEG3-F2-1a	0.88 (0.06)	3.13	2.83	826	10.79 (0.06)
m PEG3-F2-1b	0.88 (0.06)	3.13	2.83	805	11.30 (0.06)
m PEG3-F2-1c	0.88 (0.06)	3.13	2.83	784	11.76 (0.06)
m PEG3-F2-1d	0.88 (0.06)	3.13	2.83	847	10.41 (0.06)
m PEG3-F2-1e	0.88 (0.06)	3.13	2.83	868	9.95 (0.06)
m PEG3-F2-3a	3.15 (0.07)	10.57	2.61	704	10.30 (0.06)
m PEG3-F2-3b	3.15 (0.07)	10.57	2.61	684	10.86 (0.06)
m PEG3-F2-3c	3.15 (0.07)	10.57	2.61	664	11.30 (0.06)
m PEG3-F2-3d	3.15 (0.07)	10.57	2.61	644	11.96 (0.06)

continued

m	PEG3-F2-3e	3.15	(0.07)	10.57	2.61	724	9.93	(0.06)
m	PEG3-F5-Da	***0.21***	(0.01)	0.73	8.04	873	9.75	(0.06)
m	PEG3-F5-Db	***0.21***	(0.01)	0.73	8.04	835	10.46	(0.06)
m	PEG3-F5-Dc	***0.21***	(0.01)	0.73	8.04	806	11.05	(0.06)
m	PEG3-F5-Dd	***0.21***	(0.01)	0.73	8.04	787	11.49	(0.06)
m	PEG3-F5-De	***0.21***	(0.01)	0.73	8.04	768	11.87	(0.06)
m	PEG3-F5-1a	1.35	(0.08)	4.56	7.73	709	10.77	(0.06)
m	PEG3-F5-1b	1.35	(0.08)	4.56	7.73	694	11.23	(0.06)
m	PEG3-F5-1c	1.35	(0.08)	4.56	7.73	683	11.48	(0.06)
m	PEG3-F5-1d	1.35	(0.08)	4.56	7.73	678	11.58	(0.06)
m	PEG3-F5-1e	1.35	(0.08)	4.56	7.73	658	12.23	(0.06)
m	PEG3-F5-1f	1.28	(0.07)	4.33	7.75	730	10.33	(0.06)
m	PEG3-F5-1g	1.28	(0.07)	4.33	7.75	701	11.01	(0.06)
m	PEG3-F5-1h	1.28	(0.07)	4.33	7.75	682	11.49	(0.06)
m	PEG3-F5-1k	1.28	(0.07)	4.33	7.75	663	12.09	(0.06)
m	PEG3-F5-3a	3.23	(0.07)	10.44	7.25	653	10.10	(0.06)
m	PEG3-F5-3b	3.23	(0.07)	10.44	7.25	625	10.82	(0.06)
m	PEG3-F5-3c	3.23	(0.07)	10.44	7.25	605	11.40	(0.06)
m	PEG3-F5-3d	3.23	(0.07)	10.44	7.25	586	12.01	(0.06)
m	PEG3-B-1a	1.08	(0.07)	3.92		886	10.47	(0.06)
m	PEG3-B-1b	1.08	(0.07)	3.92		860	10.97	(0.06)
m	PEG3-B-1c	1.08	(0.07)	3.92		797	12.25	(0.06)
m	PEG3-B-1d	1.08	(0.07)	3.92		829	11.67	(0.06)
m	PEG3-B-3a	2.92	(0.07)	10.11		751	10.17	(0.06)
m	PEG3-B-3b	2.92	(0.07)	10.11		725	10.75	(0.06)
m	PEG3-B-3c	2.92	(0.07)	10.11		699	11.47	(0.06)
m	PEG3-B-3d	2.92	(0.07)	10.11		673	12.37	(0.06)
m	PEG3-B-4a	3.88	(0.1)	13.12		684	11.00	(0.06)
m	PEG3-B-4b	3.88	(0.1)	13.12		673	11.83	(0.06)
m	PEG3-B-4c	3.88	(0.1)	13.12		656	12.30	(0.06)
m	PEG3-P2-1a	1.08	(0.06)	4.12		849	11.19	(0.06)
m	PEG3-P2-1b	1.08	(0.06)	4.12		875	10.76	(0.06)
m	PEG3-P2-1c	1.08	(0.06)	4.12		901	10.27	(0.06)
m	PEG3-P2-3a	2.94	(0.07)	10.47		751	10.45	(0.06)
m	PEG3-P2-3b	2.94	(0.07)	10.47		777	10.01	(0.06)
m	PEG3-P2-3c	2.94	(0.07)	10.47		725	11.17	(0.06)
m	PEG3-P3-Da	***0.08***	(0.01)	0.30		1124	10.28	(0.06)
m	PEG3-P3-Db	***0.08***	(0.01)	0.30		1109	10.62	(0.06)
m	PEG3-P3-Dc	***0.08***	(0.01)	0.30		1093	10.91	(0.06)
m	PEG3-P3-Dd	***0.08***	(0.01)	0.30		1067	11.38	(0.06)
m	PEG3-P3-1a	1.11	(0.06)	4.08		798	11.98	(0.06)
m	PEG3-P3-1b	1.11	(0.06)	4.08		823	11.43	(0.06)
m	PEG3-P3-1c	1.11	(0.06)	4.08		829	11.24	(0.06)
m	PEG3-P3-1d	1.11	(0.06)	4.08		860	10.58	(0.06)
m	PEG3-P3-1e	1.11	(0.06)	4.08		880	10.27	(0.06)
m	PEG3-P3-3a	2.86	(0.08)	10.04		772	10.27	(0.06)
m	PEG3-P3-3b	2.86	(0.08)	10.04		746	10.64	(0.06)
m	PEG3-P3-3c	2.86	(0.08)	10.04		725	11.26	(0.06)
m	PEG3-P3-4a	4.07	(0.09)	13.86		694	11.05	(0.06)
m	PEG3-P3-4b	4.07	(0.09)	13.86		678	11.36	(0.06)
m	PEG3-P3-4c	4.07	(0.09)	13.86		668	11.73	(0.06)
m	PEG3-P3-4d	4.07	(0.09)	13.86		709	10.60	(0.06)

Characters in the sample name refer to micropenetration technique (m), base composition (e.g. PEG3-base), the synthesized sample (1,2,3,4) and the order of subsequent experiments with the same sample (a,b,c,...).

H_2O contents measured by KFT and IR (*italic*)

B.6.1. Temperature effect on viscosity

Figures B.2a to B.2e show plots of viscosity (expressed as log η) versus temperature (expressed as 10^4/T) for different water contents and for compositions PEG3-base, PEG3-F2, PEG3-F5, PEG3-B and PEG3-P3.

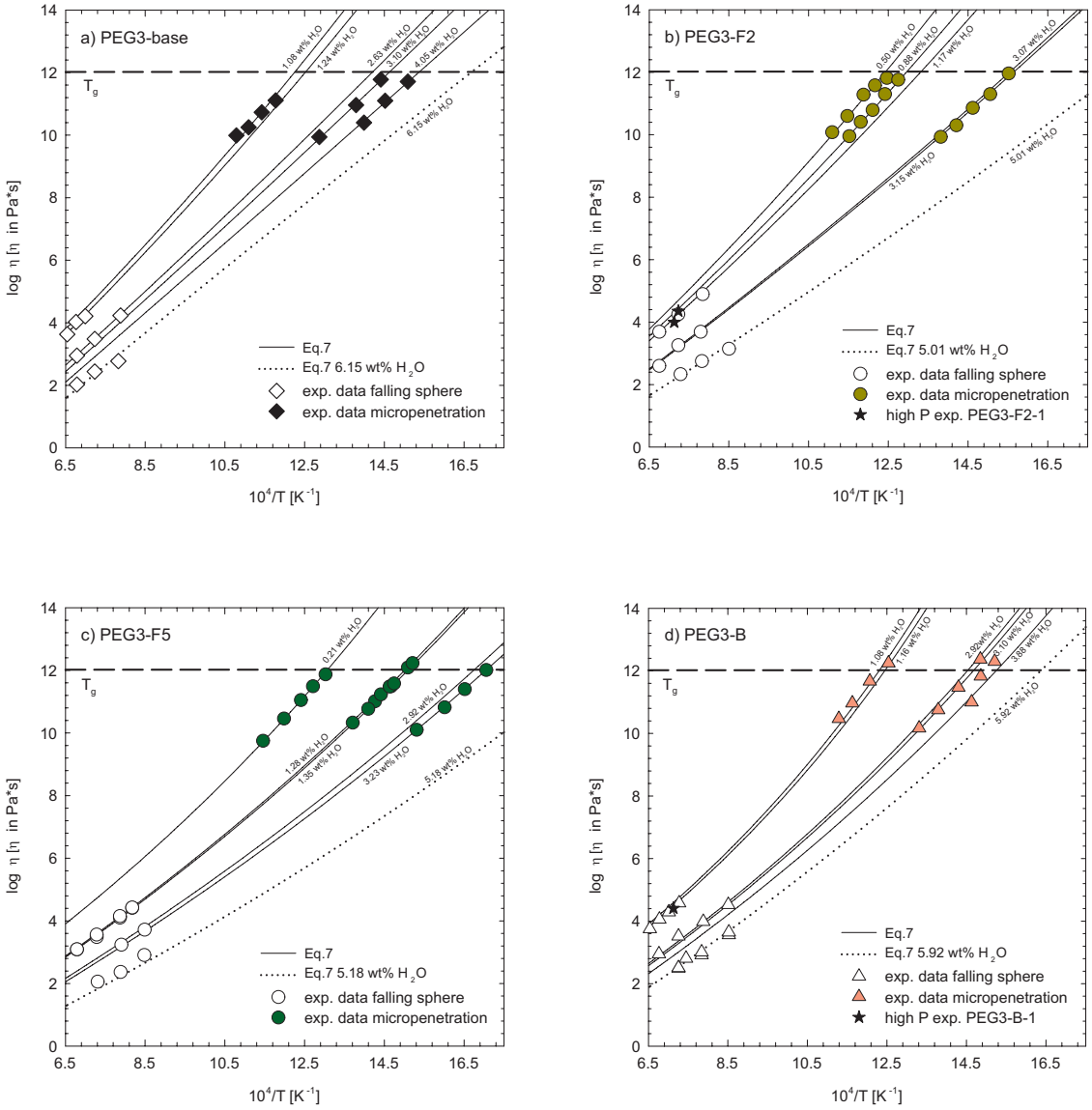

Figure B.2a-B.2e Viscosity data for the investigated melt compositions. S*ymbols* correspond to experimental data obtained using the falling sphere method (*open symbols)* and the micropenetration technique (*filled symbols*). *Stars* in Fig. B.2b, B.2d and B.2e represent experimental data from high pressure experiments (≥ 500 MPa). *Solid lines* represent the best fit of viscosity values for given water contents calculated using Eq. B.7 and the fitting parameters for each composition (Table B.4). The fitting of experimental data for high water contents using Eq. B.7 is extrapolated in the high viscosity range and is marked by the d*otted lines*.

In the low viscosity range, the measured viscosity ranges from $7.9 \cdot 10^4$ Pa·s (for PEG3-F2 at 1273 K and 1.17 wt% H_2O) to 106 Pa·s (for PEG3-base at 1474 K and 5.61 wt% H_2O). In the high viscosity range, values between $2.3 \cdot 10^{12}$ Pa·s (for PEG3-B at 673 K and 2.92 wt% H_2O) to $5.6 \cdot 10^9$ Pa·s (for PEG3-F5 at 873 K and 0.21 wt% H_2O) were determined. For all compositions the viscosity decreases with increasing temperature. This decrease is more pronounced for low water contents (compare fitting curves of the samples with ~1 wt% water and ~6 wt% water in Figs. B.2a-B.2e) and also low temperatures (compare fitting curves in the low temperature range with curves in the high temperature range, Figs. B.2a-B.2e).

To calculate the activation energy for viscous flow the single datasets of all compositions in the low and high temperature ranges were fitted separately by linear regression using the following Arrhenian equation:

$$\log \eta = \log \eta_0 + \frac{E_a}{2.303 \cdot R \cdot T} \qquad [B.6]$$

where η_0 is the pre-exponential factor, E_a the activation energy (kJ/mol) of the viscous flow, 2.303 is the conversion factor of ln to log, R the gas constant ($J \cdot mol^{-1} \cdot K^{-1}$) and T the temperature (K). Although this approach is proved to be invalid over a wide temperature range (e.g. Richet and Bottinga, 1995; Hess et al., 1995; Richet et al., 1996; Giordano et al., 2000; Whittington et al., 2000, 2001; Romano et al., 2003; Giordano and Dingwell, 2003) it is useful for comparison with studies of other authors within a limited temperature range. The calculated values for $log\ \eta_0$ and E_a are given in Table B.3. In the high temperature range E_a´s strongly decrease with increasing water content for all compositions and tend to converge to a value between 120 and 150 kJ/mol at water contents >15 mol% (in this study mol% refers to oxide components except for calculations by the Hui and Zhang (2007) model) (Fig. B.3a). This dependence on water is in good agreement with previous studies on natural and synthetic

melt compositions (Dingwell, 1987; Persikov, 1991; Schulze et al., 1996; Holtz et al., 1999; Romano et al., 2001; Romano et al., 2003). In the low temperature range a similar trend is observable but E_a´s are typically larger in this range (Fig. B.3b).

Table B.3 Activation energies and pre-exponential coefficients for viscosity

	sample	H_2O [wt%]	*T* range [K]	E_a [kJ/mol]	Log η_0 [η in Pa*s]	
	PEG3-base-1	1.24	1430-1529	243 (55)	-4.64	(1.94)
	PEG3-base-3	2.63	1269-1474	224 (3)	-4.99	(0.10)
	PEG3-base-6	6.15	1278-1474	136 (20)	-2.76	(0.76)
	PEG3-F2-1	1.17	1275-1481	211 (7)	-3.75	(0.25)
	PEG3-F2-3	3.07	1283-1481	201 (35)	-4.43	(1.33)
	PEG3-F2-6	5.01	1176-1372	128 (11)	-2.51	(0.44)
	PEG3-F5-1	1.35	1223-1473	186 (4)	-3.51	(0.16)
	PEG3-F5-3	2.92	1178-1265	n.d.	n.d.	
	PEG3-F5-6	5.70	1179-1368	139 (21)	-3.29	(0.85)
	PEG3-B-1	1.16	1375-1530	212 (7)	-3.48	(0.27)
	PEG3-B-3	3.10	1175-1478	169 (10)	-2.97	(0.42)
	PEG3-B-6	5.92	1173-1378	156 (12)	-3.36	(0.49)
	PEG3-P2-1	1.18	1376-1529	218 (5)	-3.75	(0.19)
	PEG3-P3-1	0.94	1375-1528	205 (15)	-3.16	(0.56)
	PEG3-P3-3	2.58	1275-1480	185 (10)	-3.63	(0.38)
	PEG3-P3-6	5.81	1273-1375	n.d.	n.d.	
m	PEG3-base-1a	1.08	849-927	224 (15)	-2.66	(0.87)
m	PEG3-base-3a	3.10	694-777	225 (10)	-5.22	(0.68)
m	PEG3-base-4a	4.05	663-715	228 (14)	-6.22	(1.05)
m	PEG3-F2-0.5a	0.50	802-902	251 (18)	-4.39	(1.11)
m	PEG3-F2-1a	0.88	784-868	282 (6)	-7.03	(0.36)
m	PEG3-F2-3a	3.15	644-724	228 (9)	-6.56	(0.66)
m	PEG3-F5-Da	0.21	768-873	261 (3)	-5.89	(0.22)
m	PEG3-F5-1a	1.35	658-709	248 (8)	-7.45	(0.58)
m	PEG3-F5-1f	1.28	663-730	242 (7)	-7.02	(0.51)
m	PEG3-F5-3a	3.23	586-653	210 (4)	-6.71	(0.35)
m	PEG3-B-1a	1.08	797-886	275 (10)	-5.75	(0.65)
m	PEG3-B-3a	2.92	673-751	274 (13)	-8.92	(0.96)
m	PEG3-B-4a	3.88	656-684	415 (118)	-20.59	(9.20)
m	PEG3-P2-1a	1.08	849-901	260 (14)	-4.77	(0.84)
m	PEG3-P2-3b	2.94	725-777	242 (29)	-6.28	(1.99)
m	PEG3-P3-Da	0.08	1067-1124	438 (18)	-10.05	(0.85)
m	PEG3-P3-1a	1.11	798-880	283 (10)	-6.55	(0.65)
m	PEG3-P3-3a	2.86	725-772	225 (43)	-5.00	(3.03)
m	PEG3-P3-4a	4.07	668-709	238 (16)	-6.93	(1.22)

n.d. = not determined because only 2 viscosity values were measured; mPEG3-B-4a is not included in figure B.3b because of a very high error.

1σ standard deviation is given in parentheses.

errors given in bracket are taken into account the uncertainty of regression lines

Nevertheless the difference in activation energy in the different temperature ranges is smaller than expected. Additionally, the E_a for the fluorine-bearing melts seem to be lower compared

to the fluorine-free melts. The errors for the activation energy were calculated taking into account the uncertainties of the regression lines.

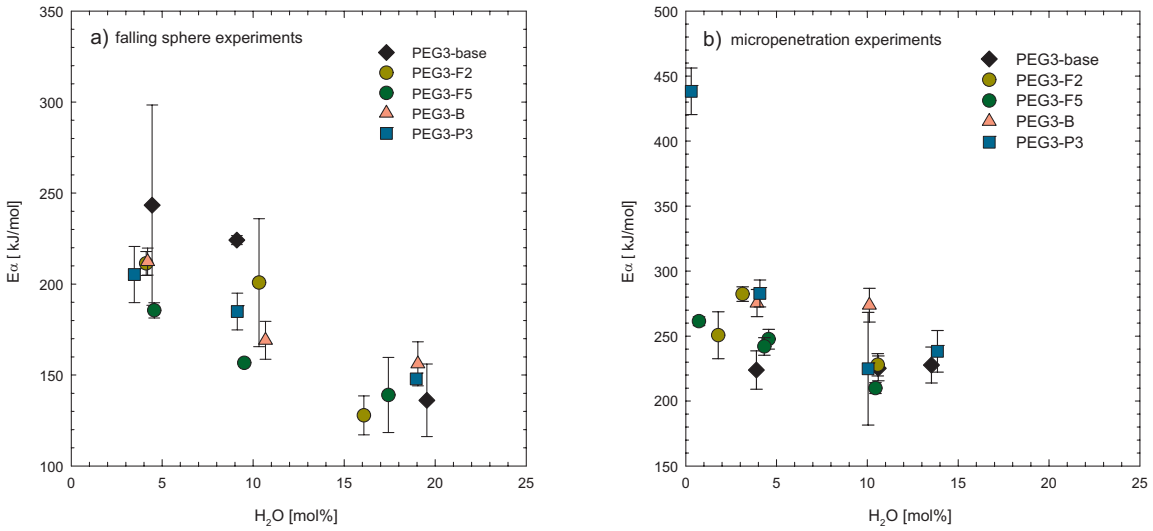

Figure B.3 Activation energies for viscosity as a function of water content calculated for each composition in the high (a) and low (b) temperature range. Arrhenian behaviour was assumed for both. Error bars account for uncertainty in the regressions.

Within the total investigated temperature range of this study the viscosity data for each composition can be described by the following modified Tamann-Vogel-Fulcher equation (Romano et al., 2003):

$$\log\eta = a_1 + a_2 \ln w_{H_2O} + \frac{b_1 + b_2 w_{H_2O}}{T - \left(c_1 + c_2 \ln w_{H_2O}\right)} \qquad [B.7]$$

where η is the viscosity, a_1 a_2 b_1 b_2 c_1 *and* c_2 are fitting parameters and w the water content in wt%. The results of the fitting parameters for each composition are given in Table B.4. Strictly, this type of equation is only valid above T_g (glass transition temperature) since the Tamann-Vogel-Fulcher model shows significant deviation from experimental data below T_g (Scholze, 1988). T_g values, defined by a viscosity of 10^{12} Pa·s, are indicated by dashed lines in

Figures B.2a-B.2e. However, the few data slightly above 10^{12} Pa·s do not significantly deviate from predicted trends and have also been considered. The accuracy of the fitting curves can be evaluated by comparing the calculated and experimentally determined viscosity values. Considering the whole dataset, the experimental data are reproduced within an error of ±8 % except for experiment PEG3-F5-6b for which there is an error of ±11 %.

Table B.4 Fitting parameters for Eq. B.7

fitting parameters	PEG3-base	PEG3-F2	PEG3-F5	PEG3-B	PEG3-P3
a	-3.86	-3.49	-2.21	-1.55	-3.03
b	-0.8	0.1	-0.3	-0.9	-0.5
c	10845.6	10476.5	7469.1	6663.3	8916.3
d	-2.0	-632.1	-313.1	81.2	-173.9
e	143.1	127.5	179.2	325.3	226.4
g	-92.5824	-34.8103	-30.3376	-103.0312	-64.0286
Standard deviation	0.12	0.09	0.05	0.17	0.09

B.6.2. Pressure effect on viscosity

A set of experiments was conducted to test the influence of pressure on the viscosity of selected melt compositions. The samples PEG3-F2-1, PEG3-B-1 and PEG3-P3-1 containing ~1 wt% H_2O were studied at temperature of approximately 1373K in the pressure range 200 - 650 MPa. Figures B.2b, B.2d and B.2e and Table B.2a show good agreement between high pressure data (star symbols) and low pressure data, indicating that pressure does not have a significant effect in this pressure-range. This result is consistent with previous investigations of Schulze et al. (1996) on haplogranitic melt compositions. Therefore, we consider that the results obtained by the micropenetration technique (P = 0.1 MPa) and the falling sphere method (P = 200 - 650 MPa) can be directly compared without adding a pressure dependence term.

B.6.3. Effect of melt composition

The fitting curves are used to discuss the effect of melt composition on viscosity of pegmatite forming melts. Because of the lack of experimental data in the high viscosity range, samples with high water contents (~ 6 wt% H_2O) were extrapolated towards low temperature for rough estimate of viscosities at these conditions (dotted lines in Figs. B.2a-B.2e) but are not included in the following discussion.

B.6.3.1. Comparison of PEG3-base with granitic and pegmatitic compositions

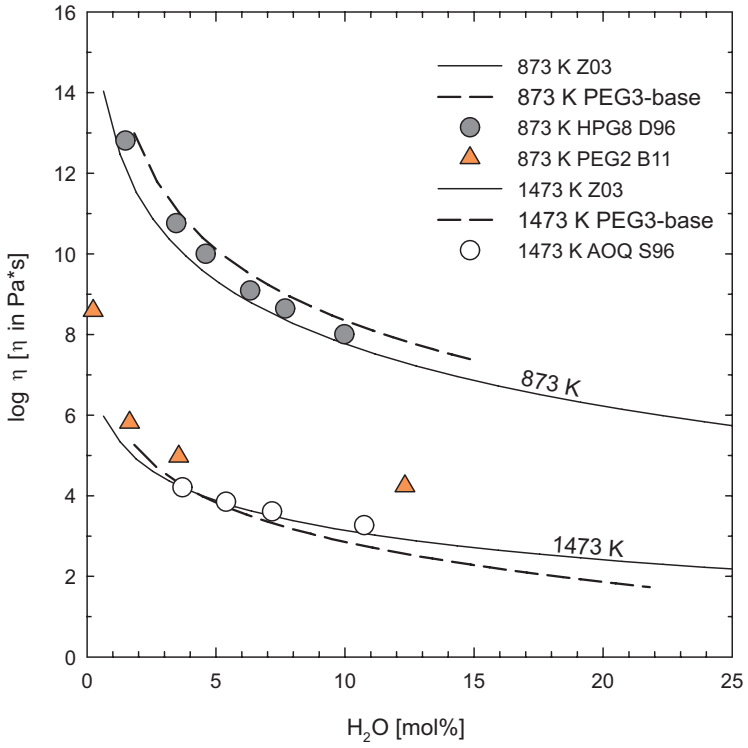

Figure B.4 Calculated viscosity isotherms for PEG3-base using Eq. B.7 in comparison with other rhyolitic and pegmatitic melt compositions at 873 K (*filled symbols*) and 1473 K (*open symbols*). Note the lower viscosity of PEG2 when compared to PEG3-base and HPG8. Z03: calculated viscosity values for granitic melts using the model from Zhang et al., 2003; D96: haplogranite melt HPG8, experimental data of Dingwell et al., 1996; S96: haplogranite melt AOQ, experimental data of Schulze et al. 1996; B11: Li-bearing pegmatite PEG2, experimental data of Bartels et al., 2011

Figure B.4 shows a plot of viscosity versus water content (mol% on oxide basis) for melt PEG3-base at temperatures of 873 and 1473 K. As expected, for both temperatures the viscosity decreases with increasing water content. Additionally the 873 K data for melt composition HPG8 from Dingwell et al. (1996a), the F-, B-, P- and Li-bearing melt PEG2 from Bartels et al. (2011) and the 1473 K data for melt composition AOQ from Schulze et al. (1996) are plotted together with the predictions of the viscosity model of Zhang et al. (2003). Viscosities of PEG3-base are almost identical with those of HPG8 and AOQ, and are well represented by the Zhang et al. model at both investigated temperatures, although PEG3-base is depleted in silica compared to the other systems. Comparing the viscosity of these melts with that of PEG2, two main observations can be made:

1.) The subtraction of F, B, P and Li from a pegmatite forming melt composition causes a significant increase of the viscosity by about 2.5 orders of magnitude at high water contents, and the difference is even larger at low water contents.

2.) The dependence on water content is more pronounced at low water content but less pronounced at high water content for the flux-containing melt PEG2 than for haplogranitic melts (HPG8, PEG3-base).

B.6.3.2. Influence of Fluorine

Figures B.5a and B.5b show the viscosities for PEG3-base and the F-bearing melts, calculated for 873 and 1473K, against the total molar content of $H_2O + F_2O_{-1}$. This term takes into account that two fluorine ions are exchanged for one oxygen ion within the silicate network. These figures show that the addition of fluorine and water to the melt is less efficient in reducing melt viscosity than the addition of water only. However, the more water is added to the F-bearing melt, the more the viscosity tends to converge to that of the hydrous PEG3-base composition, consistent with findings of Giordano et al. (2004) for haplogranitic melts.

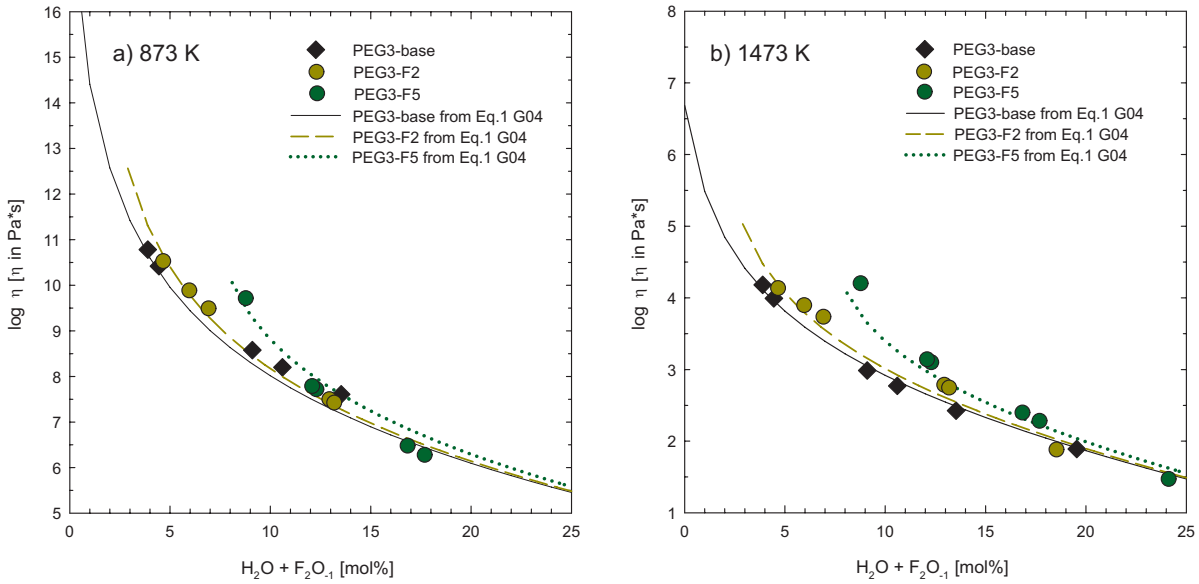

Figure B.5 Isothermal viscosities for 873 K (a) and 1473 K (b) for melt compositions PEG3-base, PEG3-F2 and PEG3-F5 calculated using Eq. B.7 as a function of water and fluorine content (expressed as molar sum of $H_2O+F_2O_{-1}$). *Lines*: calculated viscosities using the model of Giordano et al., 2004 (G04).

B.6.3.3. Influence of boron and phosphorus

Figure B.6 shows the effect of water on the viscosity of PEG3-base and PEG3-B with 0.93 wt% B_2O_3 at 873 and 1473 K. For comparison, the viscosity of HPG8, HPG8B5 and HPG8B10 containing 0.00, 4.35 and 8.92 wt% B_2O_3, respectively, from Dingwell et al. (1992, 1996a) are plotted. For the boron-bearing compositions only nominally dry melts were studied by Dingwell et al. (1992). The viscosity for the boron-free sample HPG8 is similar to that of the PEG3-base composition. At 873 K the addition of 4.35 wt% B_2O_3 to anhydrous HPG8 lowers melt viscosity by almost 4.5 log units (Dingwell et al. 1992) whereas for water-bearing melts of the present study, no significant influence of B_2O_3 content is observed (Fig. B.6).

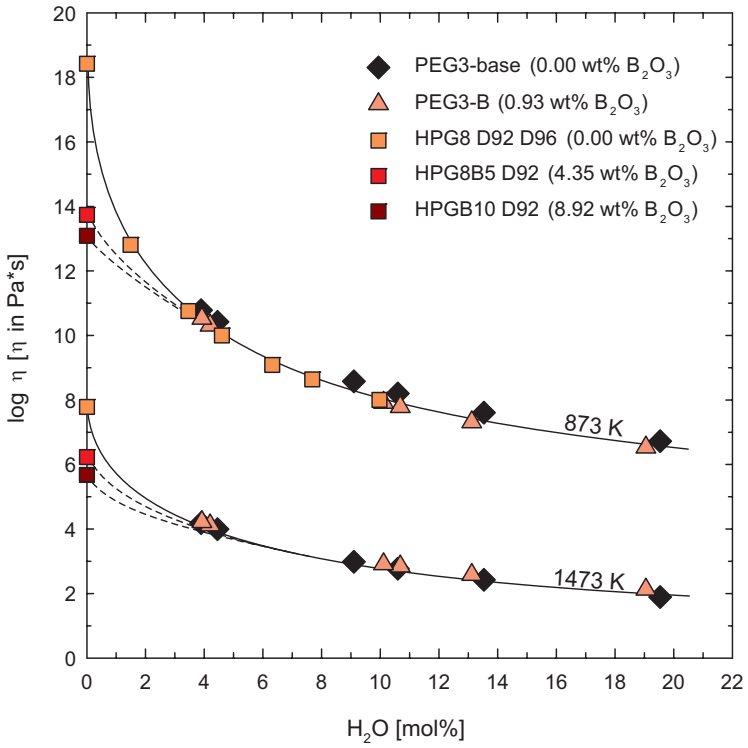

Table B.6 Influence of boron on the viscosity of melts as a function of water content for 873 and 1473 K. D92 and D96: experimental data of melts containing 0.00, 4.35 and 8.92 wt% B_2O_3 from Dingwell et al., 1992 and Dingwell et al., 1996. *Solid lines*: trends for boron-free melts (HPG8 and PEG3-base). *Dashed lines*: trend for boron-bearing melts (HPG8B5, HPG8B10, PEG3-B).

Speciation of boron in our glasses was studied by ^{11}B NMR spectroscopy to clarify its structural role in the melt. The NMR data show that BO_3 groups are the dominant species, producing a broad quadrupolar pattern due to quadrupolar interaction of second-order (Fig. B.7a) in all samples of PEG3-B. No tetrahedral coordinated boron could be identified within error of analysis. Additional measurements on the F-, B-, P- and Li-bearing PEG2 composition show a second minor Lorentzian resonance located around 0 ppm (Fig. B.7b), representing a small fraction of BO_4. This fraction of BO_4, determined by fitting the spectra and comparing the respective areas of the signals of both species, slightly increases with water content from 9.4 % at 0.07 wt% H_2O to 13.2% at 9.02 wt% H_2O.

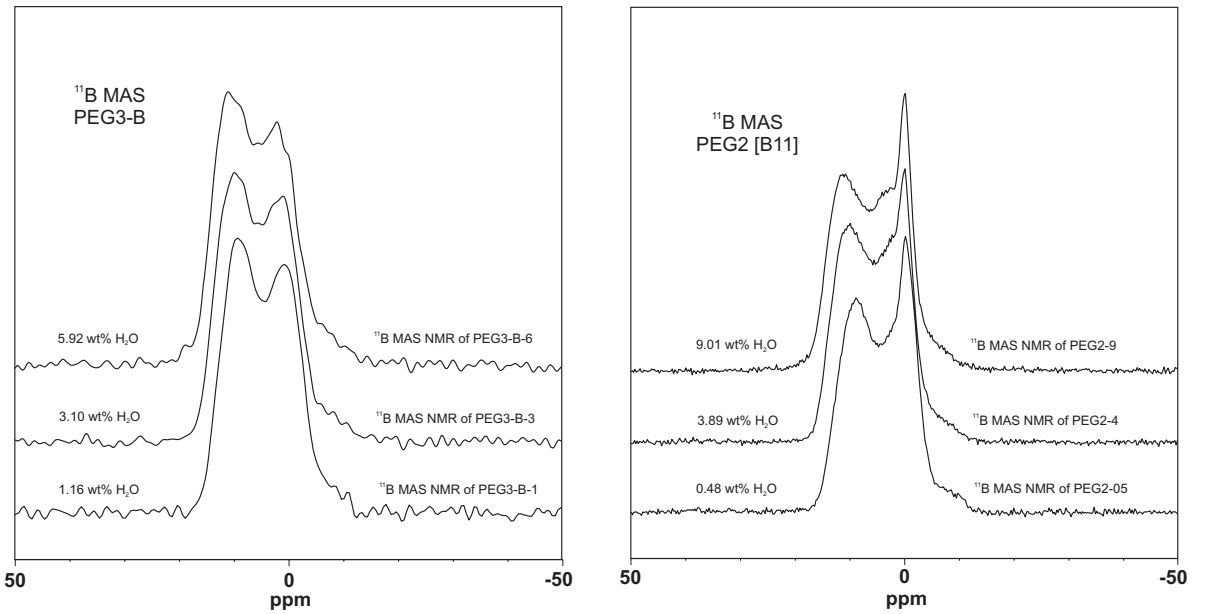

Figure B.7 (a) NMR spectra of hydrous PEG3-B glasses containing 0.93 wt% % B_2O_3. For conditions of acquisition, see text. The two peaks at ~10 and ~0 ppm are attributed to trigonal coordinated boron. (b) NMR spectra of hydrous PEG2 glasses containing 2.75 wt% % B_2O_3 synthesized by Bartels et al., 2011. The sharp peak at 0 ppm is attributed to tetrahedrall coordinated boron.

In Figure B.8, the viscosity for PEG3-base, PEG3-P2 (2.20 wt% P_2O_5) and PEG3-P3 (2.98 wt% P_2O_5) are compared to literature data for different water contents at 873 and 1473 K. In the anhydrous haplogranitic system, investigated by Dingwell et al. (1993), the addition of phosphorus has a small decreasing effect on melt viscosity. In contrast, the experimental data of the present study indicate that at high H_2O concentrations the effect of phosphorus disappears.

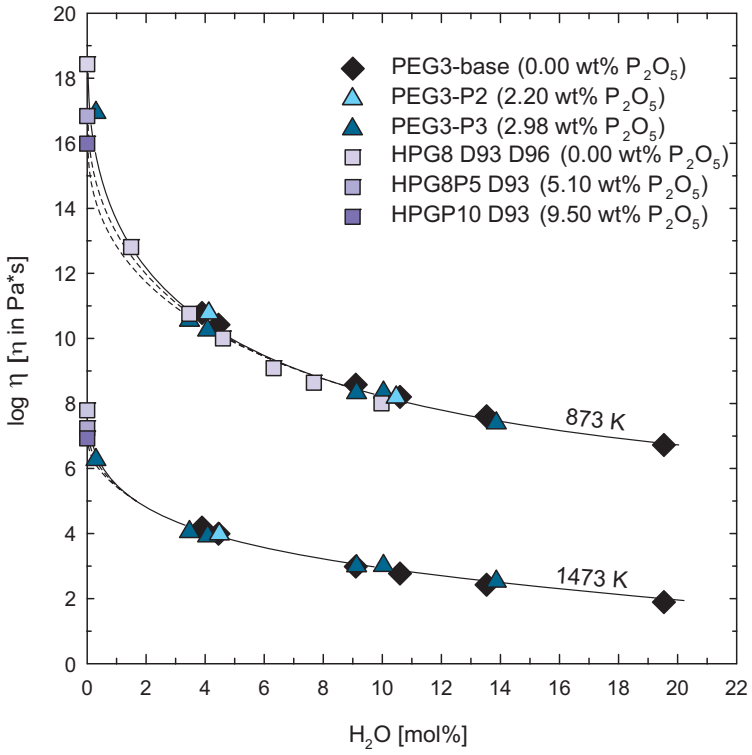

Figure B.8 Influence of phosphorus on the viscosity of melts in dependence to water content for 873 and 1473 K. D93 and D96: experimental data in melts containing 0.00, 5.10 and 9.50 wt% P_2O_5 from Dingwell et al., 1993 and Dingwell et al., 1996. *Solid lines*: trends for phosphorus-free melts (HPG8 and PEG3-base). *Dashed lines*: trend for phosphorus -bearing melts (HPG8P5, HPG8P10, PEG3-P).

B.7. Discussion

B.7.1. Speciation of water

The speciation of water as measured with IR is representing the ratio of molecular OH and H_2O at a fictive glass transition temperature (T_f), which is the temperature at which the frozen distribution of hydrous species corresponds to the equilibrium speciation in the melt (Behrens and Nowak, 2003). According to Scherer (1984) T_f can be defined for a given quench rate q by the relationship $\log \eta = 11.3 - \log |q|$, provided that the viscosity in function of temperature is known in the range of glass transition. The cooling rate after synthesis or viscosity experiments in the IHPV was typically 3.3 K/s corresponding to a viscosity of $10^{10.78}$ Pa·s at

T_f. Using Eq. B.7 the fictive temperatures for the different melt compositions were calculated. The equilibrium constant for water speciation (K) is defined as

$$K = \frac{(OH)^2}{(H_2O)\cdot(O)} \qquad [B.8]$$

where parentheses represent the molar fractions of species on a single oxygen basis. As shown in Figure B.9 *lnK* values for the PEG3-base composition are similar to those for haplogranitic and rhyolitic composition (Zhang et al., 1997; Nowak and Behrens, 2001; Behrens and Nowak, 2003). The addition of boron and fluorine to the melts increases the equilibrium constant by ~0.5 log units, indicating that both elements promote the dissociation of water within the silicate melt. This observation could explain the increased solubility of water in a haplogranitic system with increasing boron and fluorine content reported by Holtz et al. (1993). The observation of new hydroxyl-related bands in NIR spectra of hydrous boro-alumino-silicate melts by Schmidt et al. (2004a) is consistent with this interpretation. In contrary, the addition of phosphorus to the PEG3-base composition lowers *lnK* values by ~ 0.5 log units, i.e. the formation of OH^- groups is depressed in the phosphorus-bearing melt.

Despite of the variation in the relative abundance of OH^- groups, the viscosity does not significantly differ between PEG3-base, PEG3-B and PEG3-P at a given temperature and water content. The differences in OH^- concentrations are large only at high water contents where the dependence of viscosity on water content becomes less pronounced.

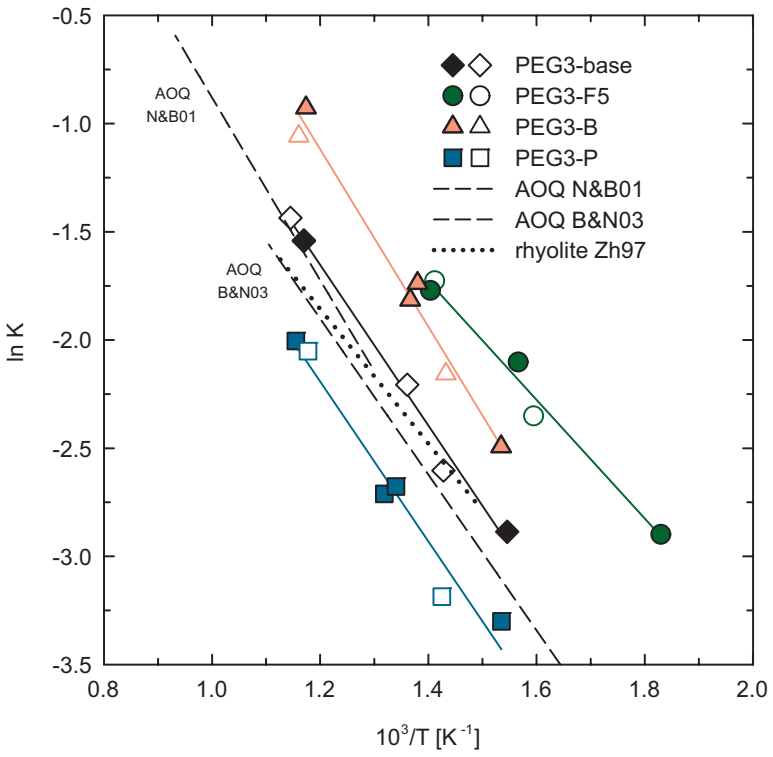

Figure B.9 Comparison of equilibrium constants for water speciation (*lnK*) in the investigated silicate melts. *Open symbols* refer to micropenetration experiments, *filled symbols* refer to falling sphere experiments. For comparison: N&B01, B&N03: in situ data from Nowak and Behrens (2001) and controlled cooling data from Behrens and Nowak (2003) for the AOQ melt composition; Zh97: isothermal heating data from Zhang et al. (1997) for rhyolitic composition.

B.7.2 Glass transition temperature and fragility

The glass transition temperature was calculated for all investigated compositions except for PEG3-P2 using Eq. B.7 and parameters listed in Table B.4. T_g decreases with increasing water content for all melt compositions (Fig. B.10). This decrease is more pronounced at low water contents where H_2O is mainly dissolved as hydroxyl groups. In melts with >3 wt% H_2O, the influence of H_2O is reduced due to the increasing amount of molecular H_2O_m. T_g values of the base composition and the P- and B-bearing melts coincide. The addition of 1.68 and 4.81 wt% F decreases the glass transition temperature by approx. 50 and 140 K, respectively, at ~1 wt% water.

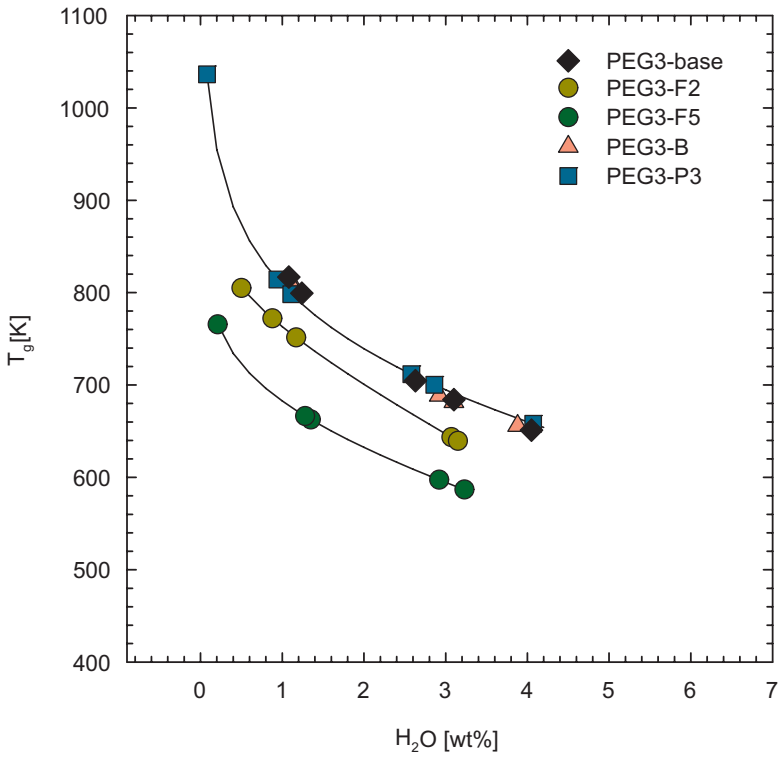

Figure B.10 Glass transition temperatures (calculated to be the viscosity at 10^{12} Pa·s using Eq. 7 and parameters listed in Table 4) for the investigated melt compositions as a function of water. *Solid lines*: calculated values (using Eq. 7) for complete range of investigated water contents. *Symbols*: experimentally investigated water contents.

The knowledge of the fragility of a silicate melt is essential to understand the rheological behaviour of a magmatic system over a broad temperature range. In an Arrhenian diagram one can distinguish between strong melts showing a linear dependence and fragile melts displaying strong curvature (Angell, 1988). Near the glass transition the temperature dependence is more pronounced in fragile melts while in high temperature melts strong melts show larger variation with temperature. The fragility *m* is given by the slope of viscosity curves (log η against reciprocal temperature) at T_g on a reduced temperature scale (Plazek and Ngai, 1991; Böhmer and Angell, 1992; Toplis et al., 1997):

$$m = \frac{B}{T_g \cdot \left(1 - \frac{C}{T_g}\right)^2} \qquad [B.9]$$

where B and C are the parameters of the VFT equation which can be calculated for each melt composition and water content using the data in Table B.4 ($B = b_1 + b_2 \cdot w_{H2O}$, $C = c_1 + c_2 \cdot \ln w_{H2O}$).

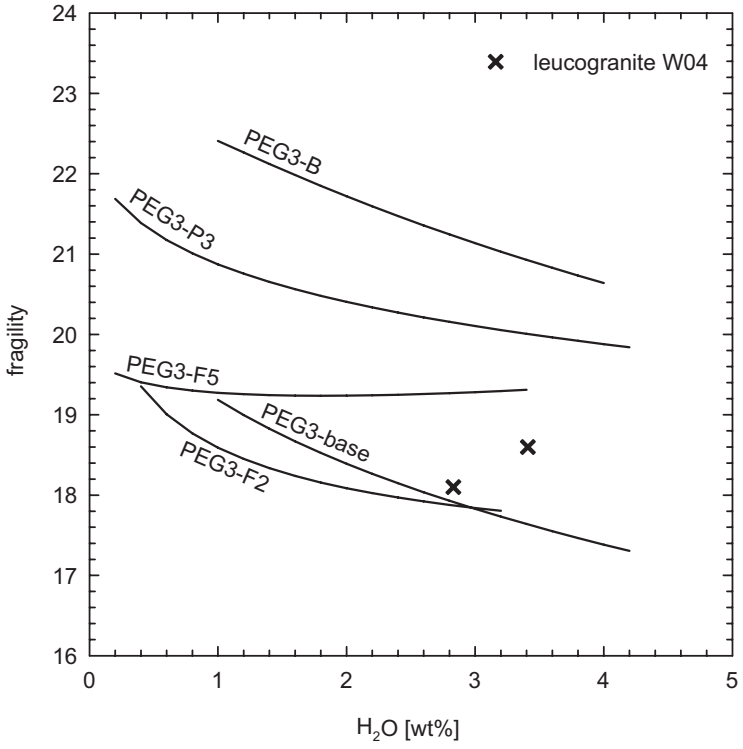

Figure B.11 Fragility (m) of glasses as a function of water content calculated using Eq. 9 and data from Table B.4. Data for a leucogranitic melt composition from Whittington et al., 2004 (W04) is shown for comparison (fragility value for anhydrous leucogranite is 29, not shown due to scaling).

Figure B.11 shows a plot of fragility against water content for the investigated melt compositions. All compositions show fragility values which are typical for highly polymerised melts (e.g. m ~18 for hydrous leucogranite; Whittington et al., 2004). This strong behaviour is confirmed by similar activation energies determined by micropenetration and

falling sphere experiments. Small difference in absolute values of *m* should not be overemphasised and may simply originate from the fitting of the viscosity data, but the dependence of *m* on water content is well resolved. For melt compositions PEG3-base, PEG3-B and PEG3-P3 a decrease of *m* with increasing water content is observed. This is consistent with studies from Whittington et al., (2004) on albitic and leucogranitic glasses (note: value for anhydrous leucogranite is 29 (Whittington et al., 2004, not shown in Fig. B.11 due to scaling). The decreasing effect of water on fragility is smaller in the presence of F (PEG3-F2) and is not observed at high concentrations of fluorine (PEG3-F5).

None of the melts investigated so far showed an increase of fragility with water content (see Fig. 10 of Del Gaudio et al., 2007). This contrasts the effect of alkali addition or, more general, melt depolymerisation on fragility indicating that the structural role of H_2O in silicate melts strongly deviates from alkaline and alkaline-earth elements.

B.7.3. Effect of melt composition

As shown in Figure B.4, there is no significant difference in viscosity between PEG3-base and previous datasets obtained for F-, B-, and P-free compositions (HPG8 and AOQ), which may be surprising, considering that the silica content is not identical. However, the addition of F, B, P and Li to PEG3-base causes a significant decrease of the viscosity by almost 2.5 orders of magnitude at high water contents (Bartels et al., 2011). This difference becomes even larger at lower water contents. This large viscosity drop from PEG3-base to PEG2 must be somehow related to the presence of F, B, P and Li. One additional reason for the lower viscosity of the F-, B- and P-bearing PEG2 melt is probably the difference in A.S.I. which is lower by 0.25 (A.S.I. = 0.91, if Li is included in the calculation) when compared to PEG3-base (A.S.I. = 1.16). According to Riebling (1966) and Toplis and Dingwell (1996) A.S.I. can have a very large impact on viscosity, especially when the melt changes from peraluminous to

peralkaline. In the following sections, the role of silica on melt viscosity and the possible effects of F, B and P are discussed successively.

B.7.3.1. Comparison of PEG3-base with haplogranitic compositions

According to Holtz et al. (1999) the viscosity of simple granite-like melts decreases with decreasing silica content and therefore, the viscosity of PEG3-base (68.0 wt% SiO_2) is expected to be lower than that of HPG8 (78.6 wt% SiO_2) and AOQ (76.1 wt% SiO_2 compositions studied by (Dingwell et al., 1996; Schulze et al., 1996). However, such a difference in viscosity is not evident (Fig. B.4). One explanation might be the higher A.S.I. of about 1.16 of PEG3-base compared to HPG8 and AOQ with an A.S.I. of ~1.00. Another reason may be the scatter of experimental data and uncertainties in extrapolating the data to the same reference temperature.

B.7.3.2. Comparison of PEG3-base with F-bearing compositions

The addition of fluorine to a silicate melt leads to a significant decrease of the viscosity with a similar magnitude as water on a molar basis (Fig. B.5a/B.5b). A simplified approach describing the effect of fluorine on melt viscosity in dependence to water content was proposed by Giordano et al. (2004) who developed a model based on different F-free and F-bearing melt compositions. Assuming that fluorine mainly forms complexes like AlF_6^{3-} and AlF_5^{2-} at low water contents, the depolymerising effect is much lower when compared to H_2O, assuming that one H_2O will lead to the formation of two hydroxyl groups being equivalent to two non-bridging oxygens (NBO´s). On the other hand, at high water contents the presence of H_2O probably inhibits the formation of such Al-F complexes and favours a mechanism where two fluorine substitutes for one bridging oxygen in the melt structure, directly depolymerising the silicate network. This mechanism would be comparable to that of water; hence the

influences of both components on melt viscosity are the same. We have tested the applicability of the computation model of Giordano et al. (2004) to our experimental data for the F-free PEG3-base and the F-bearing PEG3-F2 and PEG3-F5 melts (Fig. B.12). Good agreement was found although at high $H_2O + F_2O_{-1}$ and low temperatures the model seems to overestimate melt viscosities (Fig. B.5a). A possible explanation is that molecular H_2O becomes the dominant species at high water content.

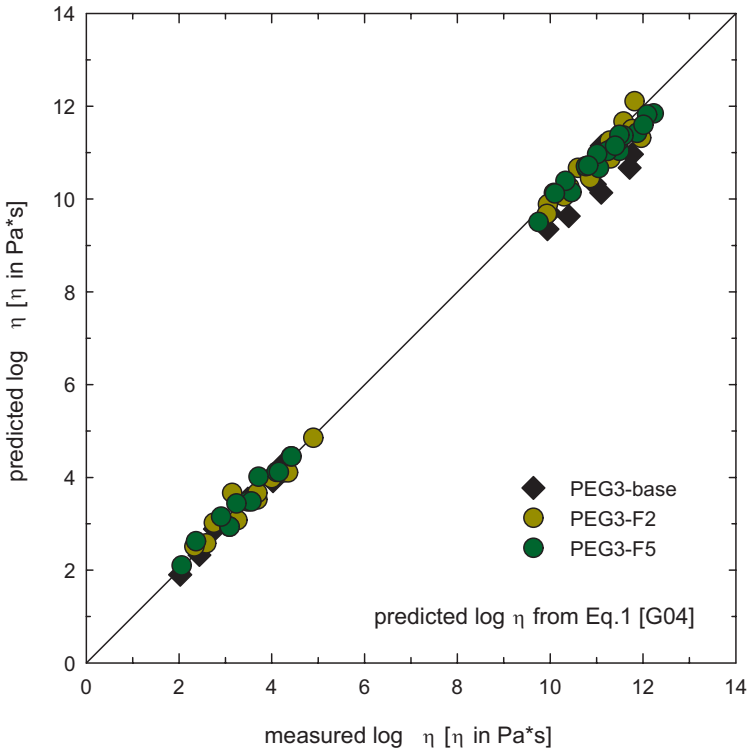

Figure B.12 Experimental viscosity data for melt compositions PEG3-base, PEG3-F2 and PEG3-F5 compared with calculated values using Eq.1 from Giordano et al., 2004 (G04).

B.7.3.3. Comparison of PEG3-base with B-bearing compositions

Figure B.6 indicates that boron significantly influences viscosity of dry haplogranitic melts. This influence is not observable for the investigated melt compositions of the present study at hydrous conditions. It is emphasized that the B_2O_3 content in PEG3-B is only 0.93 wt%, which is approximately 3.5 wt% less than the B_2O_3 content in the HPG8B5 composition, used

to investigate the role of boron in dry melts by Dingwell et al. (1992). By interpolating the dataset of Dingwell et al. (1992), the addition of 0.93 wt% B_2O_3 at dry conditions should result in a viscosity decrease by roughly 1.5 log units at 873 K.

To understand the different effect of boron on dry and hydrous melts the knowledge about how boron is incorporated in the melt structure is essential. It is well known that boron forms two species in silicate melts with different coordination to oxygen: tetrahedral and trigonal planar (e.g. Konijnendijk and Stevels, 1975; London, 1987). The ratio of tetrahedral/trigonal species increases with increasing peralkalinity (Bray, 1978; Konijnendijk and Stevels, 1978; Dell et al., 1983). Due to the excess of aluminum with respect to alkalis in the PEG3-base composition, only a small fraction of tetrahedral boron is expected which is confirmed by NMR analysis (Fig. B.7a).

In polymerised boroaluminosilicate glasses, trigonal boron joins the silicate network forming Si-O-B or Al-O-B bonds (Schmidt et al. (2004b). Taking the effective ionic radii of B, Al and Si (Shannon and Prewitt, 1969; Shannon, 1976), the ionic potential (defined as the ratio charge/radius) of these elements decreases in the order $B^{3+}(3)>B^{3+}(4)>Si^{4+}(4)>Al^{3+}(4)$ (coordination number is given in parentheses). Consequently, the bridging oxygens within Si-O-B or Al-O-B structures are more strongly bond to B than to Si or Al. Thus Si-O or Al-O bonds are weakened which facilitates viscous flow in these polymerised networks. Such a mechanism can explain the reduction of viscosity by replacement of boron for aluminium in silicate melts (Tait et al. 1984; Dingwell 1990; Dingwell al., 1992, 1993).

In hydrous melts, the depolymerising effect of water is much more efficient in lowering viscosities than the weakening of bond strength within the silicate network. Combining our viscosity data for PEG3-B with the interpolated viscosity of a haplogranitic melt with same boron content (Dingwell et al., 1992), a depressing effect of boron on viscosity is expected only at water contents below 4 mol% (dashed lines in Fig. B.6). The described effects may be

different in peralkaline silicate melts where a large fraction of tetrahedral boron is present (B.7b) since the ionic field strength is smaller for $B^{3+}(4)$ than for $B^{3+}(3)$.

B.7.3.4. Comparison of PEG3-base with P-bearing compositions

According to Toplis and Dingwell (1996), phosphorus should decrease the viscosity of anhydrous peraluminous compositions. One interpretation is that only a fraction of P is combined with the excess aluminium, resulting in an increase of viscosity, whereas most P interacts with network-forming aluminates like $NaAlO_2$ forming both Al and alkali phosphate complexes. Gan and Hess (1992) argued that these complexes reside outside the silicate network. Accordingly, the addition of P is equivalent to the removal of equimolar amounts of Na_2O and Al_2O_3. This confirms the data from Dingwell et al. (1993) for a dry, P-bearing haplogranitic composition that show a small depolymerising effect of P in anhydrous systems. The present study shows a decrease of viscosity at small water contents, but the decrease is negligible at high water contents (Fig. B.8).

This suggests that the effect of P on melt viscosity is small and as soon as water depolymerises the silicate network, the effect becomes negligible. Thus P cannot reasonably explain the very low viscosities of highly fractionated melts, especially of slightly peralkaline melts as PEG2. In peralkaline melts, the addition of phosphorus should lead to a small increase in melt viscosity because of the removal of network modifying cations into phosphate complexes, resulting in a polymerisation of the remaining portion of the silicate network (Toplis and Dingwell, 1996).

B.7.4. Comparison with recent models

Figure B.4 shows that the specific model for hydrous rhyolitic melts from Zhang et al. (2003) can be used to predict the viscosities of melt composition PEG3-base. However, for melts

containing F, B and P, a multi-composition model is needed. Two recent non-Arrhenian models for calculating viscosities of complex silicate melts are available: the model of Hui and Zhang (2007) and the model of Giordano et al. (2008). Both models consider effects of phosphorus but ignore boron. Fluorine is only included in the model of Giordano et al. (2008).

The Hui and Zhang (2007) model describes well the viscosities of PEG3-base and PEG3-B (Fig. B.13a), consistent with a negligible effect of boron on hydrous melt viscosity. However, the model significantly overestimates the effect of phosphorus (PEG3-P3). One possible explanation is that the model of Hui and Zhang (2007) was developed for more complex melt compositions. In more simplified systems, P becomes disproportionally more important within the model, perhaps leading to the incorrect prediction of the viscosity. Another explanation is that the model is only calibrated with melt compositions containing < 1 wt% P_2O_5. Since P has no significant effect on the viscosity of hydrous melts, the viscosity of PEG3-P can be predicted well by ignoring P in the calculation (Fig. B.13a, squares).

Although the model of Hui and Zhang (2007) does not include F, it may be considered by converting F_2O_{-1} (in wt%) into an equivalent amount of H_2O (in wt%). In doing so, the experimental data of the F-bearing melts is well described except for sample PEG3-F5-D that contains only 0.21 wt% H_2O. The discrepancy can be explained by the fact that the depolymerising effect of F is only comparable to that of water at high concentrations of both volatiles (> 15 mol%, Fig. B.5a / B.5b).

The prediction of the viscosity of the P-bearing melt is much better by the model of Giordano et al. (2008) than by the model of Hui and Zhang (2007) (Fig. B.13b). However, the deviation between measured and predicted values is still high and the model underestimates melt viscosities by almost 2 log units for water-poor samples (PEG3-P3-D). Ignoring phosphorus in the calculation gives better prediction of viscosity, but especially within the high viscosity

range, viscosities are not well predicted. Data for the F-poor melts (PEG3-F2) are in good agreement with the model of Giordano et al. (2008) while data for F-rich melts (PEG3-F5) is overestimated by the model.

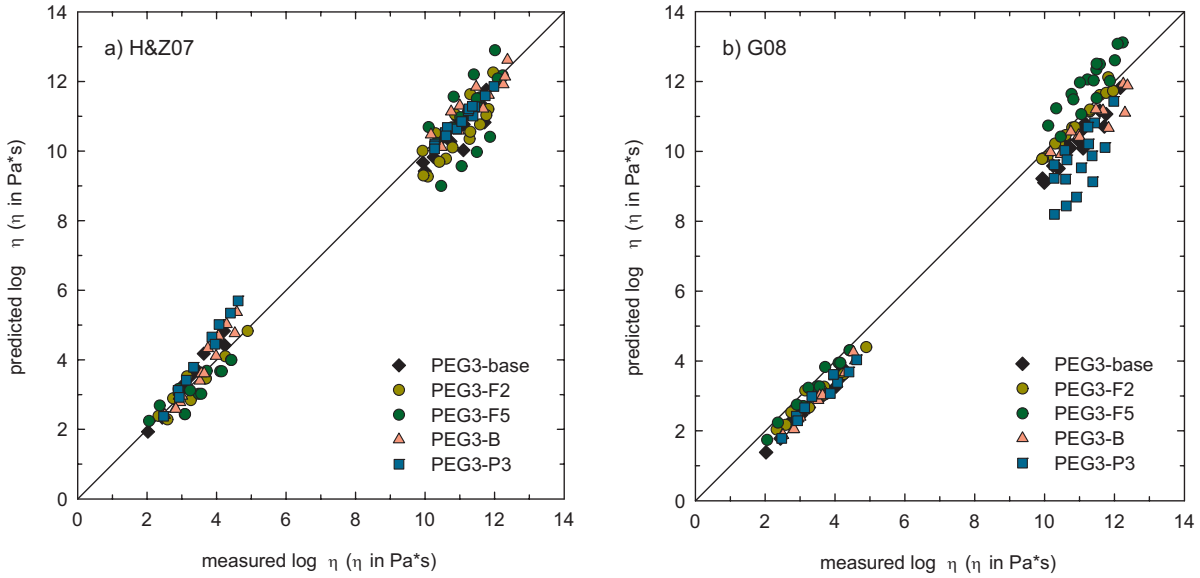

Figure B.13 Comparison of the experimental dataset with the predictions of the model of Hui and Zhang, 2007 (H&Z07) (a) and the model of Giordano et al., 2008 (G08) (b).

B.8. Conclusion

The experimental data of this study confirm that water and fluorine are the most important volatiles causing a depolymerisation of the hydrous silicate melts. Comparing our viscosity data with results for dry systems (Dingwell et al., 1992, 1993) indicates that a decreasing effect of P and B on melt viscosity occurs only at low water concentration (< 4 mol% corresponding to ~1 wt%).

Assuming that the effects of fluorine, water, boron and phosphorus on melt viscosity are additive, the calculated viscosity is still several orders of magnitude higher than the measured viscosity of a typical pegmatite forming melt as studied by Bartels et al. (2011). This discrepancy may originate from different Li-contents of the studied systems. Li plays a crucial role in the behaviour of silicate melts, i.e. by changing the A.S.I number. Furthermore,

substitution of other alkalis by lithium may change melt properties due to the high ionic field strength of Li. Additional studies on Li-bearing hydrous melts are therefore recommended to verify whether Li is the missing link to explain the low viscosities of pegmatitic melt described by Bartels et al. (2011).

Consequences of our study are, that changing the B or P content due to crystallisation of a boron- or a phosphorus-bearing mineral or partitioning into a fluid phase will not significantly affect the viscosity of the residual melt. On the other hand, changes in the H_2O and F contents in pegmatite forming melts can have dramatic influence on their flow behaviour as well as crystallisation kinetics.

B.9. Appendix

Tabel B.1.A Detailed experimental conditions and results for falling sphere experiments

sample	T [K]	P [MPa]	ρ_m [g/cm^3]	Mat.	r [µm]	d [m]	t [s]	$Log\ \eta$ [η in Pa*s]
PEG3-base-1a	1479	200	2.29	Pt	147.5	0.002200	28800	4.03
PEG3-base-1b	1529	300	2.30	Pt	147.5	0.004090	21600	3.63
PEG3-base-1c	1430	200	2.30	Pt	147.5	0.003250	64800	4.21
PEG3-base-3a	1383	200	2.24	Pt	97.5	0.003030	24900	3.48
PEG3-base-3b	1474	300	2.24	Pt	97.5	0.001543	3695	2.95
PEG3-base-3c	1269	300	2.27	Pt	97.5	0.001872	86400	4.23
PEG3-base-6a	1383	300	2.11	Pt	90.5	0.008430	7200	2.44
PEG3-base-6b	1278	300	2.14	Pt	90.5	0.005870	10800	2.77
PEG3-base-6c	1474	300	2.09	Pt	90.5	0.003160	1036	2.03
PEG3-F2-1a	1383	200	2.30	Pt	150	0.002550	54000	4.25
PEG3-F2-1b	1275	200	2.31	Pt	150	0.002310	216000	4.90
PEG3-F2-1c	1481	200	2.29	Pt	150	0.001860	10800	3.69
PEG3-F2-1d	1403	500	2.35	Pt	150	0.007640	90000	4.00
PEG3-F2-1e	1383	600	2.37	Pt	150	0.001360	36000	4.35
PEG3-F2-3a	1283	200	2.23	Pd	188	0.016926	126000	3.69
PEG3-F2-3b	1383	300	2.23	Pt	91	0.004460	24900	3.26
PEG3-F2-3c	1481	300	2.21	Pt	91	0.003030	3600	2.59
PEG3-F2-6a	1372	300	2.15	Pt	88	0.002760	1931	2.33
PEG3-F2-6b	1278	300	2.17	Pt	88	0.005880	10800	2.75
PEG3-F2-6c	1176	300	2.19	Pt	88	0.005500	25200	3.15
PEG3-F5-1a	1271	200	2.28	Pt	85	0.000970	43200	4.10
PEG3-F5-1a	1271	200	2.28	Pt	97.5	0.001130	43200	4.15
PEG3-F5-1b	1373	200	2.27	Pt	85	0.001340	14400	3.48
PEG3-F5-1b	1373	200	2.27	Pt	97.5	0.001470	14400	3.56
PEG3-F5-1c	1223	200	2.29	Pt	85	0.003780	345600	4.41
PEG3-F5-1c	1223	200	2.29	Pt	97.5	0.004800	345600	4.43
PEG3-F5-1d	1473	200	2.26	Pt	85	0.000870	3712	3.08
PEG3-F5-1d	1473	200	2.26	Pt	97.5	0.001110	3712	3.09
PEG3-F5-3a	1265	200	2.22	Pt	83.5	0.002290	14400	3.24
PEG3-F5-3b	1178	200	2.23	Pt	83.5	0.007620	144000	3.72
PEG3-F5-6a	1179	200	2.15	Pt	85	0.010200	28800	2.91
PEG3-F5-6b	1368	300	2.11	Pt	85	0.002560	1020	2.06
PEG3-F5-6c	1268	300	2.13	Pt	85	0.004570	3708	2.37
PEG3-B-1a	1375	200	2.31	Pt	132	0.003746	216000	4.58
PEG3-B-1b	1476	200	2.30	Pt	132	0.001664	28800	4.06
PEG3-B-1c	1426	200	2.30	Pt	132	0.002920	86400	4.29
PEG3-B-1d	1530	200	2.29	Pt	132	0.002100	18000	3.75
PEG3-B-1e	1403	500	2.36	Pt	132	0.002290	90000	4.41
PEG3-B-3a	1378	300	2.24	Pt	120.5	0.003032	18000	3.52
PEG3-B-3b	1269	300	2.25	Pt	120.5	0.004985	86400	3.98
PEG3-B-3c	1478	300	2.22	Pt	120.5	0.001770	2818	2.95
PEG3-B-3d	1175	300	2.27	Pt	120.5	0.004300	259200	4.53
PEG3-B-6a	1378	300	2.12	Pt	92	0.001403	1308	2.49
PEG3-B-6a	1378	300	2.12	Pd	194	0.003288	1308	2.51
PEG3-B-6b	1276	300	2.14	Pt	92	0.002457	6098	2.92
PEG3-B-6b	1276	300	2.14	Pd	194	0.004878	6098	3.01
PEG3-B-6c	1173	300	2.17	Pt	92	0.001970	21600	3.56
PEG3-B-6c	1173	300	2.17	Pd	194	0.003950	21600	3.65
PEG3-B-6d	1343	300	2.13	Pt	92	0.001300	2502	2.81
PEG3-B-6d	1343	300	2.13	Pd	194	0.003054	2502	2.82
PEG3-P2-1a	1376	200	2.30	Pt	148.5	0.002710	108000	4.52
PEG3-P2-1b	1483	200	2.28	Pt	148.5	0.002760	28800	3.94
PEG3-P2-1c	1529	200	2.28	Pt	148.5	0.002460	14400	3.68
PEG3-P3-1a	1474	200	2.30	Pt	140	0.002260	36000	4.07
PEG3-P3-1b	1375	200	2.31	Pt	140	0.003800	216000	4.62
PEG3-P3-1c	1426	200	2.30	Pt	140	0.002550	86400	4.40
PEG3-P3-1d	1528	200	2.29	Pt	140	0.001800	18000	3.87
PEG3-P3-1e	1403	500	2.35	Pt	140	0.002745	90000	4.38
PEG3-P3-1f	1378	650	2.38	Pt	140	0.001128	54000	4.55
PEG3-P3-3a	1375	300	2.25	Pt	130	0.008485	28800	3.34
PEG3-P3-3b	1480	300	2.24	Pt	130	0.003035	3711	2.90
PEG3-P3-3c	1275	300	2.26	Pt	130	0.004070	57600	3.96
PEG3-P3-3d	1433	300	2.23	Pt	130	0.005120	10800	3.13
PEG3-P3-6a	1375	300	2.12	Pt	100.5	0.004137	3117	2.47
PEG3-P3-6b	1273	300	2.14	Pt	100.5	0.005080	10800	2.92

mat. = sphere material; r = sphere radius; d = falling distance; t = experimental duration; ρ_m = melt density

Melt densities were calculated after the modified model of Ochs and Lange (1999).

Maximal uncertainties: T ± 10 K; P ± 3 MPa; density ± 0.01 g/cm^3; sphere radius ± 2 µm; distance ± 2 %; time ± 68 seconds; viscosity ± 15%

Part C

The effect of lithium on the viscosity of pegmatite forming melts

Rare element pegmatites could accumulate significant concentrations of lithium. In the previous part it is concluded, that lithium will play a crucial role in lowering melt viscosity but qualitative measurements on this effect are missing. It is well known that alkalis like Na, K but also Li will depolimerize the silicate network at least in dry systems but so far, data on the combined effects of these elements in combination with water are lacking. Therefore the third part of this work will focus on the effect of Li on the behaviour of water-bearing pegmatite forming melts. Additionally, the influence of Li in comparison to other alkalis is discussed, to verify if differences in size and cation field strength of the alkalis will cause a difference in effecting the melt viscosity.

C.1. Abstract

Based on the PEG3-base composition from part B, viscosity experiments were conducted to investigate the influence of lithium on the viscosity of pegmatite forming melts. Therefore Li_2O was added to this composition either in exchange for K_2O or as additional alkali component. The viscosity experiments of hydrous melts (~1 to ~6 wt% H_2O) were carried out in the low temperature range at ambient pressure using the micropenetration technique and in the high temperature range at 200-300 MPa pressure using the falling sphere method.

The experimental data show, that Li_2O significantly changes melt properties and decreases melt viscosity. In the high temperature range and in samples with water contents < 10 mol%, this decrease is, on a molar basis, slightly higher when compared to K_2O. Additionally it is shown, that the combined effects of fluxing elements like F, B, P and Li, could explain the low melt viscosities of pegmatite forming melts, described in previous studies from Bartels et al. (2011).

C.2. Introduction

In common magmatic systems, lithium is a rare element and the crustal average is ~20 ppm (Mason and Moore, 1982). In contrast, some highly fractionated pegmatitic systems are enriched in Li_2O up to weight percent levels, indicated by the presence of lithium minerals such as spodumene ($LiAlSi_2O_6$) or petalite ($LiAlSi_4O_{10}$).

In high concentrations lithium will become an important element governing crystallization and melt properties (London, 1987). For example in the metaluminous systems Ab-Qz-H_2O and Ab-Or-Qz-H_2O, the addition of lithium (1-4 wt.% Li_2O) depresses liquidi by approximately 80°-90°C at 100-200 MPa, and shifts minimum melt compositions in Ab-Or-Qz projections away from SiO_2 (e.g. Wyllie and Tuttle, 1964; Stewart, 1978; Martin, 1983; Martin and Henderson, 1984).

One of the most important properties controlling the crystallization of a pegmatite body is the melt viscosity. As an alkali like Na and K, Li will act as network modifier in aluminosilicate melts. De Jong and Brown (1980) proposed that the degree to which alkalis "perturb" Si-O-(Si) bonds increases with increasing cation field strength, i.e. Cs < Rb < K < Na < Li. Both, De Jong and Brown (1980) and Navrotsky et al. (1985) concluded that the smaller alkalis Li and Na should exhibit a greater tendency to weaken the silicate melt structure rather than K, Rb, and Cs. Therefore experimental investigation on the influence of Li on melt viscosity is important to understand the formation of pegmatitic features and internal zonation. Hess et al. (1995) conducted viscosity experiments in the low and high temperature range with a nominally dry haplogranitic melt and investigated the influences of excess alkalis on that melt composition. They concluded, that the effects of each of the alkalis are similar, implying that the structural role of the alkalis is common to all. However, in detail they observed an increasing viscosity with increasing size of added alkali cation. Accordingly lithium should be the most important alkali cation in depolymerizing the melt structure.

More recent Bartels et al. (2011) conducted viscosity experiments with a hydrous synthetic melt composition containing F, B, P, Li and H_2O and concluded that the enrichment of these components up to weight percent levels significantly influences the melt viscosity. In a second study (Bartels et al., submitted) they investigated the individual influences of F, B, P and H_2O on the viscosity of pegmatite forming liquids and concluded that beside water, F is the main element influencing melt viscosity and that P and B do not play a major role on viscous flow in water-rich pegmatitic systems. However, according to their observations the depolymerising effect of H_2O and F is not sufficient to explain very low viscosities of complex melts containing H_2O, F, B, P and Li (Bartels et al., 2011). Thus, they concluded that Li must play a crucial role in lowering the viscosity of natural pegmatite melts and combined effects between different constituents need to be taken under consideration.

In this study we present the results of an experimental study allowing us to discuss the influence of lithium on melt viscosity in highly fractionated systems in the low and high temperature range. Thereby the different effects of alkalis and other fluxes like H_2O and F on melt viscosity are discussed and the data is compared to the prediction of recent viscosity models.

C.3. Experimental methods

C.3.1. Starting materials

The PEG3-base composition from Part B was chosen as the starting glass. In principle this composition is equal to a previously investigated synthetic melt composition (PEG2 from Bartels et al., 2011) excluding the concentrations of F, B_2O_3, P_2O_5 and Li_2O and the molar proportions of SiO_2, Al_2O_3, Na_2O and K_2O are ~ 75.50 mol%, 13.17 mol%, 8.32 mol% and 3.01 mol%, respectively.

Two additional starting compositions (PEG3-Li and PEG3-KLi) were synthesized to investigate the different effects of Li_2O and K_2O on melt viscosity and to figure out to what extend the excess of alkalis will affect the viscosity of the melt. For the PEG3-Li composition, the total molar amount of K_2O in the PEG3-base composition was replaced by Li_2O. For the PEG3-KLi, the same molar proportion of Li_2O like in the melt composition PEG2 was added to the PEG3-base composition. All investigated compositions were synthesized from a mixture of SiO_2, Al_2O_3, Na_2CO_3, K_2CO_3 and / or Li_2CO_3 powder. These mixtures were homogenized in an agate ball mill or a swing mill and fused for 2 hours at 1873 K in a platinum crucible placed in a 1 atm chamber furnace. To ensure homogeneity, the resulting glass was crushed and melted again for 2 hours at 1873 K.

The resulting glass compositions were analysed by electron microprobe (at least 15 analyses on two or three glass pieces). The Li content was analysed by Actlabs/Canada using sodium

peroxide fusion ICP-MS. The compositions of PEG3-base, PEG3-Li and PEG3-KLi together with the PEG2 composition from Bartels et al. (2011) are given in Table C.1.

Table C.1 Composition of the starting glasses.

Oxides	PEG2 [wt%]	PEG3-base [wt%]	PEG3-Li [wt%]	PEG3-KLi [wt%]
SiO_2	59.73 (0.13)	68.01 (0.72)	70.19 (1.28)	66.92 (0.47)
Al_2O_3	19.75 (0.13)	20.14 (0.25)	20.94 (0.79)	19.67 (0.28)
Na_2O	7.25 (0.1)	7.73 (0.20)	7.74 (0.38)	7.95 (0.15)
K_2O	3.82 (0.02)	4.26 (0.05)	n.d.	4.20 (0.07)
F	5.46 (0.01)	n.d.	n.d.	n.d.
P_2O_5	2.46 (0.21)	n.d.	n.d.	n.d.
Li_2O	1.68 (0.01)	n.d.	1.42 (0.01)	1.36 (0.01)
B_2O_3	2.75 (0.01)	n.d.	n.d.	n.d.
2F = O	-2.3			
total	100.6	100.14	100.29	100.1
A.S.I.Li	0.91	1.16	1.19	0.88

Values are mean of at least 15 electron microprobe analyses; n.d.: not determined

1σ standard deviation is given in parentheses

$A.S.I._{Li}$ molar ratio of Al/(Na+K+Li)

Additionally PEG2 from Bartels et al. (2011) is shown.

All glasses were found to be homogeneous (see standard deviations in Tab. C.1). The molar ratios Al/(Na + K + Li) are 1.16 and 1.19 for the peraluminous compositions PEG3-base and PEG3-Li and 0.88 and 0.91 for the peralkaline compositions PEG3-KLi and PEG2.

C.3.2. Falling sphere method

The melt viscosity at high pressure and temperature was measured with the falling sphere method (e.g. Shaw 1963; Schulze et al., 1996; Holtz et al., 1999; Vetere et al., 2006; Bartels et al., 2011) using the exact procedure described in part A and B of this study. Hence, only the main principles of this method are described in the following:

The falling sphere method implies the synthesis of a water-bearing glass cylinder containing a Pt-horizon used as immobile marker and noble metal spheres. This setup will be brought to experimental conditions and the effective settling distance of the sphere within the cylinder can be calculated using the Pt-horizon as a reference, considered to be static, and the positions

of the spheres before and after the experiment. The measured falling distance will be used to calculate the viscosity of the melt. In this study, for each composition three cylinders with water contents of approximately 1, 3 and 6 wt% were synthesized. For the falling sphere experiments, Pt spheres with radii ranging from 84 to 178 μm were used (Tab. C.1.A). In cases of sample PEG3-Li-1 two spheres were placed within one cylinder. This allows determining two viscosity values within a single experiment.

C.3.3. Micropenetration technique

The melt viscosity at low temperatures was measured using the micropenetration technique. Water-bearing samples were synthesized in an IHPV from the GZG (Geowissenschaftliches Zentrum der Universität Göttingen) in a temperature range of 1473 to 1523 K and pressures between 100 and 204 MPa. Heating was accomplished within 30 to 60 minutes and the experimental duration varied from 70 to 90 h. The water contents ranged from ~1 to ~4 wt%. After synthesis the samples were cut in 1mm thick slices and polished on both sides. The micropenetration technique involves determining the rate of which a sapphire sphere (diameter: 1mm) under a fixed load moves into the sample surface (e.g. Webb et al., 2004). These measurements were conducted in a vertical dilatometer (Netzsch TMA 402) at the GZG. The sample is placed in a ceramic holder. The sapphire sphere is being held in the middle of the sample by a ceramic rod which is connected to a weight pan. The metal connection of the ceramic rod and the weight pan acts as the core of a calibrated linear voltage displacement transducer (LVDT). After the whole setup is inserted into an electro furnace and brought to experimental temperature, a weight is placed onto the weight pan and the movement of the sphere into the sample is recorded by the LVDT. The temperature is measured by $Pt/Pt_{90}Rh_{10}$ thermocouples, which were calibrated against the melting temperatures of bismuth, zinc, aluminium and silver.

C.4. Analytical methods

C.4.1. Microprobe

The composition of starting glasses was measured using a Cameca SX-100 electron microprobe with 15 keV acceleration voltages, 4 nA beam current and a beam diameter of 20 µm. The counting time ranged from 4 to 30 s and the respective standards were albite (Na), wollastonite (Si), corundum (Al) orthoclase (K).

C.4.2. Karl-Fischer-Titration

The water contents of all synthesized hydrous glasses for micropenetration and falling sphere experiments and the falling sphere samples after the final viscosity experiments were determined by pyrolysis and subsequent Karl-Fischer-Titration (KFT) (Behrens et al., 1996). An increment of 0.10 wt% was added to the measured values to account for an incomplete dehydration of the samples during the analysis (Leschik et al., 2004). To check for homogeneous distribution of H_2O, especially within the water-poor samples (samples with ~1 wt% H_2O), two analyses from both ends of these cylinders were performed. The resulting values do not significantly differ from each other and mean values of both measurements are given in Table C.2 for pre-experimental water content.

The differences between the pre- and post-experimental water contents of the falling sphere samples was always within the error of analysis except for PEG3-KLi-3 and PEG3-Li-1, where a leakage was observed after the final viscosity experiment. In these cases the pre-experimental water content was used for discussion. The molar value for H_2O on the basis of oxide components (Tab. C.2) were calculated from mean values of pre- and post-experimental water contents.

C.4.3. Infrared (IR) spectroscopy

IR spectroscopy was used to test the homogeneity of glasses, to identify possible water loss after falling sphere experiments and to determine the fractions of OH and molecular H_2O within the samples. Water concentrations were calculated by the Beer-Lambert-law using the peak heights of the H_2O and OH combination bands at 5200 cm^{-1} and 4500 cm^{-1} after subtraction of a linear baseline. Near infrared (NIR) spectra were recorded using a Bruker IFS88 FTIR spectrometer equipped with Mercury-Cadmium-Tellurium (MCT) narrow range detector, a tungsten lamp, a KBr beamsplitter and a Bruker IRscope II microscope.

The glass samples were prepared as both-sided polished thin sections with a thickness of around 300 µm. The thickness was measured using a digital Mitutoyo micrometer (precision ± 2 µm). For each spectrum 100 scans were collected with a spectral resolution of 4 cm^{-1}. The spot size was about 50 x 50 µm. For every sample, 4 spectra were collected to check for homogeneous distribution of the water within the sample. The densities of the samples were either determined by the Archimedean method with water and a droplet of tenside (Tween 80) per liter as immersion liquid or calculated with the model of Ochs and Lange (1999) for 292 K and 0.1 MPa. The comparison between measured and modelled values is within error, confirming the reliability of the model for the used conditions.

For each composition the absorption coefficients ε of H_2O and OH were determined using samples with water contents ranging from ~1 wt% to ~6 wt% water (determined by KFT). Assuming that no other hydrous species are present in the glass beside OH and H_2O ($C_{H_2O_t} = C_{H_2O} + C_{OH}$, where $C_{H_2O_t}$ refers to the total water content and C_{H_2O} and C_{OH} to water dissolved as molecular H_2O and OH groups, respectively) and that the ε values do not vary with water content, the ε values can be determined using plots of absorbances normalized by density ρ (after Ochs and Lange, 1999), thickness d and water content (Behrens et al., 1996):

$$\left[\frac{1802 \cdot A_{5200}}{d \cdot \rho \cdot c_{H_2O_t}}\right] = \varepsilon_{H_2O} - \frac{\varepsilon_{H_2O}}{\varepsilon_{OH}} \cdot \left[\frac{1802 \cdot A_{4500}}{d \cdot \rho \cdot c_{H_2O_t}}\right] \qquad [C.1]$$

where A_{5200} and A_{4500} are the absorbances of the bands at 4500 cm^{-1} and 5200 cm^{-1}, respectively, and ε_{H_2O} and ε_{OH} are the corresponding linear molar absorption coefficients.

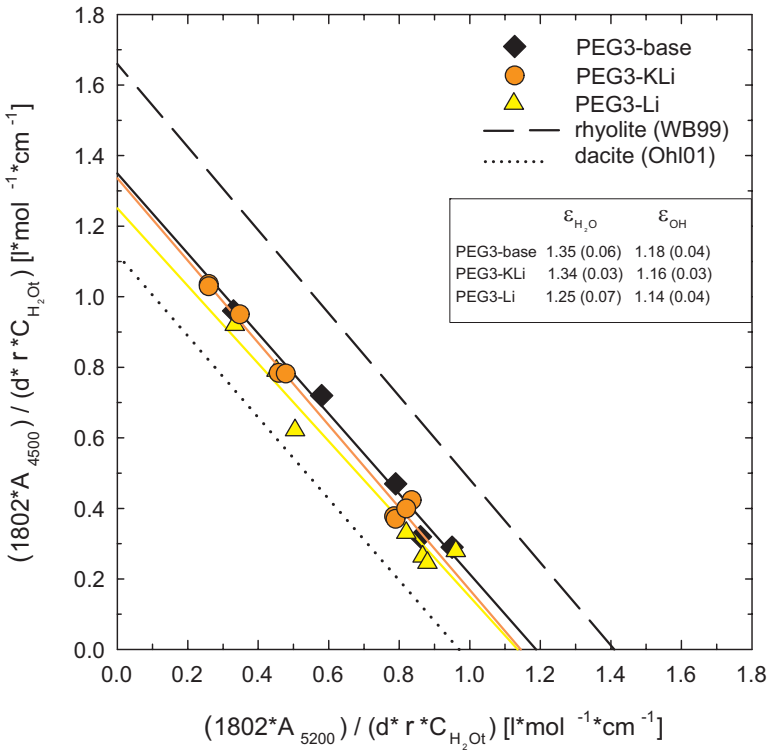

Figure C.1 Normalized absorbances of H_2O- and OH-bands for the investigated melt compositions. The dashed line represents rhyolitic data from Withers and Behrens, 1999 (WB99). The dotted line represents dacitic data from Ohlhorst et al., 2001 (Ohl01). Error bars were not shown for better clarity, max. error was ± 0.07 ($l \cdot mol^{-1} \cdot cm^{-1}$) taken into account the uncertainties of the regression lines.

The molar absorption coefficients were determined by linear regression as the intercepts of the straight line with both axes (Fig. C.1). There are no significant differences of the molar absorption coefficients for the investigated melt compositions. All compositions have a similar ratio of $\varepsilon_{H_2O}/\varepsilon_{OH}$ of 1.1 as found for rhyolite and dacite (Withers and Behrens, 1999;

Ohlhorst et al., 2001) when using the same spectra evaluation (i.e. tangential baselines). The determined coefficients were used to calculate water contents of samples for which KFT measurements were not successful (for example due to explosion caused by rapid dehydration of samples during the KFT measurement (e.g. PEG3-KLi-3, PEG3-Li-3, PEG3-Li6 and mPEG3-base-4 (Tabs. C.2 and C.3, italic numbers)).

C.5. Viscosity calculation

C.5.1. Falling sphere experiments

The viscosity values for falling-sphere experiments (Tab. C.2) were calculated using the following modified Stokes law:

$$\eta = \frac{2 \cdot t \cdot g \cdot \Delta\rho \cdot r^2 \cdot C_F}{9 \cdot d} \qquad [C.2]$$

where d is the settling distance, t is the run duration, $\Delta\rho$ is the density difference between the sphere and the melt, g is the acceleration due to gravity (9.81 m/s^2), r is the radius of the sphere and C_F is the Faxen correction (Faxen, 1923) to account for the effect of viscous drag by the capsule wall on the settling sphere. The run duration, sphere radius, settling distance, calculated melt density (after Ochs and Lange, 1999) and temperature of the experiments is given in table C.1.A. The Faxen correction is given by the equation:

$$C_F = 1 - 2.104\left(\frac{r}{R}\right) + 2.09\left(\frac{r}{R}\right)^3 - 0.95\left(\frac{r}{R}\right)^5 \qquad [C.3]$$

where r is the radius of the sphere and R is the inner radius of the capsule. For experiments where the dwell on target temperature was less than 2 hours a time correction was used to account for sinking of the sphere during heating and cooling. This was done assuming a constant heating ramp of 80 K/min and a constant cooling rate of 120 K/min and using the following equation (Vetere et al., 2006):

$$t_{effective} = \int \exp\left[\frac{-E_a}{R}\left(\frac{1}{T(t)} - \frac{1}{T_{target}}\right)\right] \cdot dt \qquad [C.4]$$

E_a is the activation energy for viscous flow and R is the universal gas constant. A preliminary value of the activation energy was determined using viscosity data without time correction, i.e. using the experimental dwell at the target temperature and assuming an Arrhenian behaviour over the investigated temperature range. The values of t for experiments with run durations of less than 2 h given in table C.1.A are already corrected using equation C.4. The melt densities at given P and T were calculated after Ochs and Lange (1999) and are listed in table C.1.A. The model of Ochs and Lange (1999) had to be extended with Li_2O and the partial molar volume for this element was taken from Knoche et al. (1995). Taking into account the uncertainties of temperature, falling distance, sphere radius, run duration and melt density the calculated total error of viscosity is always less than ± 10 %, except for sample PEG3-base-3a where a high temperature gradient of 10 K was observed during experiment resulting in a relative error of ± 15 %.

Table C.2 Experimental conditions and results for falling sphere experiments

experiment	H_2O [wt%]	H_2O^* [wt%]	H_2O^{**} [wt%]	H_2O [mol%]	Li_2O [mol%]	T [K]	P [MPa]	*Log η* [η in Pa*s]
PEG3-base-1a	1.28 (0.08)		1.24 (0.08)	4.45		1479 (6)	200	4.03 (0.04)
PEG3-base-1b						1529 (6)	300	3.63 (0.04)
PEG3-base-1c		***1.19 (0.02)***				1430 (6)	200	4.21 (0.04)
PEG3-base-3a	2.63 (0.07)		2.63 (0.07)	9.10		1383 (10)	200	3.48 (0.07)
PEG3-base-3b						1474 (1)	300	2.95 (0.02)
PEG3-base-3c		n.d.				1269 (4)	300	4.23 (0.04)
PEG3-base-6a	6.14 (0.07)		6.15 (0.08)	19.54		1383 (5)	300	2.44 (0.03)
PEG3-base-6b						1278 (5)	300	2.77 (0.03)
PEG3-base-6c		6.15 (0.08)				1474 (1)	300	2.03 (0.04)
PEG3-Li-1a	1.07 (0.06)		1.07 (0.06)	3.75	2.96	1428 (5)	300	4.01 (0.04)
PEG3-Li-1b						1374 (2)	300	4.36 (0.02)
PEG3-Li-1b						1374 (2)	300	4.40 (0.02)
PEG3-Li-1c[1]						1526 (3)	300	3.40 (0.02)
PEG3-Li-1c[1]		1.39 (0.06)				1526 (3)	300	3.39 (0.02)
PEG3-Li-3a	***2.84 (0.03)***		2.82 (0.05)	9.46	2.78	1475 (3)	300	2.86 (0.02)
PEG3-Li-3b						1275 (3)	300	3.83 (0.02)
PEG3-Li-3c						1376 (3)	300	3.19 (0.02)
PEG3-Li-3d		***2.79 (0.05)***				1426 (3)	300	2.93 (0.02)
PEG3-Li-6a	***6.34 (0.06)***		6.24 (0.07)	19.33	2.48	1379 (6)	300	2.34 (0.04)
PEG3-Li-6b						1276 (3)	300	2.80 (0.03)
PEG3-Li-6c						1223 (1)	300	3.17 (0.02)
PEG3-Li-6d		6.13 (0.07)				1326 (3)	300	2.51 (0.03)
PEG3-KLi-1a	1.09 (0.08)		1.10 (0.06)	3.85	2.96	1483 (10)	200	3.23 (0.05)
PEG3-KLi-1b						1531 (8)	300	3.10 (0.04)
PEG3-KLi-1c						1428 (5)	300	3.50 (0.03)
PEG3-KLi-1d		1.10 (0.06)				1374 (2)	300	3.78 (0.02)
PEG3-KLi-3a	***2.43 (0.03)***		2.43 (0.03)	8.23	2.82	1475 (3)	300	2.43 (0.03)
PEG3-KLi-3b						1430 (6)	300	2.55 (0.04)
PEG3-KLi-3c						1373 (1)	300	2.74 (0.02)
PEG3-KLi-3d[1]		3.05 (0.06)				1328 (5)	300	2.84 (0.02)
PEG3-KLi-6a	6.15 (0.07)		6.13 (0.07	19.04	2.49	1379 (6)	300	2.04 (0.04)
PEG3-KLi-6b						1276 (3)	300	2.40 (0.03)
PEG3-KLi-6c						1223 (1)	300	2.95 (0.02)
PEG3-KLi-6d		6.11 (0.07)				1326 (3)	300	2.33 (0.03)

H_2O contents measured by KFT and IR (***italic***); H_2O* = water content after experiments; mean value (H_2O**) of both measurements was taken for calculation in mol% (calculation based on oxide components); Li_2O [mol%] calculated

[1)] leak during experiment; n.d. = not determined

The error on T takes into account the temperature gradient along the sample and the temperature fluctuation over time.

Characters in the sample name refer to base composition (e.g. PEG3-base), the synthesized sample (1,2,3,4) and the order of subsequent experiments with the same sample (a,b,c,...).

Maximal uncertainties: T ± 10 K; P ± 3 MPa; density ± 0.01 g/cm^3; sphere radius ± 2 µm; distance ± 2 %; time ± 83 seconds; viscosity ± 15%. Images used for viscosity calculation are given in the appendix of this work.

C.5.2. Micropenetration

The temperature, water content and viscosity of conducted micropenetration experiments are given in table C.3. The absolute shear viscosity of micropenetration experiments is determined by the following equation:

$$\eta = \frac{0.1875 \cdot F \cdot t}{\sqrt{r} \cdot \sqrt{l^3}} \qquad [C.5]$$

(Pocklington, 1940), where η is the viscosity, F the applied force given by the used weight and the gravitational force, t the experimental duration, r the radius of the sphere and l the penetration depth. The uncertainty of the micropenetration apparatus was determined from measurements of a standard glass from the Deutsche Glastechnische Gesellschaft e.V. (DGG) to be 0.06 log units.

Table C.3 Experimental conditions and results for micropenetration experiments

experiment	H_2O [wt%]	[mol%]	Li_2O [mol%]	T [K]	*Log η* [η in Pa*s]
m PEG3-base-1a	1.08 (0.06)	3.89		901	10.25 (0.06)
m PEG3-base-1b				875	10.73 (0.06)
m PEG3-base-1c				849	11.11 (0.06)
m PEG3-base-1d				927	9.99 (0.06)
m PEG3-base-3a	3.10 (0.06)	10.60		777	9.94 (0.06)
m PEG3-base-3b				725	10.96 (0.06)
m PEG3-base-3c				694	11.76 (0.06)
m PEG3-base-4a	***4.05*** **(0.06)**	13.53		715	10.40 (0.06)
m PEG3-base-4b				689	11.10 (0.06)
m PEG3-base-4c				663	11.71 (0.06)
m PEG3-Li-1a	0.99	3.48	2.97	930	10.16 (0.06)
m PEG3-Li-1b				904	10.57 (0.06)
m PEG3-Li-1c				878	11.15 (0.06)
m PEG3-Li-1d				853	11.74 (0.06)
m PEG3-Li-3a	3.11	10.36	2.76	762	10.64 (0.06)
m PEG3-Li-3b				749	10.90 (0.06)
m PEG3-Li-3c				735	11.50 (0.06)
m PEG3-Li-3d				709	12.23 (0.06)
m PEG3-Li-4a	3.67	12.06	2.70	772	9.75 (0.06)
m PEG3-Li-4b				747	10.41 (0.06)
m PEG3-Li-4c				721	10.90 (0.06)
m PEG3-Li-4d				695	11.59 (0.06)
m PEG3-Li-4e				668	12.40 (0.06)
m PEG3-KLi-1a	1.04	3.65	2.96	810	10.17 (0.06)
m PEG3-KLi-1b				794	10.50 (0.06)
m PEG3-KLi-1c				768	10.86 (0.06)
m PEG3-KLi-1d				756	11.44 (0.06)
m PEG3-KLi-1e				742	12.00 (0.06)
m PEG3-KLi-1f				724	12.40 (0.06)
m PEG3-KLi-3a	3.11	10.36	2.76	698	10.10 (0.06)
m PEG3-KLi-3b				672	10.80 (0.06)
m PEG3-KLi-3c				646	11.70 (0.06)
m PEG3-KLi-3d				620	12.50 (0.06)
m PEG3-KLi-4a	4.04	13.16	2.67	644	10.50 (0.06)
m PEG3-KLi-4b				620	11.35 (0.06)
m PEG3-KLi-4c				594	12.30 (0.06)
m PEG3-KLi-4d				631	11.00 (0.06)

Characters in the sample name refer to micropenetration technique (m), base composition (e.g. PEG3-base), the synthesized sample (1,2,3,4) and the order of subsequent experiments with the same sample (a,b,c,...).

H_2O contents measured by KFT and IR (***italic***)

C.6. Experimental results

The results of the viscosity determination for the compositions PEG3-base (from Bartels et al., submitted), PEG3-Li and PEG3-KLi are shown in figure C.2a-C.2c and are given in table C.2 and C.3. In the low viscosity range, the measured viscosity data range from $2.5 \cdot 10^4$ Pa·s

(for PEG3-Li at 1374 K and 1.07 wt% H_2O) to $1.0 \cdot 10^2$ Pa·s (for PEG3-KLi at 1379 K and 6.13 wt% H_2O). In the high viscosity range, values between $3.2 \cdot 10^{12}$ Pa·s (for PEG3-KLi at 620 K and 3.11 wt% H_2O) and $5.6 \cdot 10^9$ Pa·s (for PEG3-Li at 772 K and 3.67 wt% H_2O) were measured.

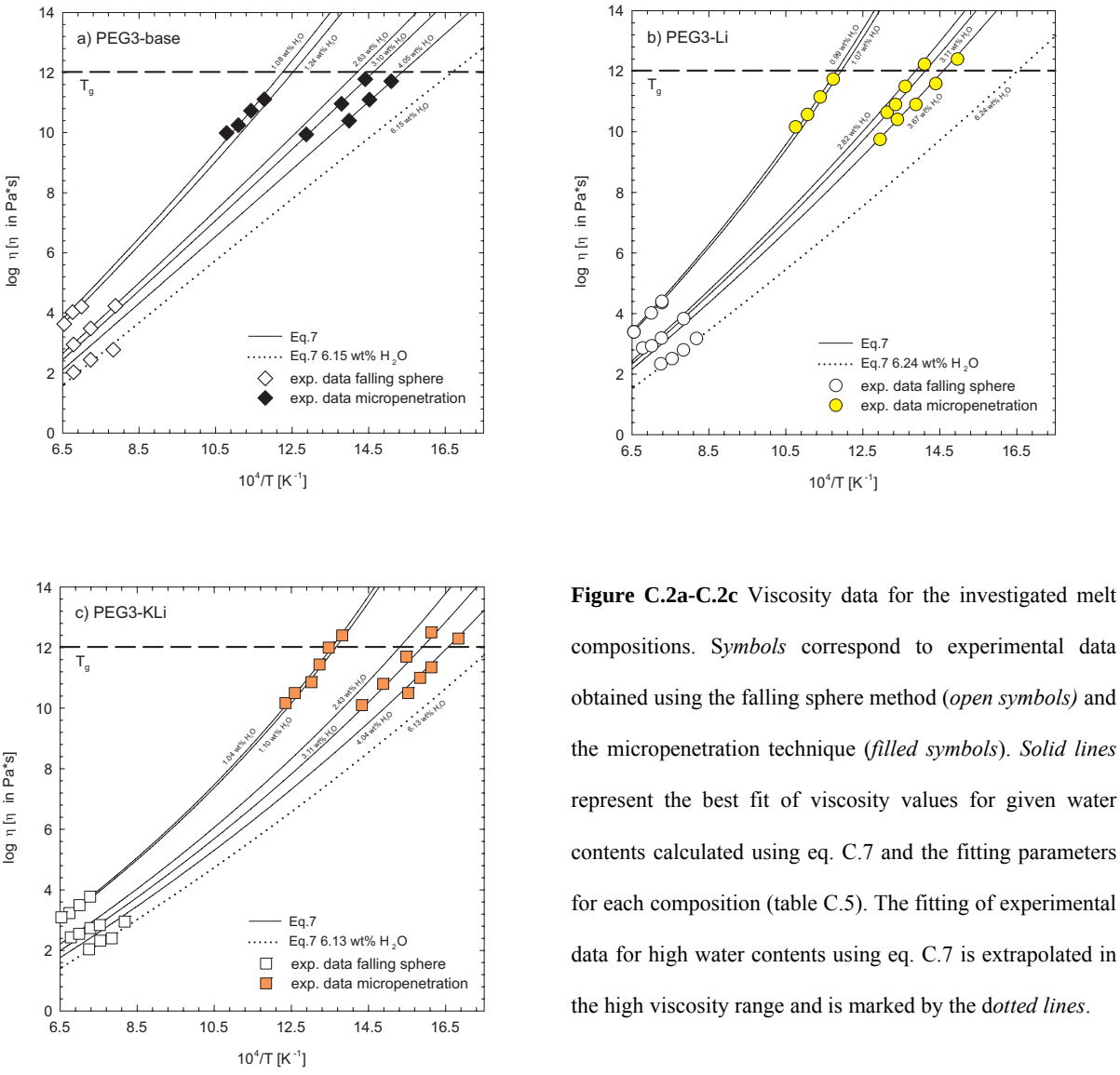

Figure C.2a-C.2c Viscosity data for the investigated melt compositions. S*ymbols* correspond to experimental data obtained using the falling sphere method (*open symbols)* and the micropenetration technique (*filled symbols*). *Solid lines* represent the best fit of viscosity values for given water contents calculated using eq. C.7 and the fitting parameters for each composition (table C.5). The fitting of experimental data for high water contents using eq. C.7 is extrapolated in the high viscosity range and is marked by the d*otted lines*.

To calculate the activation energy for viscous flow the single datasets of all compositions in the low and high temperature range were fitted separately by linear regression using the following Arrhenian equation:

$$\log \eta = \log \eta_0 + \frac{E_a}{2.303 \cdot R \cdot T} \qquad [C.6]$$

where η_0 is the pre-exponential factor, E_a the activation energy (kJ/mol) of the viscous flow, 2.303 is the conversion factor of ln to log, R the gas constant ($J \cdot mol^{-1} \cdot K^{-1}$) and T the temperature (K). The calculated values for $log\ \eta_0$ and E_a are given in Table C.4.

Table C.4 Activation energies and pre-exponential coefficients for viscosity

	sample	H_2O [wt%]	T range [K]	E_a [kJ/mol]	Log η_0 [η in Pa*s]	
	PEG3-base-1	1.24	1430-1529	243 (55)	-4.64	(1.94)
	PEG3-base-3	2.63	1269-1474	224 (3)	-4.99	(0.10)
	PEG3-base-6	6.15	1278-1474	136 (20)	-2.76	(0.76)
	PEG3-Li-1	1.07	1374-1526	261 (5)	-5.53	(0.17)
	PEG3-Li-3	2.82	1275-1475	182 (22)	-3.66	(0.82)
	PEG3-Li-6	6.24	1223-1379	175 (16)	-4.35	(0.64)
	PEG3-KLi-1	1.10	1374-1531	178 (11)	-2.99	(0.38)
	PEG3-KLi-3	2.43	1328-1475	109 (5)	-1.44	(0.18)
	PEG3-KLi-6	6.13	1223-1379	178 (36)	-4.71	(1.45)
m	PEG3-base-1a	1.08	849-927	224 (15)	-2.66	(0.87)
m	PEG3-base-3a	3.10	694-777	225 (10)	-5.22	(0.68)
m	PEG3-base-4a	4.05	663-715	228 (14)	-6.22	(1.05)
m	PEG3-Li-1	0.99	853-930	312 (14)	-7.39	(0.79)
m	PEG3-Li-3	3.11	709-762	323 (24)	-11.52	(1.73)
m	PEG3-Li-4	3.67	668-772	247 (8)	-6.94	(0.56)
m	PEG3-KLi-1	1.04	724-810	300 (26)	-9.29	(1.78)
m	PEG3-KLi-3	3.11	620-698	258 (7)	-9.24	(0.56)
m	PEG3-KLi-4	4.04	594-644	262 (8)	-10.70	(0.65)

1σ standard deviation is given in parentheses.

errors given in bracket are taken into account the uncertainty of regression lines

In the high temperature range, E_a decreases with increasing water content for PEG3-base and PEG3-Li (Fig. C.3a). This dependence on water is in good agreement with previous studies on natural and synthetic melt compositions (Dingwell, 1987; Persikov, 1991; Schulze et al., 1996; Holtz et al., 1999; Romano et al., 2001; Romano et al., 2003). The values for the PEG3-KLi composition are significantly lower at low water contents when compared to the other melt compositions but viscosity of all three melt compositions become similar at increased water contents.

In the low temperature range E_a values are typically higher and a decrease with increasing water content for PEG3-Li and PEG3-KLi is observable. In contrast, the PEG3-base composition shows similar values over the whole range of water concentrations (Fig. C.3b).

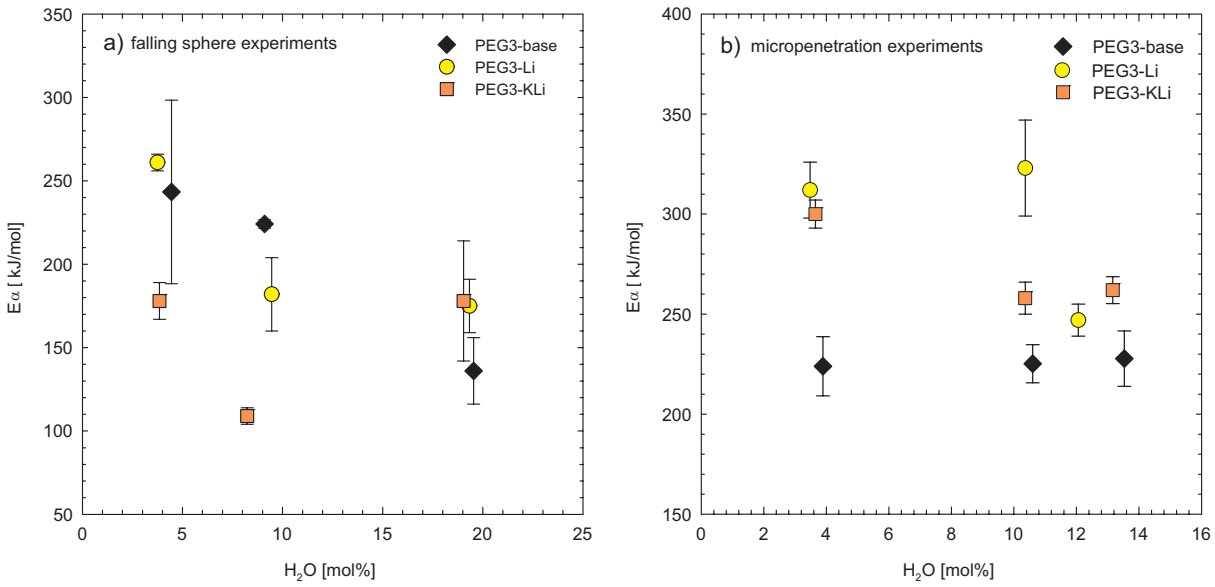

Figure C.3 Activation energies for viscosity as a function of water content calculated for each composition in the high (a) and low (b) temperature range. An Arrhenian behaviour has been assumed for both. Error bars take the uncertainty of the regression lines into account.

The observed difference in E_a between both methods is smaller than expected from previous viscosity studies and especially for the PEG3-base composition the E_a values of high and low temperature are almost equal. Within the total investigated temperature range of this study the viscosity data for each composition can be described by the following modified Tamann-Vogel-Fulcher equation (Romano et al., 2003):

$$\log\eta = a_1 + a_2 \ln w_{H_2O} + \frac{b_1 + b_2 w_{H_2O}}{T - \left(c_1 + c_2 \ln w_{H_2O}\right)} \qquad [C.7]$$

where η is the viscosity, a_1 a_2 b_1 b_2 c_1 *and* c_2 are fitting parameters, T is the temperature in Kelvin and w the water content in wt%. The results of the fitting parameters for each composition are given in Table C.5.

Table C.5 Fitting parameters for Eq. C.7

fitting parameters	PEG3-base	PEG3-Li	PEG3-KLi
a	-3.86	-3.83	-2.06
b	-0.8	-0.2	-0.6
c	10846	9410	6351
d	-2.0	-169.2	15.0
e	143.1	261.9	289.6
g	-92.6	-93.0	-82.0
Standard deviation (log η)	0.12	0.12	0.16

Strictly, this type of equation is only valid above T_g since the Tamann-Vogel-Fulcher model shows significant deviation to experimental data below T_g (Scholze, 1988). T_g values, defined by a viscocity of 10^{12} Pa·s, are indicated by dashed lines in figures C.2a-C.2c. However, the few data slightly above 10^{12} Pa·s do not significantly deviate from predicted trends and have also been considered in this study. The accuracy of the fitting curves can be evaluated by comparing the calculated and experimentally determined viscosity values. Considering the whole dataset, the experimental data are reproduced within an error of ±7 % except of experiment PEG3-KLi-3d where an error of ±10 % was determined, probably caused by the observed leakage during this experiment.

The fitting curves for the viscosity data based on the modified Tamann-Vogel-Fulcher model (Eq. C.7) are used to discuss the effect of lithium on viscosity of pegmatites. Because of the lack of experimental data in the high viscosity range, samples with high water contents (~ 6 wt% H_2O) were extrapolated towards low temperature considering the validity of the fitting (dotted lines in Figs. C.2a-C.2c) but are not included in the following discussion.

C.7. Discussion

C.7.1 Effect of lithium on the rheological properties of melt

C.7.1.1. Comparison of Li with other alkalis

Figure C.4 shows a plot of viscosity (expressed as log η) against water content (mol%) for the investigated melt compositions at 873 and 1473 K. As expected, the viscosity of all three melt compositions decreases with increasing water content. This decrease is more pronounced in the low temperature range and for low added water contents.

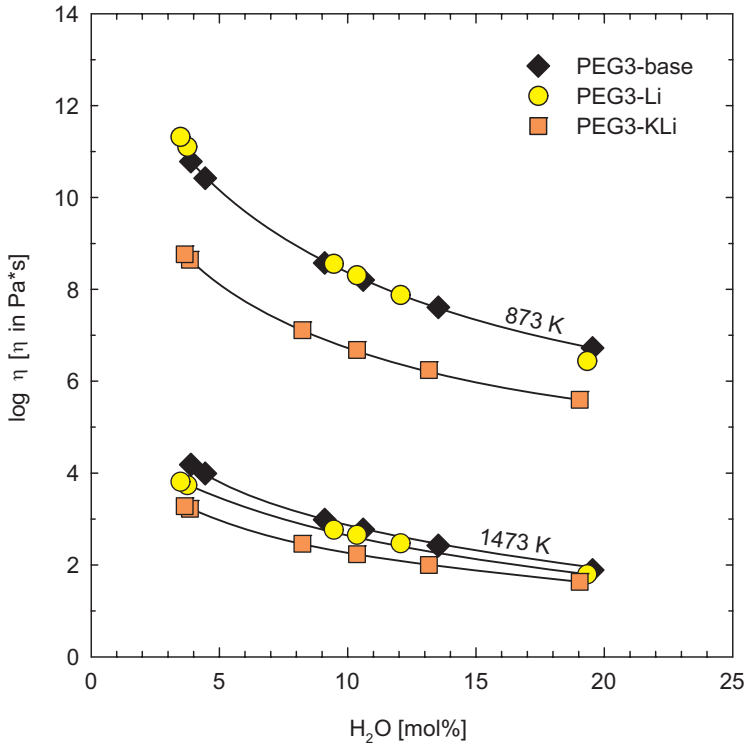

Figure C.4 Calculated viscosity values of PEG3-base, PEG3-Li and PEG3-KLi as a function of water content for 873 and 1473 K using eq. C.7.

When comparing the K_2O- and the Li_2O-bearing melt compositions (PEG3-base and PEG3-Li, respectively), no significant difference in viscosity can be observed at 873 K. At higher temperatures the viscosity is slightly decreased in the Li_2O-bearing composition, consistent with the expected effect due to different fragile behaviour of both melts (Fig. C.5).

Figures C.2a and C.2b also show, that the exchange of K_2O with Li_2O causes an increased non-Arrhenian behaviour of the melt. This trend can be described by the fragility (*m*), which allows distinguishing between strong and fragile glasses. In an Arrhenius plot (log η vs. 1/T), strong glasses show a linear behaviour, whereas fragile glasses show a curvature behaviour, normally described by an Vogel-Fulcher-Tamman equation (Angell, 1988). The fragility is given by the slope of viscosity curves (log η against reciprocal temperature) at the glass transition temperature (T_g) on a reduced temperature scale (Plazek and Ngai, 1991; Böhmer and Angell, 1992). The fragility *m* can be calculated by the following equation and is given in Table C.6:

$$m = \frac{B}{T_g \cdot \left(1 - \frac{C}{T_g}\right)^2} \qquad [C.9]$$

where *B* and *C* are the fitting parameters of the VFT equation. Smaller values of *m* are indicating a less fragile behaviour of the melt. Figure C.5 shows a plot of fragility against water content for the investigated melt compositions. The comparison of the PEG3-base with the PEG3-Li composition shows, that the fragility increases significantly, if lithium is incorporated into the melt structure (e.g. from ~19 to ~23 at 4 mol% H_2O). The change in fragility also implies an increase of the slope of the viscosity-temperature dependence in the high viscosity range and therefore affects the glass transition temperature (T_g). The glass transition temperature, taken to be the temperature where the viscosity is equal to 10^{12} Pa·s, was calculated for all investigated compositions by using the VFT-approach (log η = A+B/(T-C) and is shown in Figure C.6 and given in Table C.6. The substitution of 3.01 mol% K_2O with 3.07 mol% Li_2O causes a small increase of glass transition temperature of ~25 K.

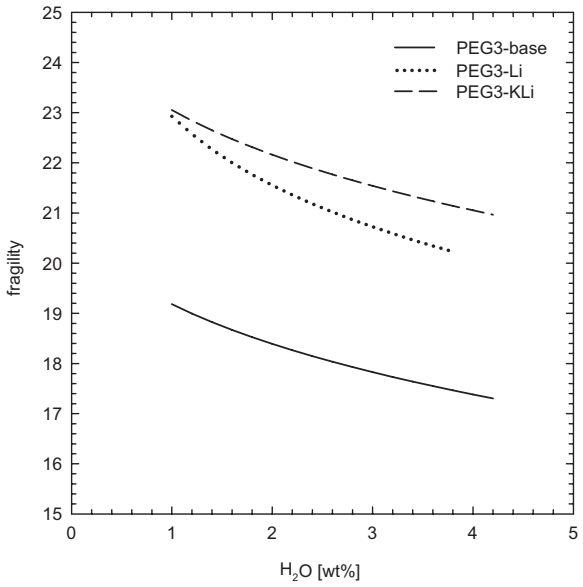

Figure C.5 Fragility (*m*) of glasses as a function of water content calculated using Eq. p and data from table C.5

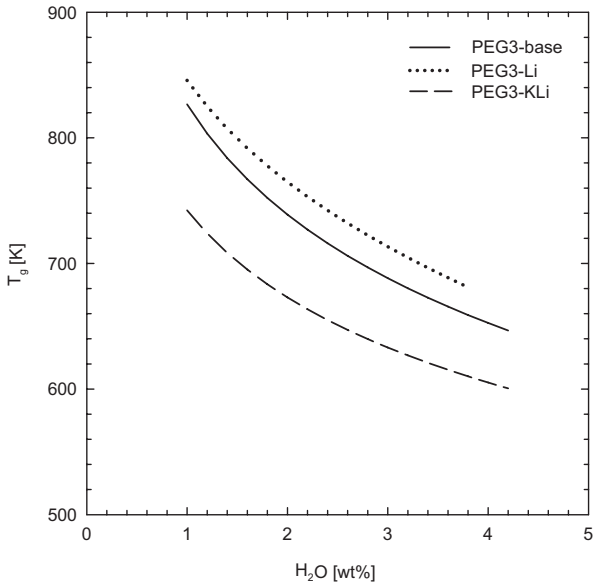

Figure C.6 Glass transition temperatures (calculated to be the viscosity at 10^{12} Pa·s using Eq. 7 and parameters listed in Table C.5) for the investigated melt compositions as a function of water.

In a slightly peraluminous melt, the alkali cation is charge balancing the Al^{3+} -ion in four fold coordination bonded to the surrounding oxygens. Thereby the smaller size and the higher cation field strength of the Li cation increase the bond strength with the surrounding bridging oxygens. Accordingly, the bond strength of these oxygens with another Al will be decreased. This is consistent with previous findings described by Navrotsky et al. (1985). According to them, the perturbation and weakening of the strong SiO and AlO bonds within the melt structure occurs with increasing potential of other atoms to compete with Si or Al for the bonding with oxygen. This potential increases with increasing cation field strength. Both, De Jong and Brown (1980) additionally proposed that the smaller alkalis Li and Na should exhibit a greater tendency to weaken the silicate structure rather than K, Rb, and Cs.

Table C.6 Calculated glass transition temperature, fragility and equilibrium constant for water speciation.

	H_2O [wt%]	A	B fitting parameter	C	T_g [K]	m	lnK
PEG3-base	1.08	-3.93	10843.53	135.97	817	19.11	-1.44
	1.24	-4.04	10843.22	123.18	799	18.96	-1.54
	2.63	-4.65	10840.50	53.57	705	18.02	n.d.
	3.10	-4.78	10839.58	38.35	684	17.78	-2.21
	4.05	-5.00	10837.73	13.60	651	17.36	-2.60
	6.15	-5.34	10833.62	-25.07	600	16.64	-2.89
PEG3-Li	1.07	-3.84	9228.83	255.60	838	22.80	-1.43
	0.99	-3.83	9242.37	262.82	847	22.95	-1.48
	2.82	-4.07	8932.71	165.51	721	20.85	-2.06
	3.11	-4.09	8883.64	156.41	709	20.65	-2.34
	3.67	-4.13	8788.89	141.02	686	20.30	-2.63
	6.24	-4.25	8354.01	91.67	606	19.15	-2.85
PEG3-KLi	1.10	-2.12	6366.98	281.74	733	22.94	-2.00
	1.04	-2.08	6366.08	286.34	738	23.01	-2.03
	2.43	-2.62	6386.93	216.74	654	21.87	-2.42
	3.11	-2.77	6397.13	196.51	629	21.48	-2.74
	4.04	-2.94	6411.08	175.05	604	21.03	-3.21
	6.13	-3.20	6442.44	140.86	565	20.25	-3.44

A, B and C are parameters for VFT fit: $\log \eta = A+B/(T-C)$

T_g is the temperature at which viscosity is 10^{12} Pa*s; *m* is the fragility parameter; *lnK* is the equilibrium constant for water speciation

C.7.1.2. The effect of changing A.S.I.

The comparison of the peraluminous composition PEG3-base with the peralkaline composition PEG3-KLi demonstrates, that the addition of 1.36 wt% Li_2O to the PEG3-base composition changes the Al / (Al + Na + Li) ratio from 1.16 to 0.88 (Tab. C.1). This change has a dramatically effect on melt viscosity because it changes the composition from a peraluminous to a peralkaline system. This shift causes a viscosity decrease at all investigated conditions (Fig. C.4). This decrease is more pronounced at low water contents and low temperatures and is around 2 log units at 873 K and ~5 mol% water.

The addition of Li_2O also causes a change in fragility and decreases T_g about ~80 K from ~820 to ~740 K at water contents of ~4 mol% (Fig. C.6). This drop in T_g with the addition of Li_2O decreases with increasing water content at is ~40 K at ~20mol% H_2O.

Due to the change from a slightly peraluminous to a peralkaline melt composition, caused by the addition of Li_2O, an additional mechanism will effect the melt structure. The excess of alkali cations leads to a depolymerisation of the silicate melt structure due to the formation of non-bridging oxygens (NBO´s) rather than just the weakening of bond strengths as described above (C.7.1.1.). Because of the higher cation field strength, the bond strength of Li with NBO´s is stronger when compared to other alkalis, which additionally causes a weakening of the AlO or SiO bonds.

C.7.1.3. Comparison of Li_2O with H_2O and F_2O_{-1}

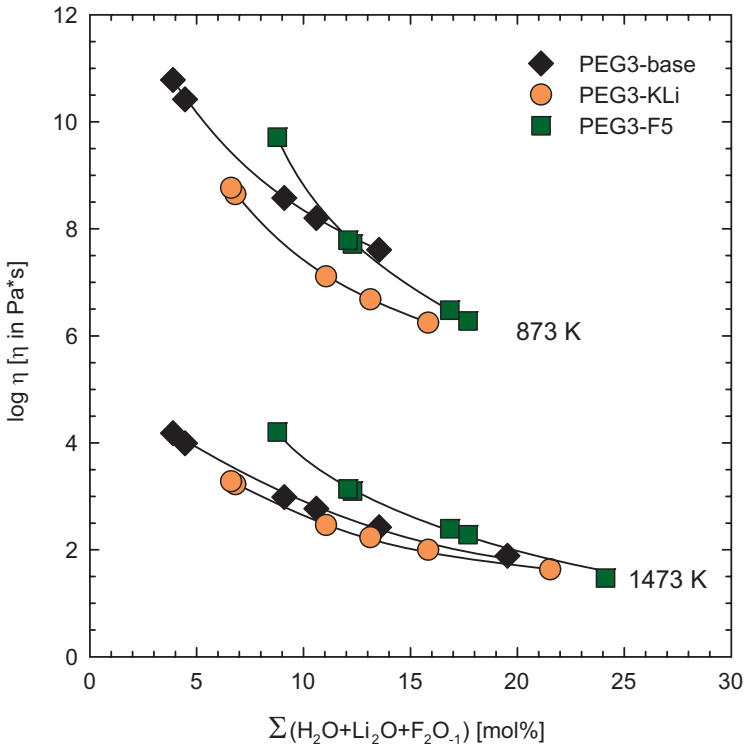

Figure C.7 Isothermal viscosities for 873 K and 1473 K for melt compositions PEG3-base, PEG3-KLi and PEG3-F5 (from Bartels et al. (submitted)) as a function of water lithium and fluorine content (expressed as molar sum of $H_2O+Li_2O+F_2O_{-1}$).

To which extent Li is influencing the melt viscosity when compared to other depolymerizing melt components like H_2O and F_2O_{-1} is still under debate. Figure C.7 shows a plot of viscosity

(expressed as log η) against the total molar content of the fluxes $H_2O + Li_2O + F_2O_{-1}$ at 873 and 1473 K. When comparing the PEG3-base with the PEG3-KLi composition at 873 K, H_2O is not as effective in lowering melt viscosity as Li_2O. This is a result of the incomplete dissociation of H_2O within the silicate structure, especially at low temperatures (Table C.7). At 1473 K this difference is negligible and could be explained by increased kinetic effects but also by the increasing ratio of OH/H_2O_m (H_2O_m = molecular H_2O) with increasing temperature (Table C.7). Considering, that the effect of H_2O_m on melt viscosity is negligible, a comparison between the effect of Li_2O and H_2O^* (water content which effectively dissociates into OH^- groups) on melt viscosity is shown in Figure C.8.

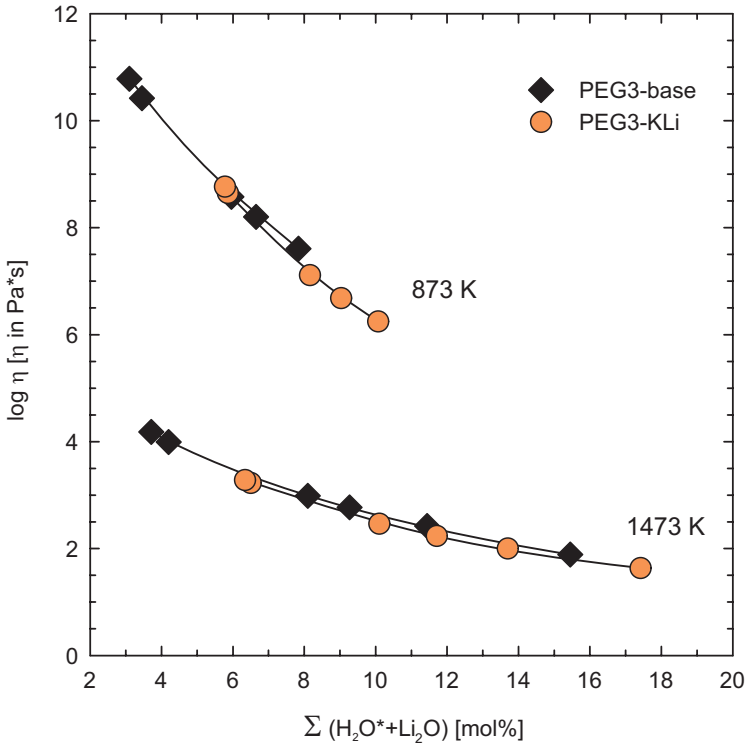

Figure C.8 Isothermal viscosities for 873 K and 1473 K for melt compositions PEG3-base and PEG3-KLi as a function of water and lithium content (H_2O^* = water content which effectively dissociates into OH^- groups)

To calculate the water speciation of both compositions for 873 and 1473 K the equilibrium constant (K) had to be determined following the procedure described in detail by Bartels et al. (submitted) using the following equation:

$$K = \frac{(OH)^2}{(H_2O)\cdot(O)} \qquad [C.8]$$

where parentheses are representing the molar fractions calculated on a single oxygen basis.

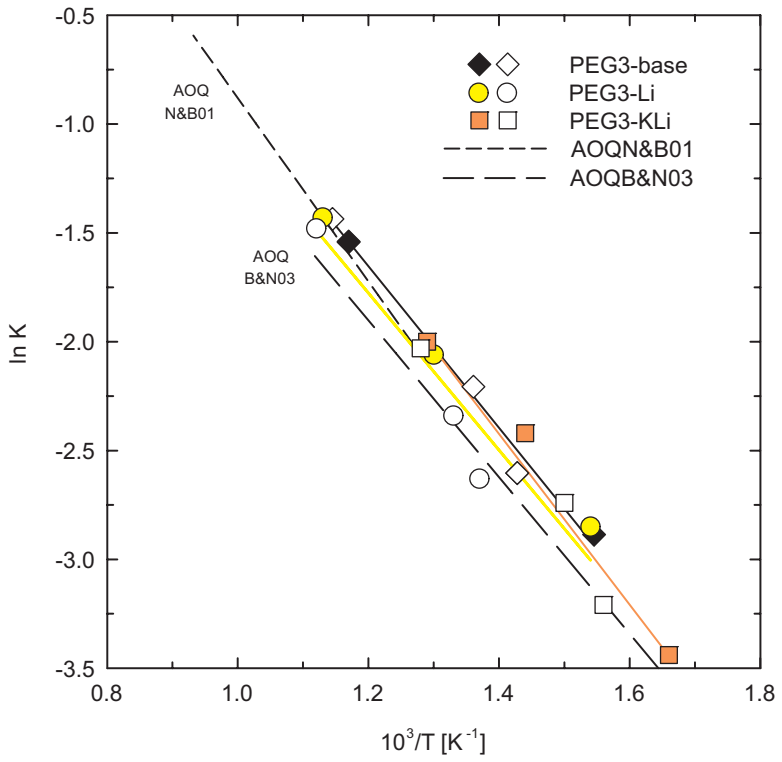

Figure C.9 Comparison of equilibrium constants for water speciation (*lnK*) in the investigated silicate melts. *Open symbols* refer to micropenetration experiments, *filled symbols* refer to falling sphere experiments. Data from Nowak and Behrens (2001) and Behrens and Nowak (2003) for the AOQ melt composition are given for comparison.

Figure C.9 shows a plot of *lnK* against the calculated fictive temperatures (T_f, expressed as $10^3/T_f$ [K^{-1}]) for all melt compositions. Additional data for the AOQ composition from Nowak

and Behrens (2001) and Behrens and Nowak (2003) are given. The *lnK* values for all composition are similar indicating similar ratios of OH and H_2O_m for all compositions at given T_f and H_2O content. Using linear regressions the equilibrium constants can be calculated for any given temperature and the water speciation for composition PEG3-base and PEG-KLi can be determined. The data shows, that the fraction of OH at the chosen temperatures (873 and 1473 K) is similar for both compositions (Table C.7) as expected from the similarity of the equilibrium constants.

Table C.7 calculated water speciation for 873 K and 1473 K

	H_2O [mol%]	OH [%]	C_{H2Om} [mol%]	C_{OH} [mol%]	log vis [vis in Pa*s]
PEG3-base	3.89	79.32	0.79	3.27	10.78
at 873 K	4.45	77.37	1.00	3.64	10.42
	9.10	65.34	3.14	6.28	8.58
	10.60	62.50	3.95	7.00	8.20
	13.53	57.82	5.69	8.24	7.61
	19.54	50.54	9.60	10.41	6.72
PEG3-KLi	3.85	79.06	0.85	3.22	8.65
at 873 K	3.65	79.83	0.74	3.11	8.76
	8.23	66.69	2.80	5.82	7.11
	10.36	62.44	3.99	6.82	6.68
	13.16	57.86	5.67	8.02	6.24
	19.04	50.60	9.54	10.14	5.60
PEG3-base	3.89	95.05	0.18	3.92	4.18
at 1473 K	4.45	94.38	0.25	4.43	3.99
	9.10	89.11	1.00	8.54	2.99
	10.60	87.52	1.33	9.76	2.77
	13.53	84.55	2.09	12.02	2.42
	19.54	78.92	4.09	16.18	1.89
PEG3-KLi	3.85	94.96	0.21	3.89	3.22
at 1473 K	3.65	95.22	0.18	3.71	3.28
	8.23	89.82	0.85	7.87	2.46
	10.36	87.49	1.31	9.65	2.24
	13.16	84.59	2.03	11.85	2.00
	19.04	78.98	4.01	15.93	1.63

C_{H2Om}: molecular water

water speciation calculated using linear regression of *lnK* vs. 1/T relationship

Additionally, when separating the effect of OH on melt viscosity, as shown in figure C.8, the effect is comparable to that of the addition of Li_2O. This observation is in contrast to the suggestions from Schulze et al. (1996). Assuming, that molecular H_2O has no effect on melt

viscosity, they concluded that H_2O is more effective in reducing melt viscosity than Li_2O and suggested that the viscosity of melt is directly related to the radii and electric-field strength of the cations following the previous findings from Hess et al. (1995), who reported an increase of viscosity with increasing size of added alkalis to a peralkaline melt. One reason for these different observations could be related to the fact, that previous studies compared the individual effects of either H_2O or different alkalis whereas this study investigates the combined effect of Li_2O and H_2O within the PEG3-KLi composition and no data on dry Li_2O-bearing melt is available.

As described by Giordano et al. (2004) and Bartels et al. (submitted), the incorporation of F into the silicate network is different in water-poor and water-rich melts, changing from complex forming to substitution for bridging oxygens with increasing H_2O content. This explains the minor decreasing effect on melt viscosity at total contents of F_2O_{-1} + H_2O + Li_2O below 12 mol% shown in Figure C.7. According to Bartels et al. (submitted) the decreasing effect of F_2O_{-1} increases and might be more important than that of H_2O at higher water contents, assuming that OH^- groups act as network modifier whereas molecular H_2O has a minor affect on re-arrangement of the silicate network during viscous flow, and that all fluorine substitutes for bridging oxygens. This assumption is confirmed by the fact, that the curves for the F- and Li-bearing melt compositions seams to become one single line at high molar concentration of H_2O + Li_2O + F_2O_{-1} indicating a similar structural role of both components within the silicate melt.

C.7.2. Comparison to recent models

The two most recent multicompositional models to calculate silicate melt viscosities are the model of Hui & Zhang (2007) and the model of Giordano et al. (2008). Both models do not include Li_2O in their calculations. Nevertheless the accuracy of the model can be tested by

adding the Li_2O content as either Na_2O or K_2O, considering that the differences of the effect on melt viscosity between the single alkalis are small. Because of the higher similarity between Li_2O and Na_2O, the Li_2O content was added into the models as Na_2O. Figure C.10 shows the comparison of the experimentally determined data from this study and the calculated values using the model of Hui and Zhang (2007) (Fig. C.10a) and Giordano et al. (2008) (Fig. C.10b).

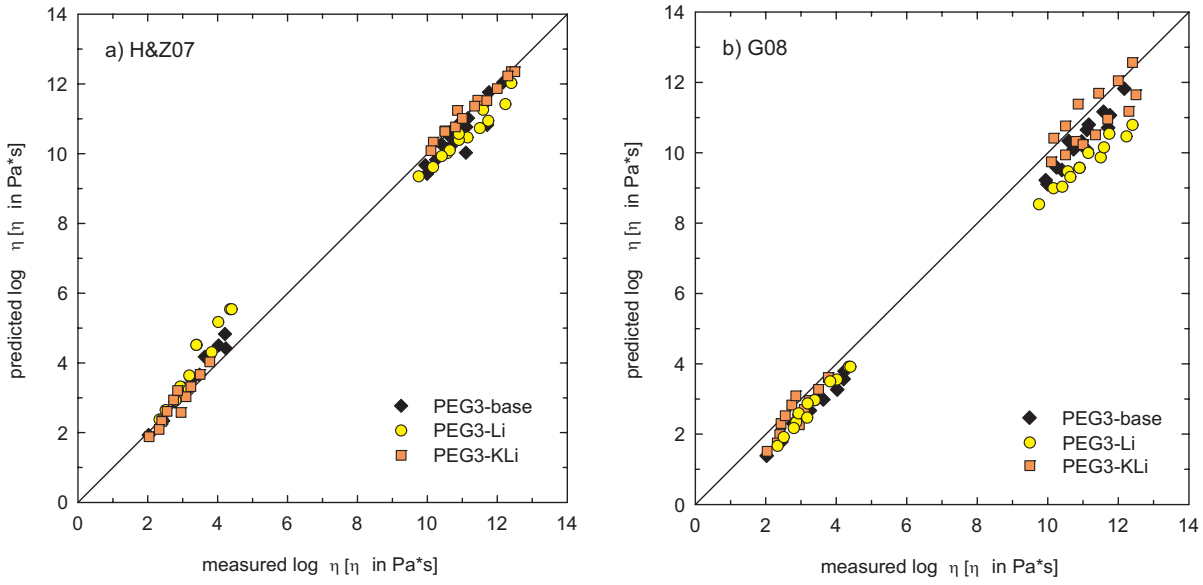

Figure C.10 Comparison of the experimental dataset with the predictions of the model of Hui and Zhang, 2007 (H&Z07) (a) and the model of Giordano et al., 2008 (G08) (b)

When using the model of Hui and Zhang (2007), the modelled values confirm the experimental data of this study. However, for melt composition PEG3-Li, some misfits could be observed in the low viscosity range, where the model overestimates melt viscosities by approximately 1 log unit. The experimental data for these misfits belong to the water-poor sample PEG3-Li-1 with ~1 wt% H_2O. This could be related to the higher decreasing effect of Li_2O on melt viscosity when compared to Na_2O, which is mainly related to differences of the cation field strength (see discussion C.7.1.1.).

When using the model of Giordano et al. (2008), especially in the high viscosity range, the prediction for the viscosity of the investigated melt compositions is less accurate when compared to the model of Hui and Zhang (2007), and a consistent underestimation of the viscosities for melt composition PEG3-Li can be observed. On the other hand, in the low viscosity range the model fits very well with the experimental data and does not show the misfits for water-poor samples as described for the model of Hui and Zhang. In summary, due to the rather small differences between the individual alkali cations (see discussion C.7.1.1. and Hess et al., 1995) in influencing melt viscosity, the prediction of melt viscosities for Li-bearing compositions is possible, by adding the Li_2O-content as Na_2O. Thereby, when looking at the complete temperature range the model of Hui and Zhang (2007) predicts viscosities more accurate, than the model of Giordano et al. (2008). However, to improve the prediction of the available models, the data of melt viscosities used for calibration of the models had to be extended with Li_2O bearing compositions.

C.7.3. Reasons for the low viscosities of pegmatite forming melts

Bartels et al. (submitted) concluded that beside water, fluorine is the main element influencing melt viscosity and that P and B do not play a major role on viscous flow in water-rich systems, from which pegmatites crystallize. However, according to their observations the depolymerising effect of both elements is not sufficient to explain very low viscosities of complex melts containing H_2O, F, B, P and Li. Accordingly they assumed, that Li will also play a major role in the rheology of pegmatitic systems. The experimental data of this study shows, that the progressive enrichment of Li within a pegmatitic system causes a decrease of the viscosity comparable to the depolymerizing effects of H_2O and F. To verify whether the additional effects of Li_2O, H_2O and F are sufficient to explain the low viscosity of a synthetic pegmatitic melt composition, the individual decreasing effects of Li_2O (known from PEG3-

KLi composition) and F_2O_{-1} (known from the PEG3-F5 composition, Bartels et al., submitted) where added to the water bearing PEG3-base composition. Figure C.11 shows the logarithmic viscosity against molar water content of the PEG3-base composition together with the individual effects of Li_2O and F_2O_{-1} for 873 K, a reasonable temperature for highly fractionated melts. Additionally the viscosity values for the synthetic pegmatite composition PEG2 from Bartels et al. (2011) are shown.

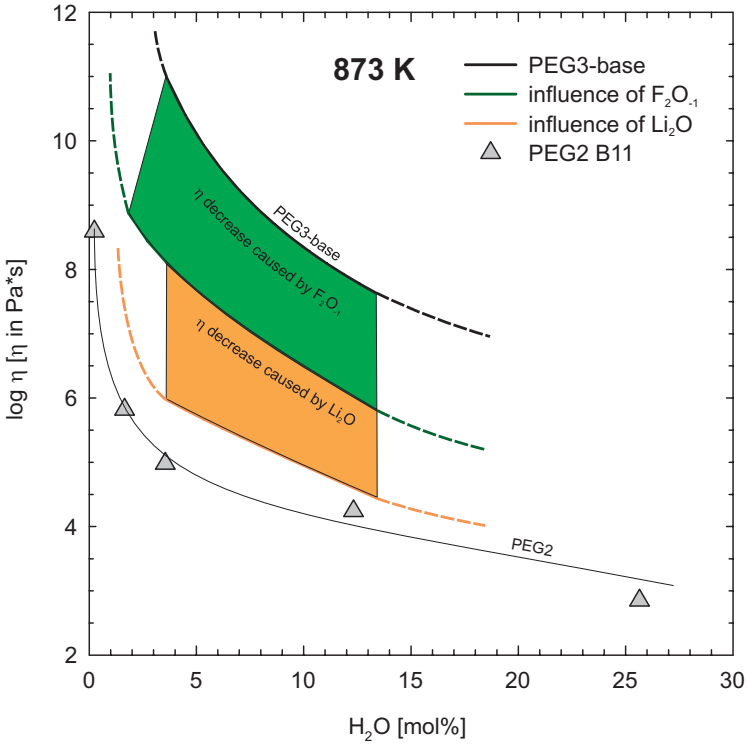

Figure C.11 Modeled viscosity decrease due to the addition of F_2O_{-1} and Li_2O to the PEG3-base composition using eq. C.7. Data for F_2O_{-1} from Bartels et al. (submitted). PEG2 from Bartels et al. (2011) (B11). Dashed lines are guide for the eyes.

Keeping in mind that the Li_2O and F_2O_{-1} contents are slightly higher in the PEG2 composition, compared to the PEG3-F5 and PEG3-KLi composition, the additive effects of these elements could reasonably explain the low viscosity of the synthetic pegmatitic melt composition. However towards lower water contents (< 10 mol%), the viscosity of the PEG2 composition increasingly deviate from the predicted viscosity caused by the combined

influence of Li_2O, F_2O_{-1} and H_2O. This could be related to coupled effects due to the interaction of all fluxes. Finally, the very low viscosities for the synthetic pegmatite forming melt composition PEG2 observed by Bartels et al. (2011) could be explained by the combined effects of all added fluxes, H_2O, F, Li, B, and P.

C.8. Conclusion

If lithium is enriched within a magmatic system, beside other fluxes, it will play a key role in controlling melt properties like fragility, activation energy, glass transition temperature and melt viscosity. It will also be one of the main constituent controlling the formation of boundary layers during pegmatite formation (London, 2008, p. 267 ff) and could keep the viscosity low even during the loss of other fluxes like H_2O or F due to diffusion or crystallization processes. In combination with the results of previous investigation on melt viscosity (Bartels et al., 2011; submitted), the data of this study also demonstrate, that the viscosity of highly fractionated melts are very low viscous mainly due to combined effects of H_2O, F_2O_{-1} and Li_2O. This also implies that even if water is lost from a magmatic system highly enriched in other fluxes, the viscosity can still be very low, which could be an important factor during pegmatite crystallization. However it has to be mentioned that Li_2O only effects melt viscosity by changing melt composition from peraluminous to peralkaline. In strong peraluminous systems, the effect of Li_2O will be less pronounced.

C.9. Appendix

Tabel C.A.1 Detailed experimental conditions and results for falling sphere experiments

sample	T [K]	P [MPa]	ρ_m [g/cm^3]	Mat.	r [µm]	d [m]	t [s]	Log η [η in Pa*s]
PEG3-base-1a	1479	200	2.29	Pt	147.5	0.002200	28800	4.03
PEG3-base-1b	1529	300	2.30	Pt	147.5	0.004090	21600	3.63
PEG3-base-1c	1430	200	2.30	Pt	147.5	0.003250	64800	4.21
PEG3-base-3a	1383	200	2.24	Pt	97.5	0.003030	24900	3.48
PEG3-base-3b	1474	300	2.24	Pt	97.5	0.001543	3695	2.95
PEG3-base-3c	1269	300	2.27	Pt	97.5	0.001872	86400	4.23
PEG3-base-6a	1383	300	2.11	Pt	90.5	0.008430	7200	2.44
PEG3-base-6b	1278	300	2.14	Pt	90.5	0.005870	10800	2.77
PEG3-base-6c	1474	300	2.09	Pt	90.5	0.003160	1036	2.03
PEG3-Li-1a	1428	300	2327	Pt	149	0.00173	21600	4.01
PEG3-Li-1b	1374	300	2333	Pt	149	0.00131	36000	4.36
PEG3-Li-1b	1374	300	2333	Pt	178	0.00166	36000	4.40
PEG3-Li-1c[1]	1526	300	2318	Pt	149	0.0033	9900	3.40
PEG3-Li-1c[1]	1526	300	2318	Pt	178	0.00467	9900	3.39
PEG3-Li-3a	1475	300	2241	Pt	139	0.00192	1911	2.86
PEG3-Li-3b	1275	300	2268	Pt	139	0.00273	25200	3.83
PEG3-Li-3c	1376	300	2254	Pt	139	0.00176	3697	3.19
PEG3-Li-3d	1426	300	2247	Pt	139	0.00266	3105	2.93
PEG3-Li-6a	1379	300	2115	Pt	97.5	0.00172	999	2.34
PEG3-Li-6b	1276	300	2135	Pt	97.5	0.00184	3085	2.80
PEG3-Li-6c	1223	300	2146	Pt	97.5	0.00182	7279	3.17
PEG3-Li-6d	1326	300	2125	Pt	97.5	0.00184	1593	2.51
PEG3-KLi-1a	1483	200	2312	Pt	141.5	0.00474	10800	3.23
PEG3-KLi-1b	1531	300	2307	Pt	141.5	0.00334	5522	3.10
PEG3-KLi-1c	1428	300	2318	Pt	141.5	0.00517	21600	3.50
PEG3-KLi-1d	1374	300	2325	Pt	141.5	0.00453	36000	3.78
PEG3-KLi-3a	1475	300	2251	Pt	139	0.00528	1965	2.43
PEG3-KLi-3b	1430	300	2257	Pt	137.5	0.00274	1357	2.55
PEG3-KLi-3c	1373	300	2265	Pt	137.5	0.00332	2547	2.74
PEG3-KLi-3d[1]	1328	300	2272	Pt	137.5	0.00374	3736	2.84
PEG3-KLi-6a	1379	300	2114	Pt	91	0.00299	998	2.04
PEG3-KLi-6b	1276	300	2135	Pt	91	0.004	3084	2.40
PEG3-KLi-6c	1223	300	2147	Pt	91	0.00265	7279	2.95
PEG3-KLi-6d	1326	300	2125	Pt	91	0.00246	1592	2.33

mat. = sphere material; r = sphere radius; d = falling distance; t = experimental duration; ρ_m = melt density

[1)] leak during experiment

Melt densities were calculated after the modified model of Ochs and Lange (1999).

Maximal uncertainties: T ± 10 K; P ± 3 MPa; density ± 0.01 g/cm^3; sphere radius ± 2 µm; distance ± 2 %; time ± 83 seconds; viscosity ± 15%

Part D

Melt-melt immiscibility in peralkaline pegmatitic systems

It often happens that new ideas in experimental petrology rise from unintended results of experiments. The idea and the experimental investigations of this part are based on a visco sity run, which was conducted below the liquidus of the melt. Consequently crystallization started during experiment. When I looked at the experimental results in detail, the following pictures, showing the segregation of a second immiscible melt phase in direct contact to the crystallization front piques my interest.

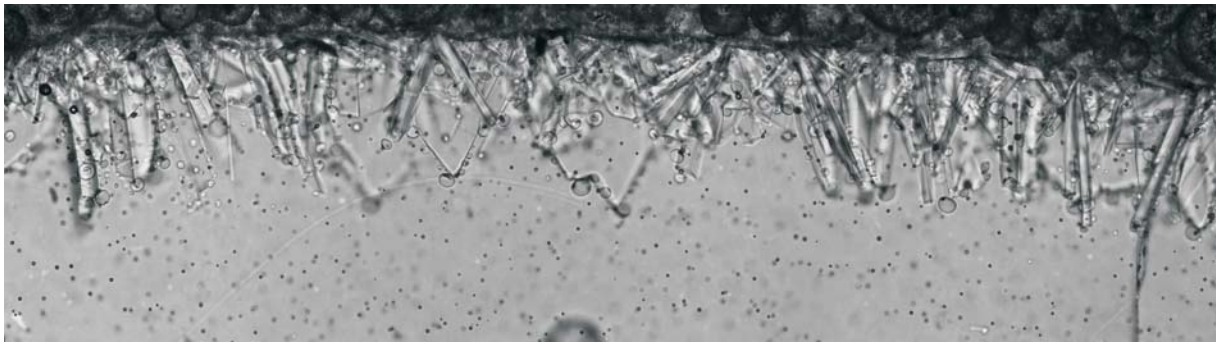

Evidences for liquid immiscibility in nature are the occurrence of fluid and melt inclusions hosted in different crystals found in pegmatites. The compositions of these inclusions are far off the typical compositions assumed for pegmatite bulk compositions. Although they might be the product of high fractionation at the end of crystallization or of boundary layer processes developed at the crystallization front, another possible explanation could be the formation of two immiscible melts during pegmatite crystallization. Recent experimental studies were able to reproduce liquid immiscibility in synthetic melts, giving new evidences, that this process is real in natural examples. This part will focus on the possible process leading to the formation of liquid immiscibility in highly fractionated melts and give new explanations for the complex story of pegmatite crystallization.

D.1. Abstract

A synthetic peralkaline melt with composition similar to natural pegmatitic examples was used to conduct crystallization experiments at 973 K and 200MPa. In samples with an initial water content of approximately 0.5 wt%, an additional immiscible melt phase segregated from the starting composition. This low density melt segregates from a boundary layer developed through rapid crystallization of feldspar in dynamic-crystallization experiments but also in normal crystallization experiments coexisting with aluminosilicate melt and feldspar crystals. Electron microprobe analyses show that the segregated melts in both types of experiments are almost similar and are mainly composed of Al_2O_3, Na_2O, F and P_2O_5. The segregation of an immiscible melt phase, which is highly enriched in F and P_2O_5 and effectively fractionates Na_2O from K_2O, gives new explanations for transport and crystallization processes within pegmatitic systems.

D.2. Introduction

Pegmatitic bodies, especially rare element pegmatites are among the most complex igneous rocks and show extreme enrichment in elements which are typically traces in other common rock forming melts. The formation of pegmatite bodies has been debated since decades (e.g. Jahns 1953a; Jahns and Burnham 1969; Černý 1991a). A classical model (Jahns and Burnham, 1969) suggests that pegmatites crystallize from coexisting highly fractionated silicate melt and aqueous fluid. More recent studies (e.g., London, 2008) showed that the role of undercooling and crystallization response might play an important role in the formation of pegmatite features rather than the crystallization from an aqueous liquid. Additionally, Nabelek et al. (2010) suggested that the retention of H_2O in pegmatite forming melts together with the degree of undercooling is the main factor causing pegmatitic textures.

In any case it is difficult to find a general model including all features observed in pegmatites because the crystallization is strongly dependent on cooling history of the melt, which might be dramatically different from one to another pegmatitic system. Beside, the possible occurrence of two or more immiscible melts might have a huge impact on crystallization processes and could explain some of the numerous textural observations in pegmatites.

Evidences for the occurrence of two coexisting melts are given by the fact that melt inclusions of different composition could be observed in natural pegmatite forming minerals. There are numerous studies investigating melt and fluid inclusions in pegmatite-related ore deposits (e.g., Webster et al. 1997; Thomas et al. 2000, 2003, 2005; Thomas and Webster 2000; Audétat and Pettke 2003; Kamenetsky et al. 2004). Additionally Rickers et al. (2006) accomplished a detailed study on natural melt and fluid inclusions from the Variscan Ehrenfriedersdorf pegmatite complex. Based on their study, Rickers et al. (2006) reported the separation of a natural melt with increasing fractionation into two coexisting immiscible phases and additional high-salinity brine, which segregates through the pegmatitic stage. More recently, Thomas et al. (2009) also reported the occurrence of immiscibility on the basis of fluid and melt inclusions hosted in beryl within the Stockscheider pegmatite of the Orlovka Massif in the Khangilay complex. They concluded that melt-melt- or melt-fluid-immiscibility are real processes in the evolution of pegmatites. Additionally volatile-rich melt fractions, although at low volume, can be efficient agents for material transport and segregation, whether volatiles, rare metals or aluminosilicates.

Experimental investigations on liquid immiscibility are rather rare. Veksler et al. (2002) and Veksler and Thomas (2002) presented the first conclusive evidence for a three phase equilibrium in a synthetic water saturated strongly peraluminous silicate system which composition is close to natural rare element pegmatites. They observed coexisting aluminosilicate melt together with a hydrosaline melt, which was preserved as surface films on precipitating crys-

tals and interstitial fillings in glass-crystal aggregates. The hydrosaline melt was highly enriched in B (15.6 wt%), F (17.5 wt%) and H_2O when compared to the starting glass and effectively fractionates Na from K.

So far melt-melt immiscibility was demonstrated experimentally in nearly water-saturated conditions (excess water). Here, we present the first experimental data showing that immiscibility is also observable at water-undersaturated conditions in a peralkaline system with bulk composition, which is expectable for highly fractionated rare-element pegmatites. We also demonstrate that immiscible melts may form close to the interface between melt and minerals as a result of rapid growth of crystalline phases.

D.3. Experimental and analytical methods

D.3.1. Starting material

For the experimental investigations of this study, the PEG2 composition synthesized by Bartels et al. (2010) was used. The synthesis of melt composition PEG2 is described in detail by Bartels et al. (2010).

The major element composition of the glass was analyzed by electron microprobe. The lithium concentration was determined by inductively coupled plasma optical emission spectrometry (ICP-OES). Additionally, Al-, Na- and K-contents were measured with this method to check the analytical data obtained with microprobe dataset. Boron and fluorine concentrations were analyzed commercially (Actlabs/Canada). The PEG2 glass composition is given in Table D.1. The molar ratio Al/(Na+K+Li) ($A.S.I._{Li}$) is 0.92. The Li-free ratio Al/(Na+K) (A.S.I.) is 1.26.

D.3.2. Experimental setup

Two different approaches were pursued to conduct crystallization experiments with water bearing glass powder; normal crystallization experiments from a glass powder and dynamic-crystallization from a homogeneous glass cylinder. The later approach causes the formation of a crystal growth front, starting at the rim of the glass body towards the centre. For dynamic-crystallization, a glass cylinder containing 0.5 wt% water was synthesized in an internally heated gas pressure vessel (IHPV) with Ar as pressure medium at 1273 K, 200MPa and 24h. After synthesis, this glass body was clear and free of crystals. In a second step, a part of the cylinder was welded shut in a gold capsule and the dynamic-crystallization experiment was conducted in an IHPV at 973 K and 200MPa with run duration of 96 h. For normal crystallization experiment, the other part of the synthesized hydrous glass cylinder was grinded to a fine powder, welded shut into a gold capsule and brought to experimental conditions for 144 h using a CSPV. Temperatures were measured by using Pt-$Pt_{90}Rh_{10}$ (IHPV) and Ni-CrNi (CSPV) thermocouples. Quenching in both types of autoclaves was close to isobaric. In case of IHPV experiments an initial quenching rate of 200 K/min was attained by switching off the heating power of the furnace. In the CSPV a similar cooling rate was attained by removing the pressure vessel out of the furnace and using a compressed air flux around the vessel. All capsules were weighted after the experiments to ensure that no leaks occurred during the experiments.

D.3.3. Analytical methods

The compositions of the run products were determined using a Cameca SX-100 electron microprobe. For glass measurements 15keV accelerating voltage, 4nA beam current and a beam diameter of 10 μm were used. Counting times ranged from 4 s for Na up to 20 s in case of F and P. For analysis of the crystals 15keV accelerating voltage, 15nA beam current and a fo-

cussed beam were used. The respective standards for all measurements were albite (Na), wollastonite (Si), corundum (Al), orthoclase (K), apatite (P) and SrF_2 (F). Additionally, element mapping measurements were conducted for both samples using 15keV accelerating voltage, 40nA beam current, a focused beam with 0.1 s dwell time and a step size of 0.4 µm. This method also enables a qualitative analysis of boron.

D.4. Results

D.4.1. Dynamic-crystallization

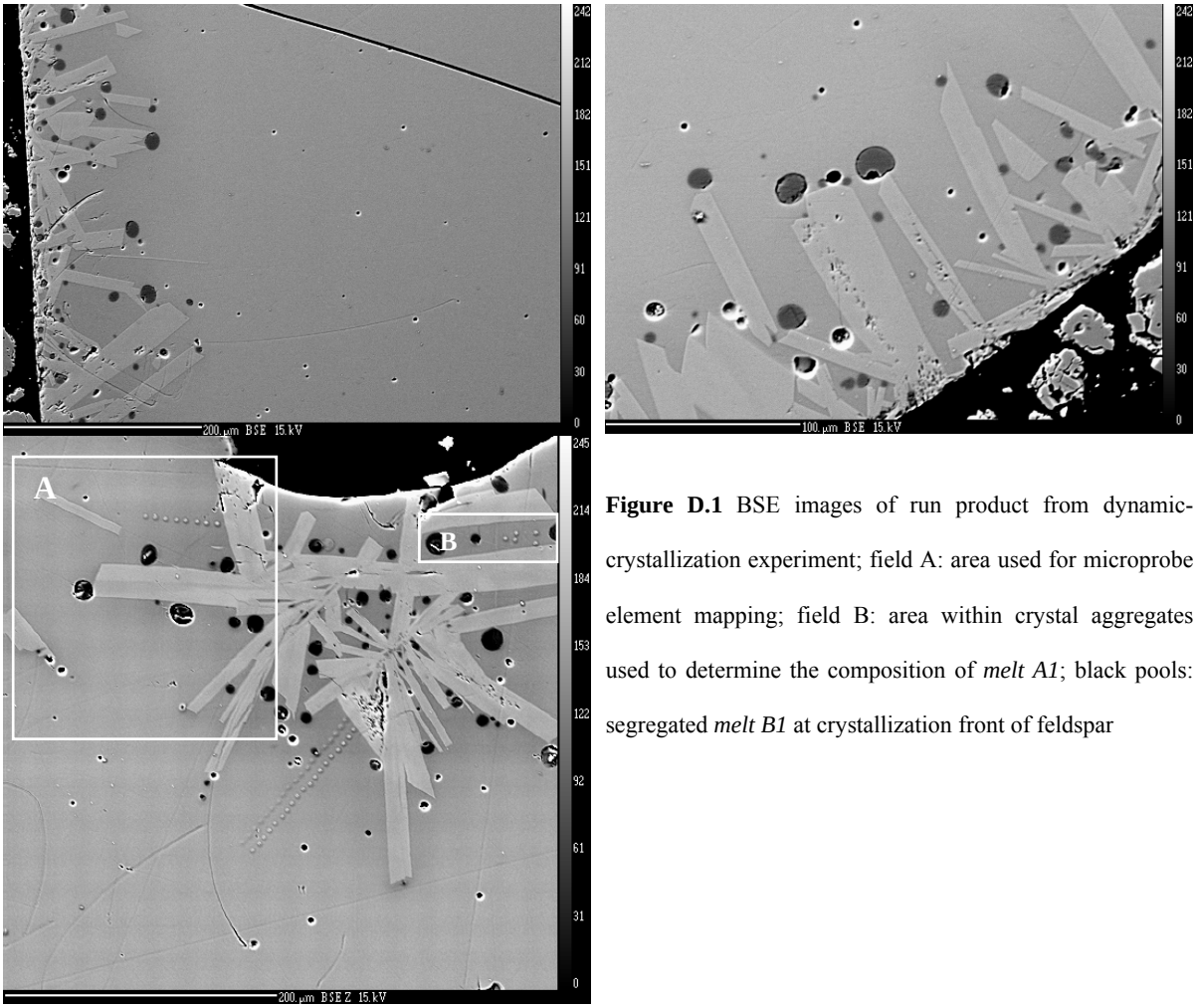

Figure D.1 BSE images of run product from dynamic-crystallization experiment; field A: area used for microprobe element mapping; field B: area within crystal aggregates used to determine the composition of *melt A1*; black pools: segregated *melt B1* at crystallization front of feldspar

Figure D.1 shows BSE images of the run product of the dynamic-crystallization experiment. The images show that crystallization of feldspar starts at the rim of the capsule wall towards the center and that the starting PEG2 melt composition segregated into two immiscible melt

fractions (*melt A1 (field B in Fig. D.1)* and *melt B1 (black pools around crystals, Fig.D.1)*). The compositions of the starting melt PEG2 and the two segregated melts *A1* and *B1* together with the composition of the formed crystals are given in Table D.1. All crystals show homogeneous feldspar composition of an Ab-rich alkali feldspar with approximately 1 wt% P_2O_5 incorporated by coupled exchange of $Al^{3+} + P^{5+} = 2\ Si^{4+}$.

Table D.1 analysis of starting composition and run products of dynamic-crystallization experiment

oxides	PEG2 [wt%]		melt A1 [wt%]		melt B1 [wt%]		crystals [wt%]	
SiO_2	59.73	0.13	51.36	0.87	0.21	0.04	66.77	0.46
Al_2O_3	19.75	0.13	20.19	0.42	25.21	0.30	20.64	0.25
Na_2O	7.25	0.10	7.32	0.31	11.90	0.50	10.05	0.19
K_2O	3.82	0.02	3.96	0.07	0.37	0.04	1.58	0.15
F	5.46	0.01	7.97	0.63	48.03	0.93		
P_2O_5	2.46	0.21	3.07	0.23	22.78	0.46	1.06	0.16
Li_2O	1.68	0.01	n.d.		n.d.			
B_2O_3	2.75	0.01	n.d.		n.d.			
2F = O	-2.30		-3.36		-20.22			
total	100.60		90.51		88.29		100.10	

1σ standard deviation is given in parentheses

mean of at least 10 electron microprobe analyses

Rest of melt A1 and B1 (~10 wt%) are probably Li_2O, B_2O_3 and H_2O

PEG2 composition taken from Bartels et al. (2010)

The composition of *melt A1* was measured between crystal aggregates (Fig. D.1, field B). The second *melt B1* formed melt pools at the crystallization front of the feldspar crystals. When comparing the PEG2 starting composition with the *melt A1* composition, the SiO_2 concentration is decreased by ~9 wt% from ~60 wt% down to ~51 wt%, whereas the F concentration is increased by ~2 wt% (5.46 wt% to 7.97 wt%) in the *melt A1* giving evidence for the formation of a boundary layer.

The segregated *melt B1*, located at the crystallization front of feldspar, has a dramatically different composition (Tab. D.1) mainly composed of F, Al_2O_3, P_2O_5 and Na_2O. This difference in composition between the two immiscible melts *A1* and *B1* becomes clear when looking at the results of the microprobe element mapping data of the sample (marked as field A in Fig.

D.1). Figures D.2a-D.2f are showing the element distribution of Si, Na, B, F and P in field A (Fig. D.1). The segregated *melt B1* is highly enriched in F and P when compared to *melt A1*. Although boron could not be determined quantitatively by microprobe, element mapping shows that this element is also highly concentrated within the segregates low density melt phase. Important to note is that no silica could be observed in this melt.

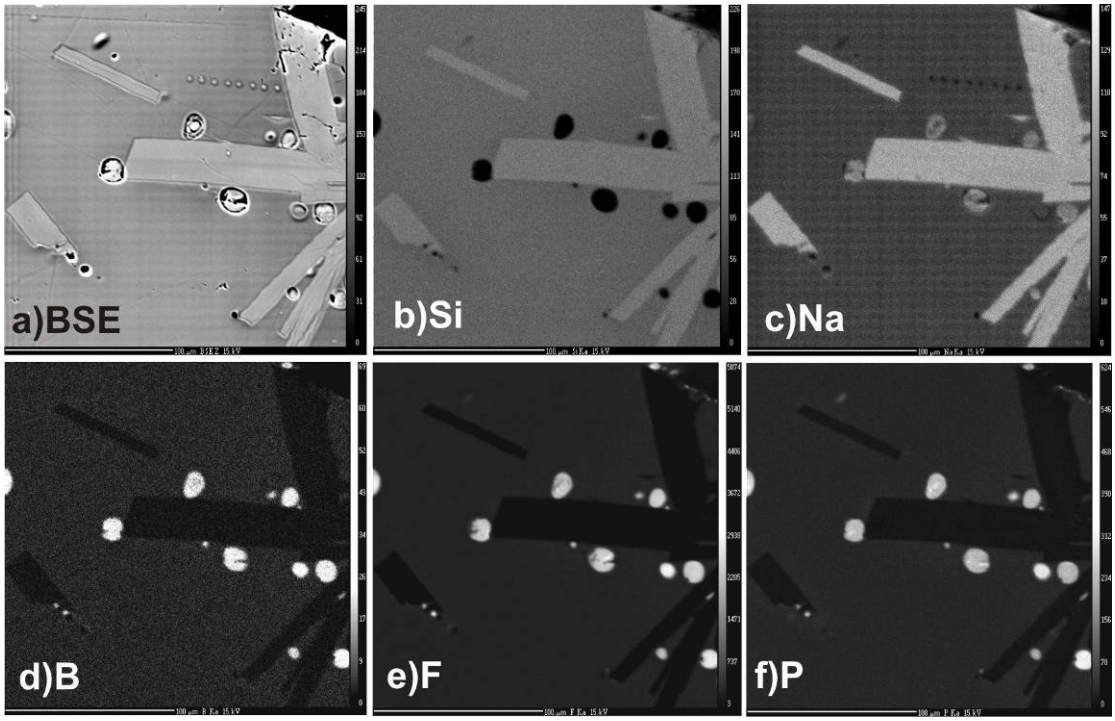

Figure D.2a-D.2f BSE image (a) and relative element distribution (b-f) in run product of dynamic-crystallization experiments. Contrast and brightness of pictures d, e and f are modified for visual clarity; therefore scale on the right side of the pictures is not transferable to images

D.4.2. Normal crystallization

Figure D.3 shows two BSE images of the run products of normal crystallization experiments. The crystallization from a glass powder promoted crystal growth all over the sample. Thereby different crystal sizes from a few µm up to 100µm could be observed. Again the PEG2 starting composition segregated into two immiscible melt compositions (*melt A2* and *B2*). The composition of *melt A2* was measured in crystal-free areas of the sample.

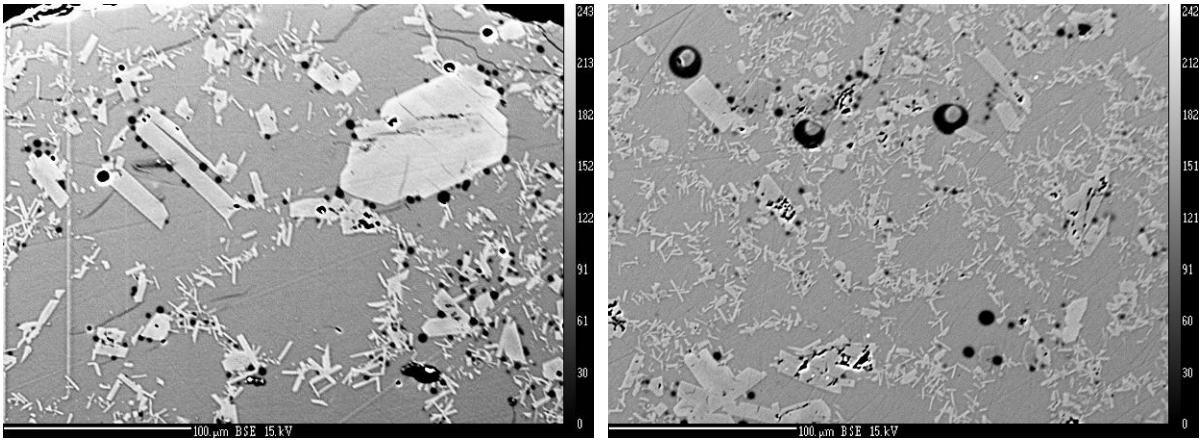

Figure D.3 BSE images of run products of normal crystallization experiments. (a) conducted in IHPV, 50 K/min heating ramp, 973 K, 200 MPa, 96 h and initial quenching rate of 200 K/min. (b) repeat experiment conducted in CSPV, ~25 K/min heating ramp, 973 K, 200 MPa, 144 h; Light grey: feldspar crystals; dark grey: *melt A2*; black pools around crystals: segregated *melt B2* Grey dots in black pools are microprobe hits.

The composition of *melt B2* was measured in the surrounding of large crystals where the largest immiscible melt pools could be observed. Both compositions are given in Table D.2.

Table D.2 analysis of starting composition and run products of normal crystallization experiments

oxides	PEG2 [wt%]		melt A2 [wt%]		melt B2 [wt%]		crystals [wt%]	
SiO_2	59.73	0.13	50.92	0.67	0.26	0.05	67.23	0.77
Al_2O_3	19.75	0.13	19.91	0.27	26.96	0.43	20.26	0.36
Na_2O	7.25	0.10	6.47	0.33	10.91	0.40	10.06	0.19
K_2O	3.82	0.02	4.49	0.10	0.54	0.05	2.03	0.41
F	5.46	0.01	8.60	0.67	48.91	0.81		
P_2O_5	2.46	0.21	3.45	0.13	21.60	0.50	1.13	0.22
Li_2O	1.68	0.01	n.d.		n.d.			
B_2O_3	2.75	0.01	n.d.		n.d.			
2F = O	-2.30		-3.62		-20.59			
total	100.60		90.22		88.59		100.71	

1σ standard deviation is given in parentheses

mean of 10 electron microprobe analyses

PEG2 composition taken from Bartels et al. (2010)

In comparison to the dynamic-crystallization experiment, *melt A2* and *B2* show similar compositions as melt *A1* and *B1*, although *A2* is slightly enriched in K_2O when compared to *A1*. The composition of the crystals is also similar to that determined in the dynamic-crystallization experiment.

D.5. Discussion

The experiments demonstrate that two immiscible melts can coexist in a pegmatitic system. In dynamic-crystallization experiments, the fast crystal growth from the border to the center of the capsule clearly shows that the oversaturation of the melt with elements which are not incorporated in the feldspar crystals leads to the formation of two immiscible melts in a boundary layer of approximately 100 µm.

D.5.1. Comparison to peraluminous systems

In previous crystallization experiments conducted with a synthetic peraluminous pegmatite, Veksler et al. (2002) reported the occurrence of melt immiscibility (formation of a second hydrosaline melt) in a broad P-T-range under water saturated conditions. However the only preserved immiscible melt pools are results of experiments conducted at 803 to 823 K and 200 MPa. Even though Veksler et al. (2002) recommended that, due to analytical problems, the given data for hydrosaline melt of their study should be treated as rough estimation, some similarities could be observed when compared to the segregated melt composition of this study (Fig. D.4). Although the concentrations of individual elements are significantly different, the relative abundance is similar. Both melts contain high amounts of aluminium and fractionate Na_2O from K_2O. They also contain high amounts of F although the concentration of this element is much higher in the immiscible melt phase of this study (~48 wt% compared to ~17 wt% in the hydrosaline melt from Veksler et al., 2002). Two significant differences are the concentration of SiO_2 and P_2O_5. The concentration of SiO_2 is ~23 wt% in the hydrosaline melt from Veksler et al. (2002) whereas no SiO_2 is incorporated in the immiscible low density melts of this study. This could be due to analytical problems in the study of Veksler et al. (2002) who reported extreme heterogeneity of the immiscible melt phase and the segregation of this melt into at least two different glasses and a number of crystalline solids during

quench. In case of P_2O_5, the immiscible melt phases of this study are strongly enriched in this component when compared to the starting glass composition (~22 compared to 2.46 wt%) whereas no significant enrichment is observable for the hydrosaline melt from Veksler et al. (2002) (2.58 compared to 5.00 wt% in their starting material).

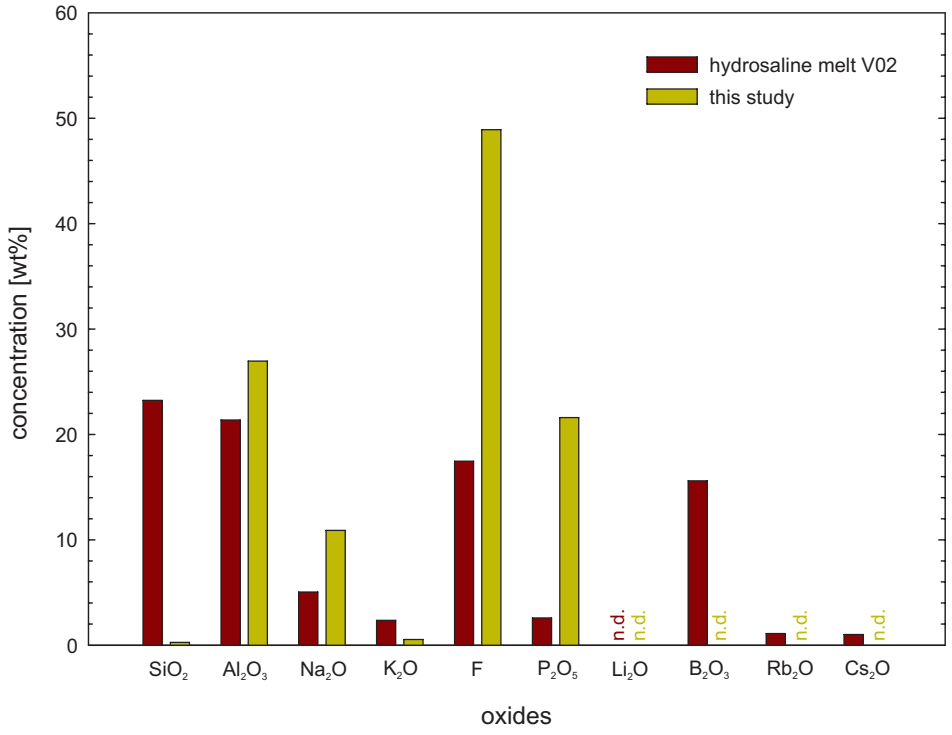

Figure D.4 Comparison of immiscible melt compositions from Veksler et al. (2002) (V02) and normal crystallization experiment of this study; n.d. = not determined

The comparison of oxides like Li_2O, B_2O_3, Rb_2O and Cs_2O is not possible because these components are either not determined in this study (Li_2O and B_2O_3) or are not included in the initial melt composition (Rb_2O and Cs_2O).

Although the comparison between the separated phases observed by Veksler and this study is difficult (differences in water content, initial melt composition and temperature), the new data show that melt-melt immiscibility is not only a process occurring in peraluminous systems. In fact it could also occur in peralkaline pegmatites and the composition of the segregated melt

shows significant similarities in relative abundance of elements when compared to peraluminous systems.

D.5.2. Implications for the formation of pegmatites

D.5.2.1. Impact on the boundary layer theory

Crystallization processes in pegmatites (or low viscosity systems) often occur under strong undercooling, which results in an enrichment of incompatible components at the crystallization front, and in a subsequent back-diffusion into the melt.

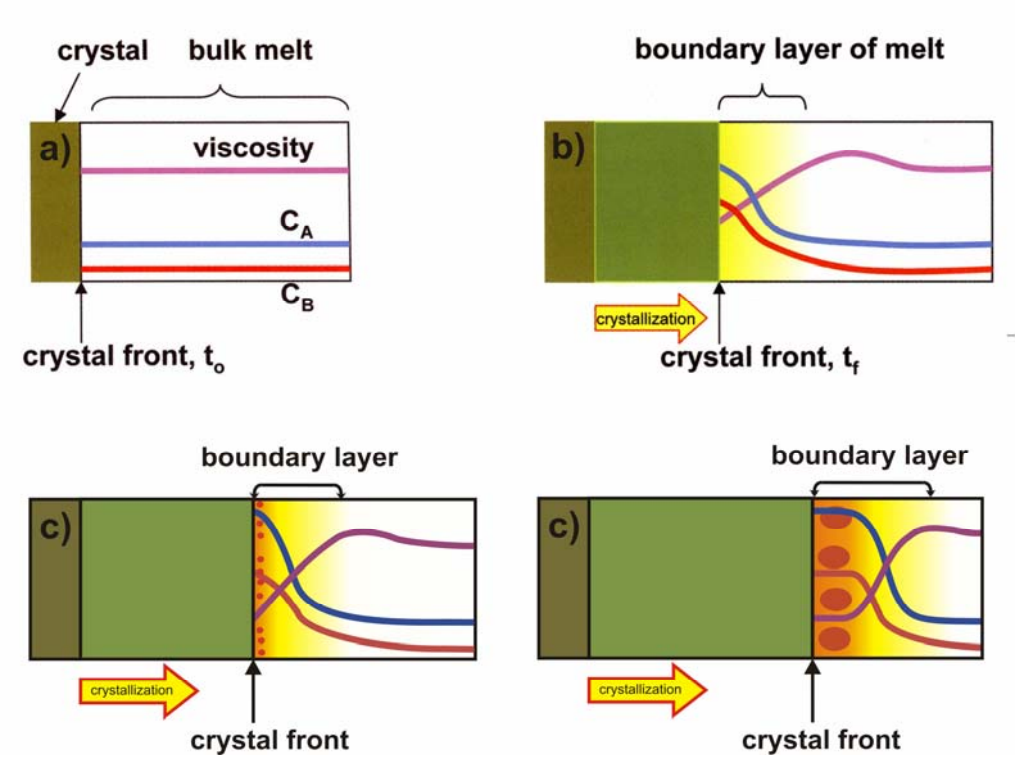

Figure D.5 Schematic illustration of the build-up of excluded components and of melt viscosity at a crystal-growth front (a and b after London, 2008; see text for details) and the segregation of a second immiscible melt (c and d).

Figure D.5a-D.5b show qualitatively the viscosity and the concentration of two components C_A and C_B (B diffuses faster than A) during a fast crystallization scenario after London et al. (2008 p. 267 ff). As a consequence the concentration (and the thermodynamic activity) of

non-deposited components such as water, F, B, Li and HFSE's may be strongly increased, which imposes fluxes of these components away from the crystallization front. The concentration profiles of components C_A and C_B shown qualitatively in Fig. D.5 are different because of the different diffusivities of elements.

Although the composition of the formed *melt A1* of the dynamic crystallization experiments do not show a typical boundary layer sequence for all elements, two main observations confirm the occurrence of a boundary layer in this experiment. First the depletion of SiO_2 in the glass surrounding the feldspar aggregates. This component together with Al_2O_3 and Na_2O is needed to build up the feldspar crystal. If the crystal growth rate is higher than the diffusivity of Si within the melt, the melt surrounding the feldspar crystal becomes progressively depleted in Si. The Al_2O_3 concentration in the glass is nearly identical to that of the formed feldspar and no change in Al_2O_3 is expected. Second the increased concentration of F in the same area. This element is incompatible for the crystallized feldspar and becomes progressively enriched in the surrounding melt. According to London (2008 p.224f) B, Li and H_2O are probably also enriched in such a boundary layer. However the analytical methods used in this work could not give any information about these melt components. The P_2O_5 content is only slightly enriched because of the incorporation of this element into the crystal structure of feldspar (Tab. D.1).

In our case study, the boundary layer development described by London (2008, p.268f) could be expanded by pictures c and d in Figure D.5. Due to an increased viscosity of the melt from the crystallization front (mineral-melt interface) towards the melt phase (~ 10^5 Pa*s at 973 K, Bartels et al., 2011) and therefore depressed back-diffusion of the incompatible elements into the surrounding melt, the melt at the crystallization front becomes progressively enriched in elements, which are not incorporated in the crystal structure of feldspar. At a specific point the melt becomes oversaturated and a second melt (*melt B1*) segregates. In this case the seg-

regated melt buffers the silicate melt in fluxing elements. On the other hand the occurrence of immiscibility and the formation of secondary melt pools highly enriched in fluxes could also act as reservoir for the boundary layer, buffering a possible loss of fluxes from that boundary layer for example due to crystallization or diffusion processes.

There are a few studies clearly indicating the presence of boundary layers in nature but also in experiments. Van Lichtervelde et al. (2007) described natural samples from the Tanco pegmatite and observed fine-grained aplite enriched in Ta oxides and F-rich mica between a giant K-feldspar crystal and dendritic amblygonite (see Fig.3 in van Lichtervelde et al. 2007). According to van Lichtervelde et al. (2007) in this case the dendritic amblygonite is evidence of high Li + P concentrations in a boundary layer and sequential crystallization of tantalum oxides and phosphates. The dendritic texture growing away from and perpendicular to the contact indicates rapid crystal growth. London (1999, 2005) conducted crystallization experiments with B-bearing haplogranitic melts and entrapped a boundary layer at the crystallization front of quartz and feldspar. The composition of this boundary layer is comparable to estimated compositions of B-rich melt inclusions in the Tanco pegmatite and these inclusions are therefore interpreted as trapped boundary layers. London (1999) additionally showed an experimental example in which cryolite (Na_3AlF_6) was entrapped by inclusions during rapid growth of synthetic quartz. Another experimental example is reported from Veksler et al. (2003) who observed berlinite ($AlPO_4$) in fluid inclusions hosted by quartz. These phases were interpreted to be precipitations from boundary layers “accidently trapped” in growing crystals. When looking at the compositions of *melt B1* and *B2* (Tab. D.1 and D.2) the described components like amblygonite, cryolite or berlinite, interpreted as crystallized boundary layers, are phases which would also crystallize most likely from these segregated low density melts. Accordingly the preliminary experiments of this study could deliver a new stage in the understanding

of the boundary layer model and offer new possible explanation for crystallization processes in pegmatites.

D.5.2.2. Impact on element transport

If melt immiscibility occurs during pegmatite crystallization, this would significantly influence material transport. In contrast to the formation of a boundary layer, the segregation of a complete new melt phase enables efficient element transport away from the crystallization front. The segregation of immiscible melts formed either in dynamic- or normal crystallization experiments could have strong impact on the distribution of HFSE´s and rare metals in pegmatite systems but also on alkali distribution. In many rare element granites an increased Na/K ratio could be observed. Plutons of typical alkali-calcic monzonite or calc-alkaline granite composition evolve roofward into a zone enriched in K-Fsp followed by albitic rocks. In addition to high concentrations of rare alkalis, niobium, tantalum and tin, the evolved albite rocks show enrichment of fluxes like F, P and in some cases B (London 2008, p.170). A similar trend could be observed in LCT pegmatite groups. With increasing distance to the source rocks, Na becomes progressively enriched within the melt and the most evolved and distal pegmatites are albite-lepidolite subtypes of the rare element class of pegmatites (Černý et al. 2005). Beside existing models, the formation of low density immiscible melt containing high concentrations of Na and almost no K (Tab. D.1/D.2) could give an additionally explanation of the fractionation of alkalis in pegmatitic systems under magmatic conditions and could explain the enrichment of sodic rocks in the upper parts of these systems. Also the increasing concentration of fluxes could be explained by transport processes through the segregated low density melt, observed in the experimental products of this study.

D.5.2.3. Impact on crystallization of HFSE- and other rare metal phases

Bartels et al. (2010) showed that the solubility of rare metals such as Nb and Ta is increased in pegmatitic systems when compared to haplogranitic systems and is strongly dependent on the presence of fluxing elements. As described above, van Lichtervelde et al. (2007) observed Ta mineralization correlated to boundary layer effects. On the other hand, Veksler et al. (2012) showed that there is no significant partitioning of Nb and Ta into fluoride melts but into phosphate melts.

The observed segregation of a F- and P-rich melt in the experiments of this study opens the question of HFSE and other rare metal behaviour. Due to the enrichment of P within the melt, partitioning of these elements into *melt B1 and B2* is expected. Assuming that transport processes due to a low density melt occur during crystallization, this could explain the described enrichment of Nb, Ta and tin in the evolved albite rocks found in the upper parts of rare element pegmatites. Accordingly beside observed associations of Nb and Ta with crystallized boundary layer structures, liquid immiscibility could give new explanation for ore-forming processes in pegmatitic systems, especially in rare-element and miarolitic pegmatites.

References

Angell, C.A., 1988. Perspectives: Perspective on the glass transition. *J. Phys. Chem. Solids* 49, 863-871

Audétat, A., Pettke, T., 2003. The magmatic-hydrothermal evolution of two barren granites: a melt and fluid inclusion study of the Rito del Medio and Caòada Pinatebe plutons in northern New Mexico (USA). *Geochim Cosmochim Acta* 67, 97–121

Audetat, A., Keppler, H., 2004. Viscosity of fluids in subduction zones. *Science* 303, 513-516

Baker, D.R., Vaillancourt, J., 1995. The low viscosities of F + H_2O-bearing granitic melts and implications for melt extraction and transport. *Earth and Planetary Science Letters* 132, 199-211

Bartels, A., Holtz, F., Linnen, R. L., 2010. Solubility of manganotantalite and manganocolumbite in pegmatitic melts. *Am Mineral* 95, 537-544

Bartels, A., Vetere, F., Holtz, F., Behrens, H., Linnen, R.L., 2011. Viscosity of flux-rich pegmatitic melts. *Contrib. Mineral. Petrol.* 162, 51-60.

Bartels, A., Behrens, H., Holtz, F., Schmidt, B.C., Fechtelkord, M., Knipping, J., Crede, L., Baasner, A., Pukallus, N., submitted. The effect of fluorine, boron and phosphorus on the viscosity of pegmatitic liquids. Submitted to *Chem. Geol.*

Behrens, H., Romano, C., Nowak, M., Holtz, F., Dingwell, D.B., 1996. Near-infrared spectroscopic determination of water species in glasses of the system $MAlSi_3O_8$ (M=Li, Na, K): an interlaboratory study. *Chem. Geol.*128, 41-63

Behrens, H., Nowak, M., 2003. Quantification of H_2O speciation in silicate glasses and melts by IR spectroscopy — in situ versus quench techniques. *Phase Transit.* 76, 45–61.

Behrens, H., Yamashita, S., 2008. Water speciation in hydrous sodium tetrasilicate and hexasilicate melts: Constraint from high temperature NIR spectroscopy. *Chem. Geol.* 256, 306-315.

Behrens, H., Zhang, Y., 2009. H_2O diffusion in peralkaline to peraluminous rhyolitic melts. *Contrib. Mineral. Petrol.* 157, 765-780

Benne, D., Behrens, H., 2003. Determination of water solubility in haplobasaltic melts using Karl-Fischer titration and IR spectroscopy on quenched glasses. *Eur. J. Mineral.* 15, 803-814.

Berndt, J., Liebske, C., Holtz, F., Freise, M., Nowak, M., Ziegenbein, D., Hurkuck, W., Koepke, J., 2002. A combined rapid-quench and H-2-membrane setup for internally heated pressure vessels: Description and application for water solubility in basaltic melts. *Am. Mineral.* 87, 1717-1726

Boettcher, S.L., Guo, Q., Montana, A. 1989. A simple device for loading gases in high-pressure Experiments. *Am. Mineral.* 74, 1383-1384

Boiret, M., Urbain, G., 1987. Mesures de viscosités d'aluminosilicates de lithium. *C. R. Acad. Sci. Paris série II* 305, 167-169

Böhmer, R., Angell, C.A., 1992. Correlations of the nonexponentiality and state dependence of mechanical relaxations with bond connectivity in Ge–As–Se supercooled liquids. *Phys. Rev.* B 45, 10091–10094.

Bray, P. J., 1978. NMR studies of borates. In: Pye L.D., Frenchette V.D., Kriedl, N.J., (Eds), Borate G1asses: Structure, Properties, Applications). *Materials Sci. Res*. 12. Plenum Press, New York, pp. 32l-351.

Černý, P., 1991. Rare-element granite pegmatites: Part I. Anatomy and internal evolution of pegmatite deposits. *Geoscience Canada* 18, 49-67

Černý, P., 1991a. Rare-element granite pegmatites.II. Regional to global environments and petrogenesis. *Geoscience Canada* 18, 68-81

Černý, P., Masau M., Goad B.E., Ferreira K., 2005. The Greer Lake Leucogranite, Manitoba, and the origin of lepidolite-subtype granitic pegmatites. *Lithos* 80, 305-321

Dell, W.J., Bray, P.J., Xiao, S.Z., 1983. ^{11}B NMR studies and structural modeling of Na_2O-B_20_3-SiO_2 glasses of high soda content. *J. Non-Cryst. Solids* 58, 1-16.

De Jong, B.H.W.S. and Brown, G.E.JR., 1980. Polymerization of silicate and aluminate tetrahedra in glasses, melts, and aqueous solutions-II. The network modifying effects of Mg^{2+}, K^+, Na^+, Li^+, OH^-, F^-, Cl^-, H_20, CO_2, and H_3O^+ on silicate polymers. *Geochim. Cosmochim. Acta* 44, 1627-1642.

Del Gaudi, P., Behrens, H., Deubener, J., 2007. Viscosity and glass transition temperature of hydrous float glass. *J. Non-Cryst. Solids* 353, 223-236.

Dingwell, D.B., 1987. Melt viscosities in the system $NaAlSi_3O_8$– H_2O–F_2O_{-1}. In: Mysen, B.O. (Ed.), *Magmatic Processes: Physicochemical Principles, Spec. Publ*., vol. 1. The Geochemical Society, Pennsylvania State University, University Park, PA, pp. 423–433.

Dingwell, D.B., Webb, S.L., 1990. Relaxation in silicate melts. *Eur. J. Mineral.* 2, 427–449.

Dingwell, D.B., Knoche, R., Webb, S.L., 1992. The effect of B_2O_3 on the viscosity of haplogranitic liquids. *Am. Mineral.* 77, 457-461.

Dingwell, D.B., Knoche, R., Webb, S.L., 1993. The effect of P_2O_5 on the viscosity of haplogranitic liquids. *Eur. J. Mineral.* 5, 133-140.

Dingwell, D.B., Hess, K.U., Knoche, R., 1996. Granite and granitic pegmatite melts: volumes and viscosities. *Transactions of the Royal Society of Edinburgh, Earth Sciences* 87, 65– 72.

Dingwell, D. B., Romano, C., and Hess, K. U., 1996a. The effect of water on the viscosity of a haplogranitic melt under P-T-X conditions relevant to silicic volcanism. *Contrib. Mineral. Petrol.* 124, 19–28.

Dingwell, D.B., Pichavant, M., Holtz, F., 1996b. Experimental studies of boron in granitic melts. In: Grew E.S., Anovitz L.M., (Eds.), *Boron: Mineralogy, Petrology and Geochemistry.* vol. 33. Mineral. Soc. Am. Rev. Mineral., Washington, DC, pp 331-385.

Dingwell, D.B., Hess, K.-U., Romano, C. 1998. Extremely fluid behavior of hydrous Peralkaline rhyolites. *Earth Planet Sci Lett* 158, 31-38

Faxen, H., 1923. Die Bewegung einer starren Kugel längs der Achse eines nit zäher Flüssigkeit gefüllten Rohres. Arkiv för Mathematik, *Astronomi och Fysik* 17, 1-28

Fersmann, A.E., 1931. Ueber die geochemish-genetishe Klassifikation der granitpegmatite. *Mineralogische Petrografische Mitteilungen* 41, 64-83

Gan, H., Hess, P.C., 1992. Phosphate speciation in potassium aluminosilicate glasses. *Am. Mineral.* 77, 495-506.

Giordano, D., Dingwell, D.B., Romano, C., 2000. Viscosities of Teide phonolites in the welding interval. *J. Volcanol. Geotherm. Res.* 103, 239–245.

Giordano, D., Dingwell, D.B., 2003. Viscosity of hydrous Etna basalt: implications to the modelling of Plinian basaltic eruptions. *Bull. Volcanol.* 65, 8 – 14.

Giordano, D., Romano, D.B., Dingwell, D.B., Poe, B., Behrens, H., 2004. The combined effects of water and fluorine on the viscosity of silicic magmas. *Geochim. Cosmochim. Acta* 68, 5159-5168

Giordano, D., Russell, J.K., Dingwell, D.B., 2008. Viscosity of magmatic liquids: A model. *Earth and Planetary Science Letters* 271, 123-134

Hess, K.-U., Dingwell, D.B., Webb, S.L., 1995. The influence of excess alkalis on the viscosity of a haplogranitic melt. *Am. Mineral.* 80, 297-304

Hess, K-U., Dingwell, D.B., 1996. Viscosities of hydrous leucogranitic melts: A non-Arrhenian model. *Am. Mineral* 81, 1297-1300.

Holtz, F., Dingwell, D.B., Behrens, H., 1993. Effects of F, B_2O_3 and P_2O_5 on the solubility of water in haplogranite melts compared to natural silicate melts. *Contrib. Mineral. Petrol.* 113, 492-501.

Holtz, F., Roux, J., Behrens, H., Pichavant, M., 1999. Water solubility in silica and quartzofeldspathic melts. *Am. Mineral.* 85, 682–686.

Hui, H., Zhang, Y., 2007. Towards a general viscosity equation for natural anhydrous and hydrous silicate melts. *Geochim. Cosmochim. Acta* 71, 403-416

Jahns, R.H., 1953. The genesis of pegmatites. I. Occurrence and origin of giant crystals. *Am Mineral* 38, 563-598

Jahns, R.H., 1953a. The genesis of pegmatites. II. Quantitative analysis of lithium-bearing pegmatite, Mora county, New Mexico. *Am Mineral* 38, 1078-1112

Jahns, R.H. and Burnham, C.W., 1969. Experimental studies of pegmatite genesis. I. A model for the derivation and crystallization of granitic pegmatites. *Economic Geology* 64, 843-864

Kamenetsky, V.S., Naumov, V.B., Davidson, P., van Achterbergh, E., Ryan, C.G., 2004. Immiscibility between silicate magmas and aqueous fluids: a melt inclusion pursuit into the magmatichydrothermal transition in the Omsukchan Granite (NE Russia). *Chem Geol* 210, 73–90

Knoche, R., Dingwell, D.B., Webb, S.L., 1995. Melt densities for leucogranites and granitic pegmatites: Partial molar volumes for SiO_2, $A1_2O_3$, Na_2O, K_2O, Li_2O, Rb_2O, Cs_2O, MgO, CaO, SrO, BaO, B_2O_3, P_2O_5, F_2O_{-1}, TiO_2, Nb_2O_5, Ta_2O_5, and WO_3. *Geochim. Cosmochim. Acta* 59, 4645-4652.

Konijnendijk W.L., Stevels J.M., 1978. Structure of borate and borosilicate glasses by Raman spectroscopy. In: Pye L.D., Frenchette V.D., Kriedl, N.J., (Eds), *Borate G1asses: Structure, Properties, Applications*. *Materials Sci. Res*. 12. Plenum Press, New York, pp. 259- 279.

Leschik, M., Heide, G., Frischat, G.H., Behrens, H., Wiedenbeck, M., Wagner, N., Heide, K., Geißler, H., Reinholz, U., 2004. Determination of H_2O and D_2O contents in rhyolitic glasses using KFT, NRA, EGA, IR spectroscopy, and SIMS. *Phys. Chem. Glasses* 45, 238-251

Liebske, C., Behrens, H., Holtz, F., Lange, R.A., 2003. The influence of pressure and composition on the viscosity of andesitic melts. *Geochim. Cosmochim. Acta* 67 (3), 473– 485.

London, D., 1987. Internal differentiation of rare-element pegmatites: effects of boron, phosphorus and fluorine. *Geochim. Cosmochim. Acta* 51, 403–420.

London, D., 1992. The application of experimental petrology to the genesis and crystallization of granitic pegmatites. *Can. Mineral*.30, 499-540

London, D., 1999. Stability of tourmaline in peraluminous granite systems: the boron cycle from anatexis to hydrothermal aureoles. *Eur. J. Mineral.* 11, 253-262

London, D., 2005. Granitic pegmatites: an assessment of current concepts and directions for the future. *Lithos* 80, 281-303

London, D., 2008. Pegmatites. *Mineralogical Association of Canada*, Special publication 10, pp 225

London, D., 2009. The origin of primary textures in granitic pegmatites. *Can. Mineral*. 47, 697-724

Martin, J.S., 1983. An experimental study of the effects of lithium on the aranite solidus. *J. Ussher Sot*. 5.4 17-420

Martin, J.S., and Henderson, C.M.B., 1984. An experimental study of the effects of small amounts of lithium on the granite system. In *Progress in Experimental Petrology* (ed. C.M.B. Henderson), pp. 30-35. *Nat. Env. Res. Council Publ. Ser.* D 25

Mason, B.H. and Moore, C.B., 1982. *Principles of Geochemistry* (4^{th} ed.). John Wiley & Sons, New York, N.Y.

Massiot, D., Fayon, F., Capron, M., King, I., Le Calvé, S., Alonso, B., Durand, J.O., Bujoli, B., Gan, Z., Hoatson, G., 2002. Modelling one- and two-dimensional solid-state NMR spectra. *Magnetic Resonance in Chemistry* 40, 70-76.

Nabelek, P.I., Whittington, A.G., Sirbescu, M.L.C., 2010. The role of H_2O in rapid emplacement and crystallization of granite pegmatites: resolving the paradox of large crystals in highly undercooled melts. *Contrib. Mineral. Petrol.* 160, 313-325.

Navrotsky, A., Geisinger, K.L., McMillan, P., Gibbs, G.V., 1985. The tetrahedral framework in glasses and melts – inferences from molecular orbital calculations and implications for structure, thermodynamics, and physical properties. *Phys. Chem. Min*. 11, 274-298

Nowak, M., Behrens, H., 2001. Water in rhyolitic magmas: getting a grip on a slippery problem. *Earth. Planet. Sci. Lett.* 184, 515–522.

Ochs, F.A., Lange, R.A., 1999. The density of hydrous magmatic liquids. *Science* 283, 1314-1317

Ohlhorst, S., Behrens, H., Holtz, F., 2001. Compositional dependence of molar absorptivities of near-infrared OH- and H_2O bands in rhyolitic to basaltic glasses. *Chem. Geol.* 174, 5-20.

Persikov, E.S., 1991. The viscosity of magmatic liquids: experiment, generalized patterns. A model for calculation and prediction. *Applications. Adv. Phys. Geochem*. 9, 1 – 40.

Plazek, D.J., Ngai, K.L., 1991. Correlation of polymer segmental chain dynamics with temperature-dependent time-scale shift. *Macromolecules* 24, 1222.

Pocklington, H.C., 1940. Rough measurements of high viscosities. *Proceedings of the Cambridge Philosophical Society* 36, 507-508.

Richet, P., Bottinga, Y., 1995. Rheology and configurational entropy of silicate melts. In: Stebbins, J.F., McMillan, P.F., Dingwell,D.B. (Eds.), Structure, Dynamics and Properties of Silicate Melts, vol. 32. *Mineral. Soc. Am. Rev. Mineral*., Washington, DC, pp. 67– 94.

Richet, P., Lejeune, A.M., Holtz, F., Roux, J., 1996. Water and the viscosity of andesite melts. *Chem. Geol.* 128, 185– 197.

Rickers, K., Thomas, R., Heinrich, W., 2006. The behavior of trace elements during the chemical evolution of the H(2)O-, B-, and F-rich granite-pegmatite-hydrothermal system at Ehrenfriedersdorf, Germany: a SXRF study of melt and fluid inclusions. *Miner Deposita* 41, 229-245

Riebling, E. F., 1966. Structure of sodium aluminosilicate melts containing at least 50 mole% SiO_2 at 1500°C. *J. Chem. Phys*. 44, 2857-2865.

Romano, C., Hess, K.-U., Mincione, V., Poe, B.P., Dingwell, B.T., 2001. The viscosities of dry and hydrous $XAlSi_3O_8$ (X = Li, Na, K, Ca0.5, Mg0.5) melts. *Chem. Geol.* 174, 115– 132.

Romano, C., Giordano, D., Papale, P., Mincione, V., Dingwell, D.B., Rosi, M., 2003. The dry and hydrous viscosities of alkaline melts from Vesuvius and Phlegrean Fields. *Chem. Geol.* 202, 23-38.

Scaillet, B., Holtz, F., Pichavant, M., Schmidt, M., 1996. Viscosity of Himalayan leucogranites: implications for mechanisms of granitic magma ascent. *Journal of Geophysical Research–Solid Earth* 101(B12), 27691– 27699.

Scherer, G.W., 1984. Use of the Adam-Gibbs Equation in the analysis of structural relaxation. *Journal of the American Ceramic Society* 67, 504–511.

Schmidt, B.C., 2004a. Effect of boron on the water speciation in (alumino)silicate melts and glasses. *Geochim. Cosmochim. Acta,* 68, 5013-5025.

Schmidt, B.C., Zotov, N., Dupree, R., 2004b. Structural implications of water and boron dissolution in albite glass. *J. Non-Cryst. Solids*, 337, 207-219.

Scholze, H., 1988. Glas: Natur, Struktur und Eigenschaften. Springer, NY.

Schulze, F., Behrens, H., Holtz, F., Roux, J., Johannes, W., 1996. The influence of H_2O on the viscosity of a haplogranitic melt. *Am. Mineral.* 81, 1155-1165.

Shannon, R.D., 1976. Revised effective ionic radii and systematic studies of interatomic distances in halides and chalcogenides. Acta Cryst. A32: 751-767

Shannon, R.D. and Prewitt, C.T., 1969. Effective ionic radii in oxides and fluorides. Acta Cryst. B25: 925-946

Shaw, H.R., 1963. Obsidian-H_2O viscosities at 100 and 200 bars in temperature range 700 degrees to 900 degrees C. *J. Geophys. Res.* 68, 6337-6343.

Simmons, W.B., Webber, K.L., 2008. Pegmatite genesis: state of the art. *Eur. J. Mineral.* 20, 421-438.

Sirbescu, M.L.C., Nabelek, P.I., 2003. Crustal melts below 400 degrees C. *Geology* 31, 685-688

Stewart, D.B., 1978. Petrogenesis of lithium-rich pegmatites. *Amer. Mineral.* 63, 970-980

Tait, J.C., Mandolesi, D.L., Rummens, H.E.C., 1984. Viscosity of melts in the sodium borosilicate system. Phys. Chem. Glasses 25: 100-104

Thomas, R., Webster, J.D., 2000. Strong tin enrichment in a pegmatiteforming melt. *Miner Depos* 35, 570–582

Thomas, R., Webster, J.D., Heinrich, W., 2000. Melt inclusions in pegmatite quartz: complete miscibility between silicate melts and hydrous fluids at low pressure. *Contrib Mineral Petrol* 139, 394−401

Thomas, R., Förster, H.J., Heinrich, W., 2003. The behaviour of boron in a peraluminous granite-pegmatite system and associated hydrothermal solutions: a melt and fluid-inclusion study. *Contrib Mineral Petrol* 144, 457–472

Thomas, R., Förster, H.J., Rickers, K., Webster., J., 2005. Formation of extremely F-rich hydrous melt fractions and hydrothermal fluids during differentiation of highly evolved tin-granite magmas: a melt/fluid inclusion study. *Contrib Mineral Petrol* 148, 582–641

Thomas, R., Davidson, P., Badanina, E., 2009. A melt and fluid inclusion assemblage in beryl from pegmatite in the Orlovka amazonite granite, East Transbaikalia, Russia: implications for pegmatite-forming melt systems. *Miner Petrol* 96, 129-140

Toplis, M.J., Dingwell, D.B., 1996. The variable influence of P_2O_5 on the viscosity of melts of differing alkalie/aluminium ratio: Implications for the structural role of phosphorus in silicate melts. *Geochim. Cosmochim. Acta* 60, 4107-4121.

Toplis, M.J., Dingwell, D.B., Lenci, T., 1997. Peraluminous viscosity maxima in Na_2O-Al_2O_3-SiO_2 liquids: The role of triclusters in tectosilicate melts. *Geochim. Cosmochim. Acta* 61, 2605-2612.

Van Lichtervelde, M., Linnen, R.L., Salvi, S., Didier, B., 2007. Textures and chemical evolutions in tantalum oxide a discussion of magmatic versus metasomatic origins for Ta mineralization in the Tanco Lower Pegmatite, Manitoba, *Canada Econ Geol* 102, 257-276

Vetere, F., Behrens, H., Holtz, F., Neuville, D.R., 2006. Viscosity of andesitic melts - new experimental data and a revised calculation model. *Chem. Geol.* 228, 233-245

Veksler, I.V. and Thomas, R., 2002. An experimental study of B-, P- and F-rich synthetic granite pegmatite at 0.1 and 0.2 GPa. *Contrib Mineral Petrol* 143, 673-683

Veksler, I.V., Thomas, R. and Schmidt, C., 2002. Experimental evidence of three coexisting immiscible fluids in synthetic granite pegmatite. *Am Mineral* 87, 775–779.

Veksler, I.V., Thomas, R., Wirth, R., 2003. Crystallization of $AlPO_4$-SiO_2 solid solutions from granitic melt and implications for P-rich melt inclusions in pegmatitic quartz. *Am Mineral* 88, 1724-1730

Veksler, I.V., Dorfman, A.M., Dulski, P., Kamenetsky, V.S., Danyushevsky, L.V., Jeffries, T., Dingwell, D.B., 2012. Partitioning of elements between silicate melt and immiscible fluoride, chloride, carbonate, phosphate and sulfate melts, with implications to the origin of natrocarbonatite. *Geochim Cosmochim Acta* 79, 20-40

Webb, S.L., Müller, E., and Büttner, H., 2004. Anomalous rheology of peraluminous melts. *Am. Mineral.,* 89, 812-818.

Webber, K.L., Falster, A.U., Simmons, W.B., Foord, E.E., 1997. The role of diffusion-controlled oscillatory nucleation in the formation of line rock in pegmatite-aplite dikes. *Journal of Petrology* 38, 1777-1791

Webster, J.D., Thomas, R., Rhede, D., Förster, H.-J., Seltmann, R., 1997. Melt inclusions in quartz from an evolved peraluminous pegmatite: geochemical evidence for strong tin enrichment in fluorine-rich and phosphorus-rich residual liquids. *Geochim Cosmochim Acta* 61, 2589–2604

Whittington, A., Richet, P., Holtz, F., 2000. Water and the viscosity of hydrous depolymerized aluminosilicate melts. *Geochim. Cosmochim. Acta* 64, 3725–3736.

Whittington, A., Richet, P., Linard, Y., Holtz, F., 2001. The viscosity of hydrous phonolites and trachytes. *Chem. Geol.* 174, 209– 223.

Whittington, A.G., Richet, P., Behrens, H., Holtz, F., Scaillet, B., 2004. Experimental temperature-X(H_2O)-viscosity relationship for leucogranites, and comparison with synthetic silicic liquids. *Trans Roy Soc Edin: Earth Sci* 95, 59-72

Withers, A.C., Behrens, H., 1999. Temperature-induced changes in the NIR spectra of hydrous albitic and rhyolitic glasses between 300 and 100 K. *Physics and chemistry of minerals* 27, 119-132.

Wyllie, P.J. and Tuttle, O.F., 1964. Experimental investigation of silicate systems containing two volatile components. Part III. The effects of SO3, P2O5, HCl, and L2O, in addition to H2O, on the melting temperatures of albite and granite. *Amer. J. Sci.* 262 930-939

Zhang, Y., Belcher, R., Ihinger, P.D., Wang, L.P., Xu, Z.J. and Newman, S., 1997. New calibration of infrared measurement of dissolved water in rhyolitic glasses, Geochim. Cosmochim. Acta 61, 3089-3100.

Zhang,Y., Xu, Z., Liu,Y., 2003. Viscosity of hydrous rhyolitic melts inferred from kinetic experiments, and a new viscosity model. *Am. Mineral.* 88, 1741–1752.

Appendix

The following images were recorded after each viscosity experiment conducted with the falling sphere method. They are used as basis for the viscosity calculation. The conditions for the single experiments could be find in the tabels A.2, B.2a, B.1.A, C.2. and C.2.A. The scalebars, given on the images are only valid for the original size of the recorded images. Sample names with an m (e.g. PEG2-1m) belong to the melting experiment, conducted to synthesize a water-bearing glass cylinder containing a Pt horizon (immobile marker) and noble metal spheres and are not used for viscosity calculation (see text for details).

PEG2-1m PEG2-1a PEG2-1b PEG2-1c PEG2-1d

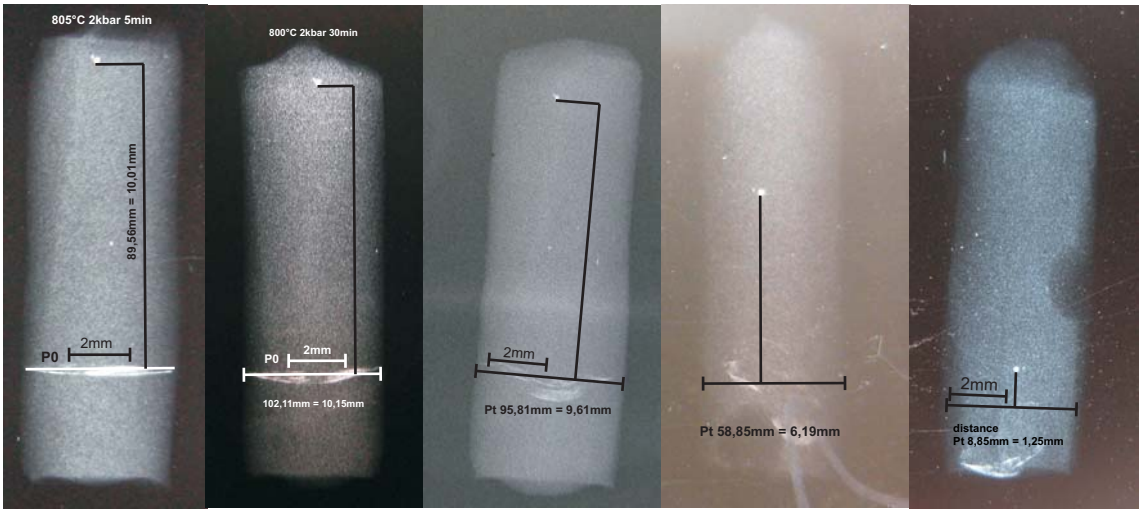

PEG2-2m PEG2-2a PEG2-2b PEG2-2c PEG2-2d

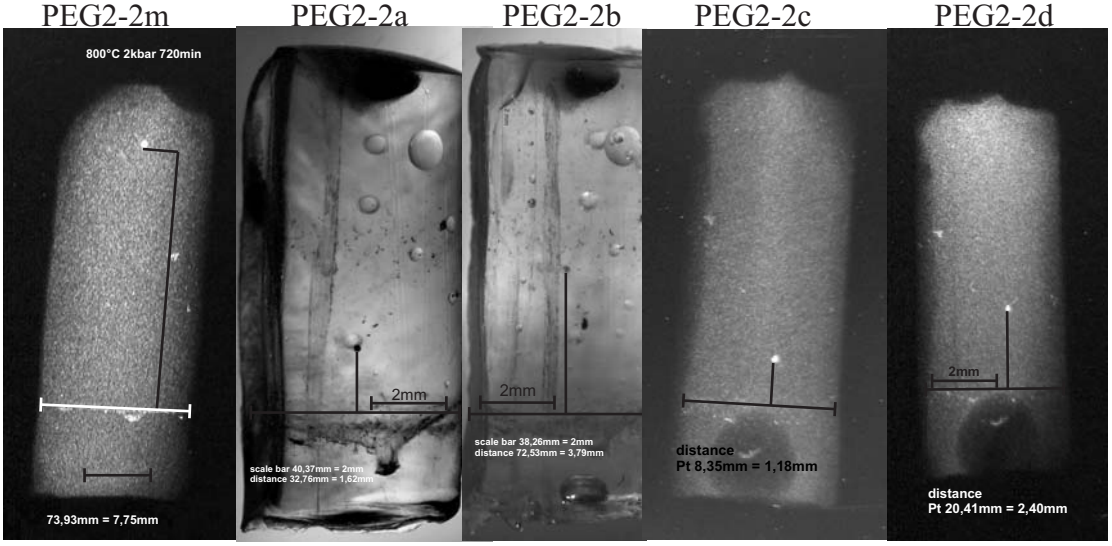

PEG2-3m PEG2-3a PEG2-3b PEG2-3c PEG2-3d PEG2-3e PEG2-3f

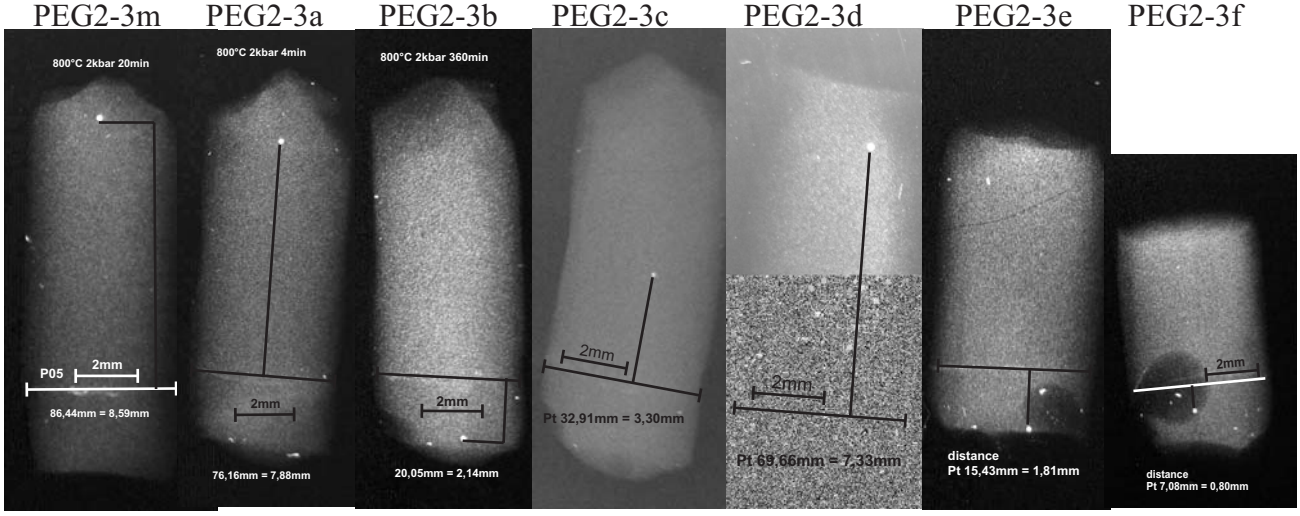

PEG2-4a

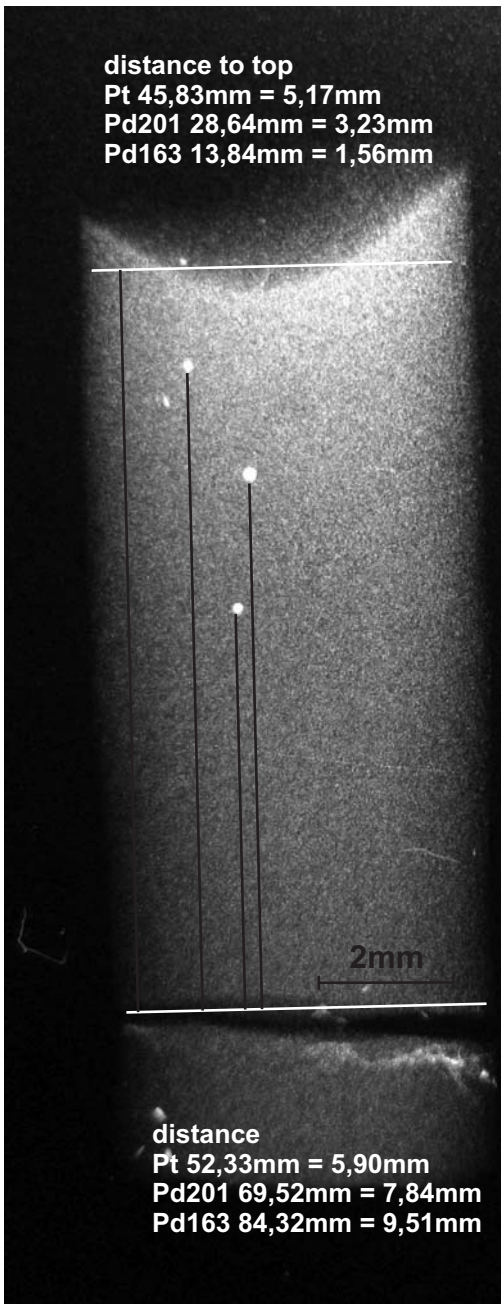

PEG2-4b

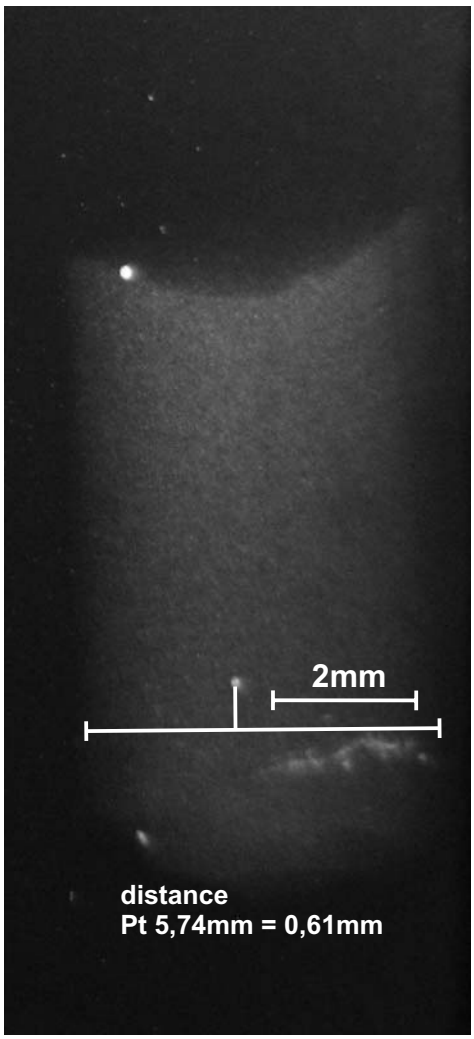

PEG2-4m is missing

PEG3-base-1m

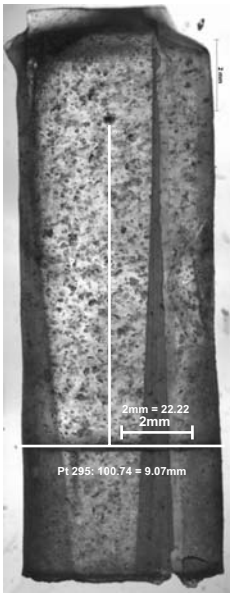

PEG3-base-1a

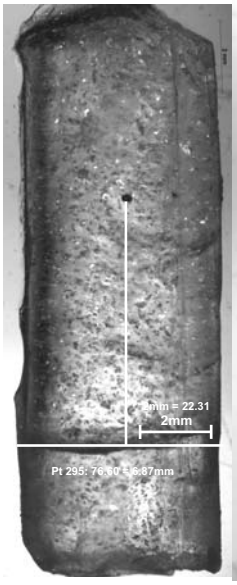

PEG3-base-1b

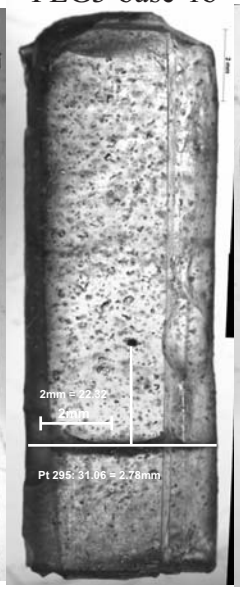

PEG3-base-1c

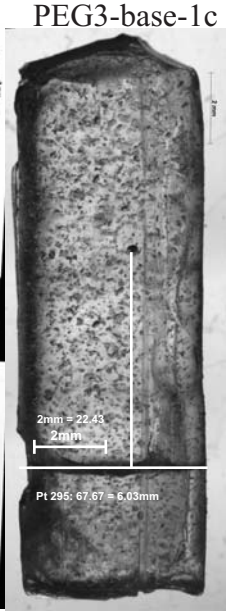

PEG3-base-3m

PEG3-base-3a

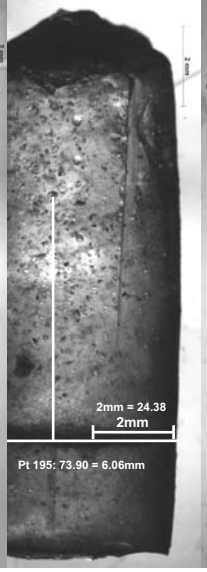

PEG3-base-3b

PEG3-base-3c

PEG3-base-6m

PEG3-base-6a

PEG3-base-6b

PEG3-base-6c

PEG3-F2-1m PEG3-F2-1a PEG3-F2-1b PEG3-F2-1c PEG3-F2-1d PEG3-F2-1e

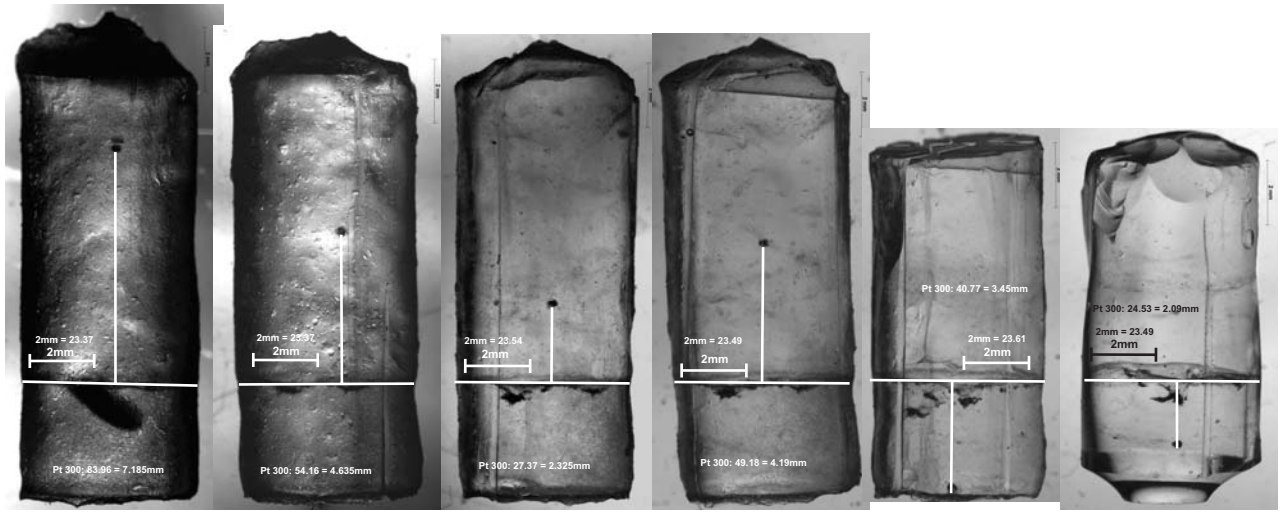

PEG3-F2-3m PEG3-F2-3a PEG3-F2-3b

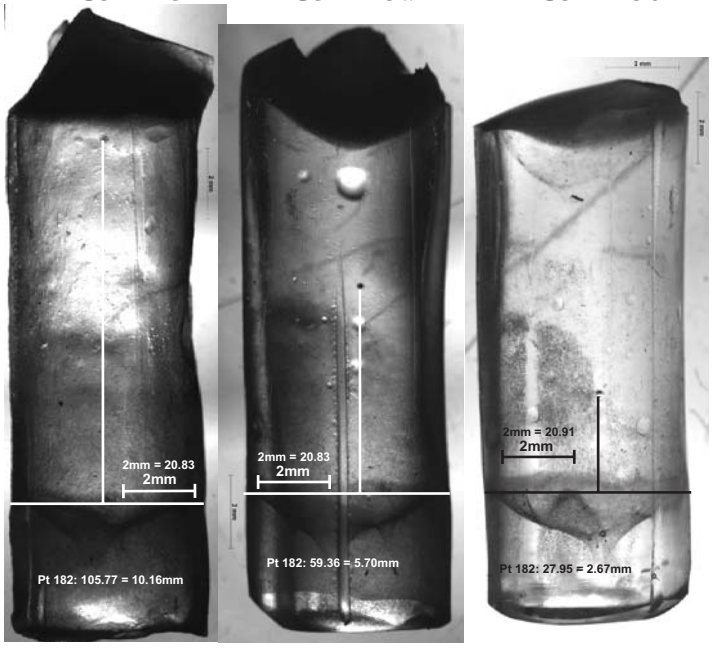

PEG3-F2-6m PEG3-F2-6a PEG3-F2-6b PEG3-F2-6c

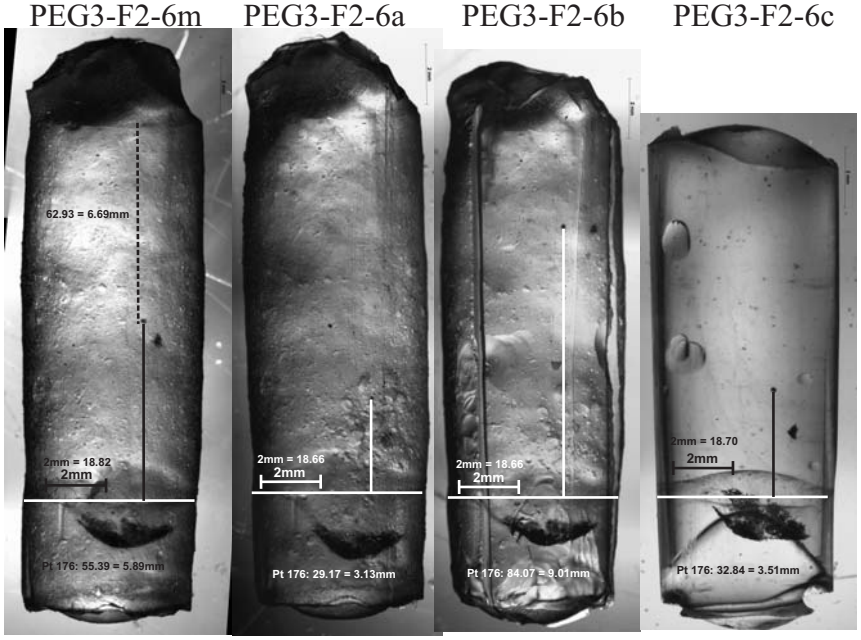

PEG3-F5-1m PEG3-F5-1a PEG3-F5-1b PEG3-F5-1c PEG3-F5-1d

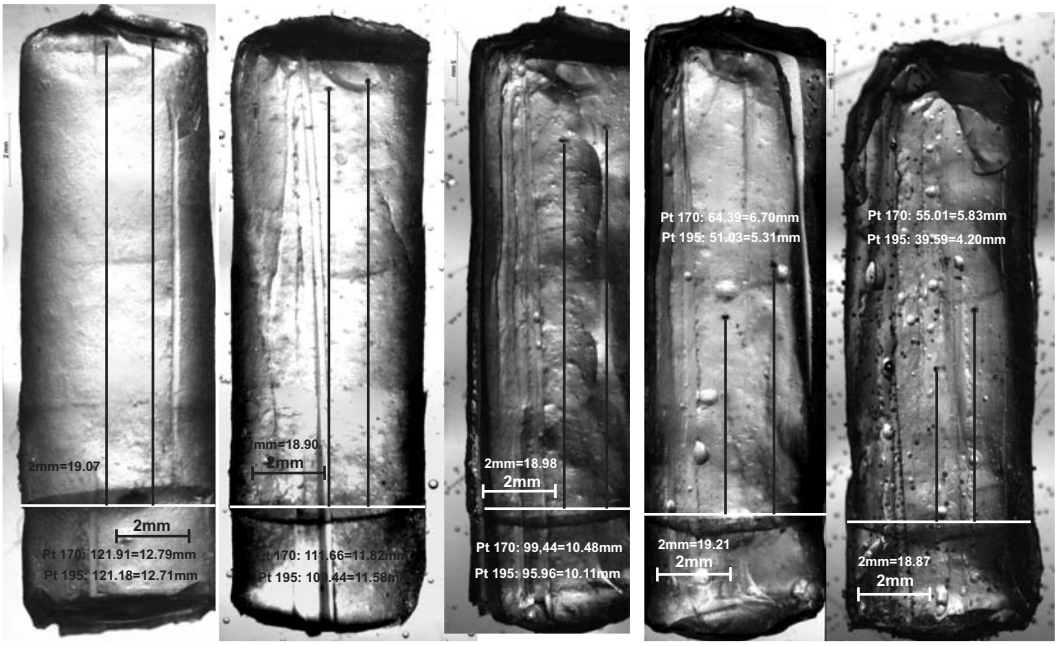

PEG3-F5-3m PEG3-F5-3a PEG3-F5-3b

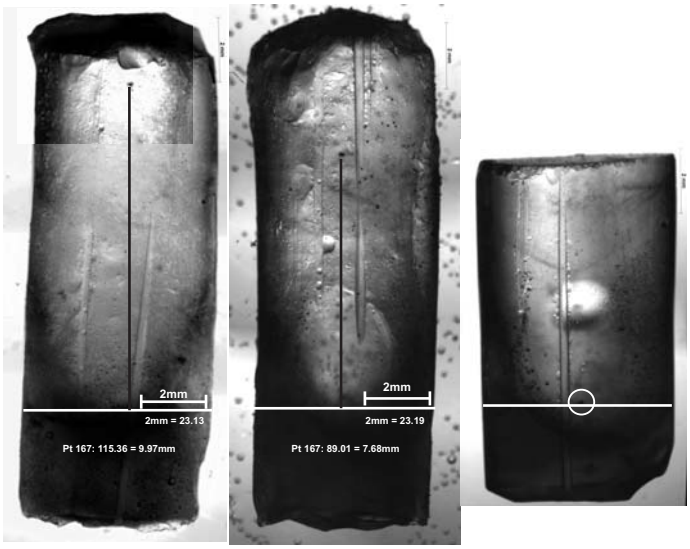

PEG3-F5-6m PEG3-F5-6a PEG3-F5-6b PEG3-F5-6c

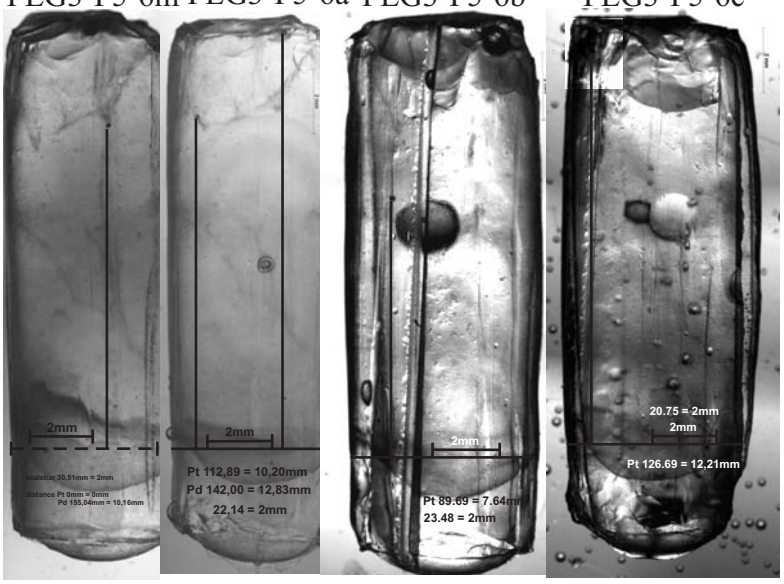

PEG3-B-1m

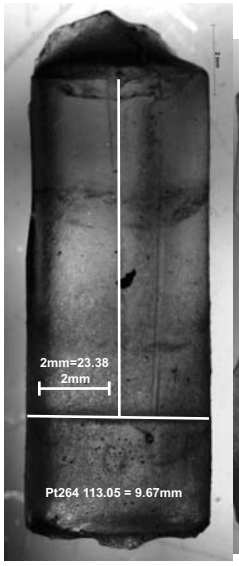

PEG3-B-1a

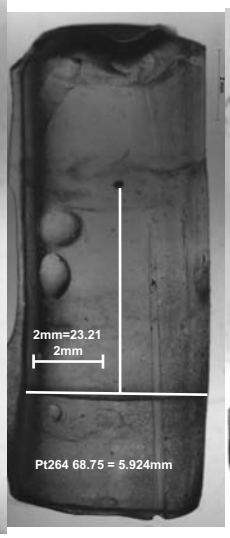

PEG3-B-1b

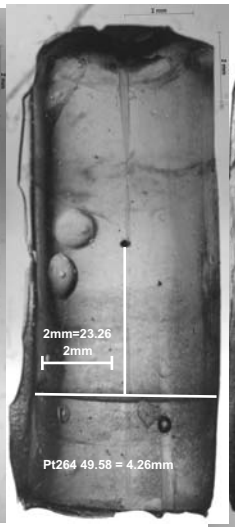

PEG3-B-1c

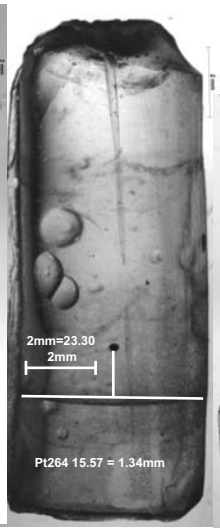

PEG3-B-1d

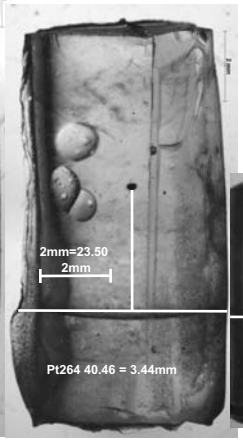

PEG3-B-1e

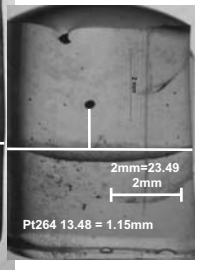

PEG3-B-3m

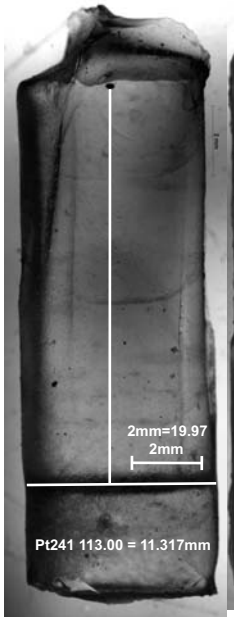

PEG3-B-3a

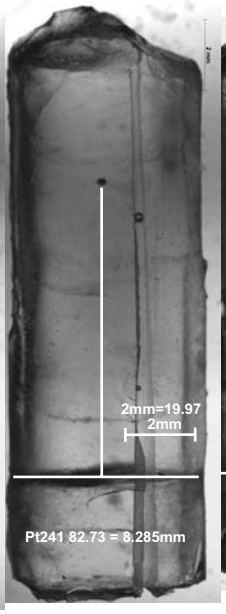

PEG3-B-3b

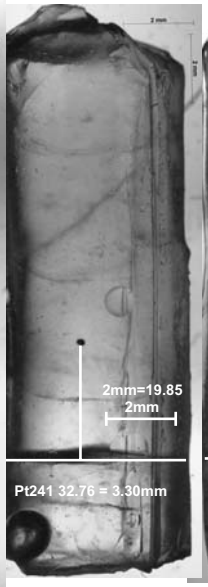

PEG3-B-3c

PEG3-B-3d

PEG3-B-6m

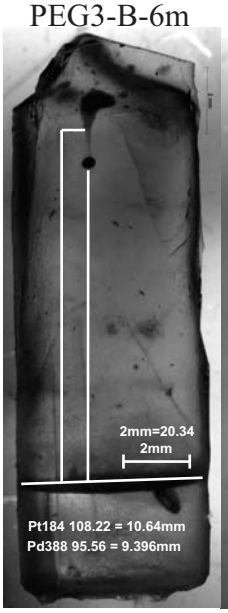

PEG3-B-6a

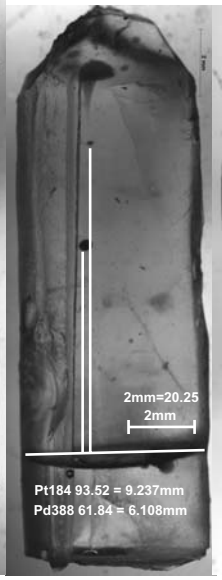

PEG3-B-6b

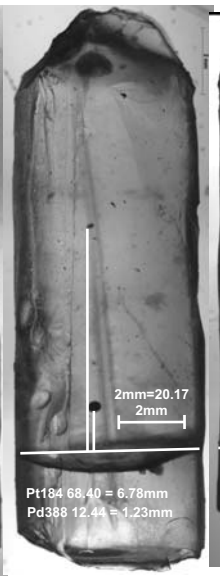

PEG3-B-6c

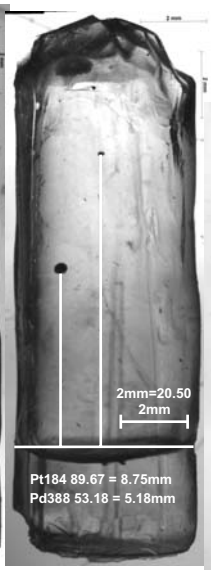

PEG3-B-6d

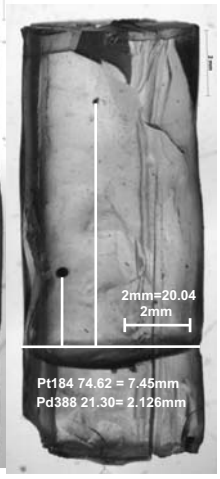

PEG3-P2-1m

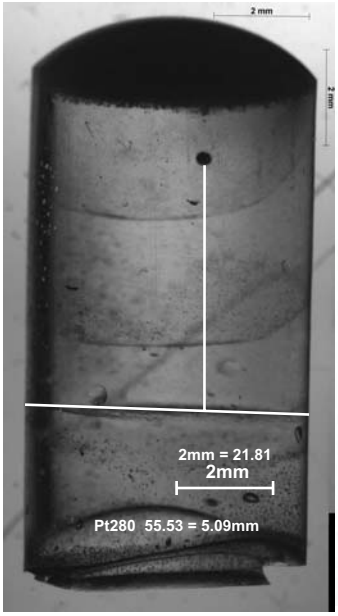

PEG3-P2-1a

PEG3-P2-1b

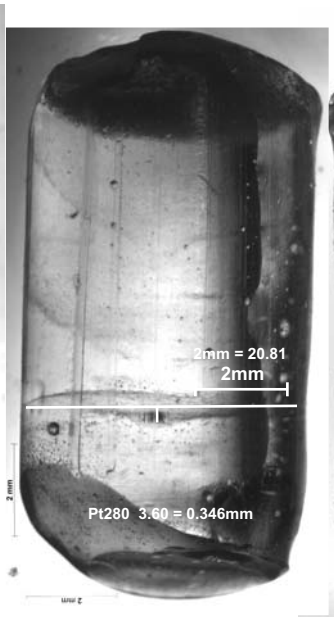

PEG3-P2-1c

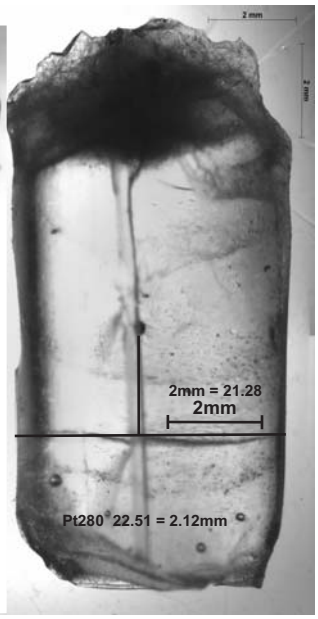

PEG3-P3-1m PEG3-P3-1a PEG3-P3-1b PEG3-P3-1c PEG3-P3-1d PEG3-P3-1e PEG3-P3-1f

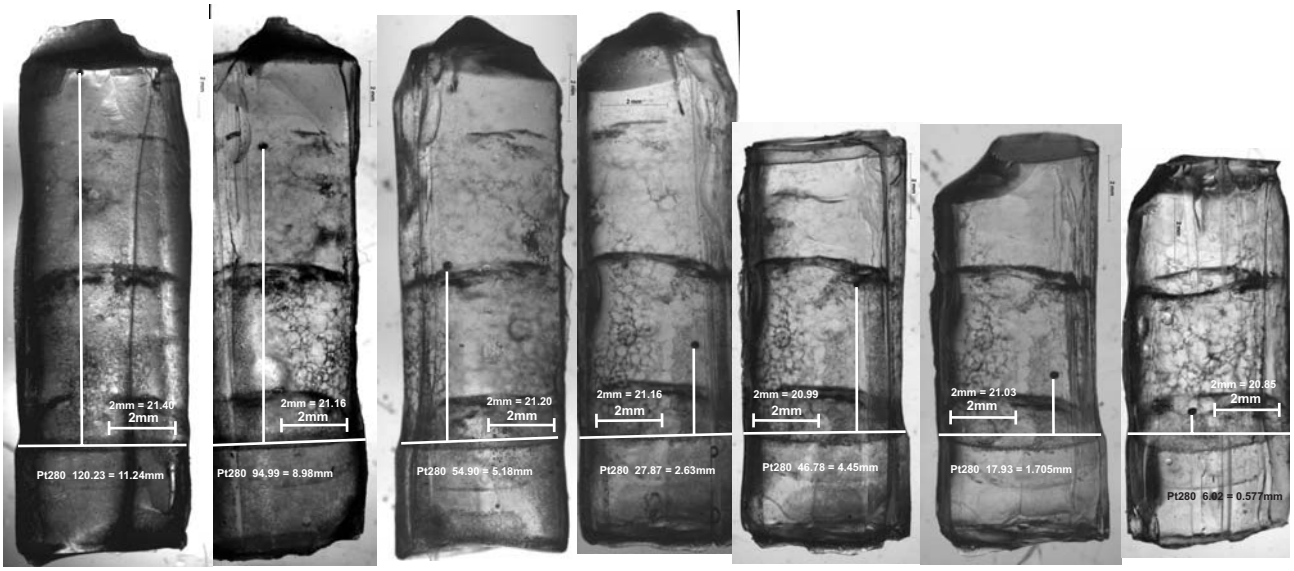

PEG3-P3-3m PEG3-P3-3a PEG3-P3-3b PEG3-P3-3c PEG3-P3-3d

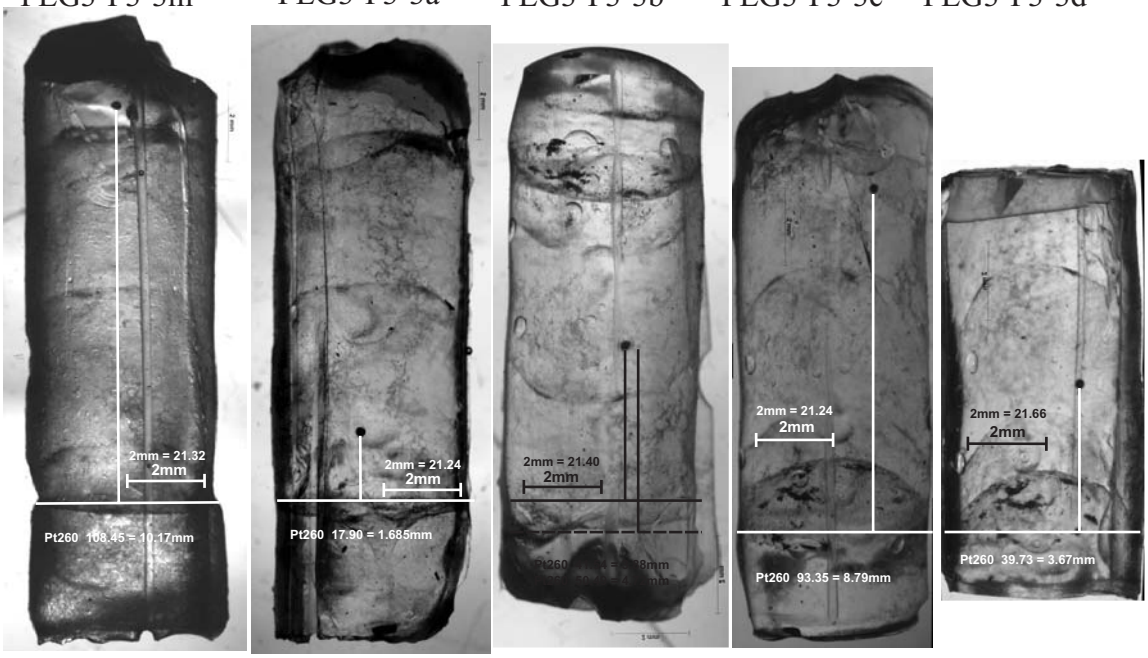

PEG3-P3-6m PEG3-P3-6a PEG3-P3-6b

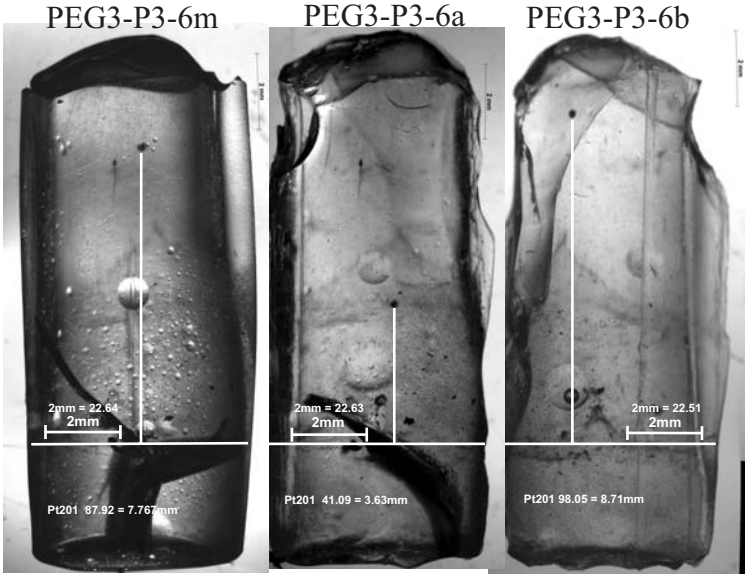

PEG3-Li-1m

PEG3-Li-1a

PEG3-Li-1m$_2$

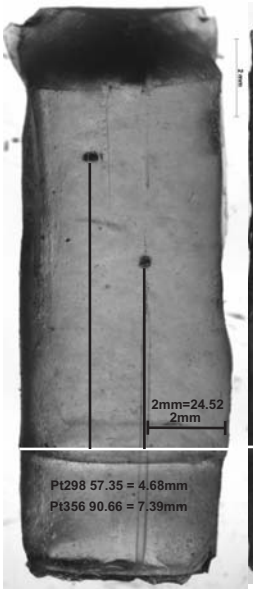

PEG3-Li-1b

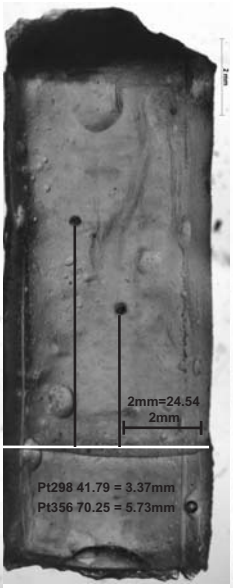

PEG3-Li-1c

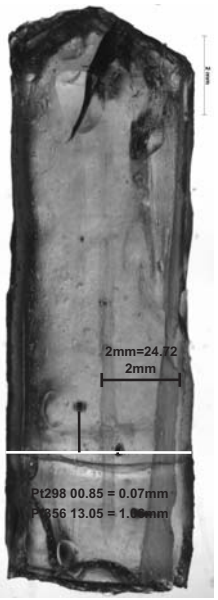

PEG3-Li-3m

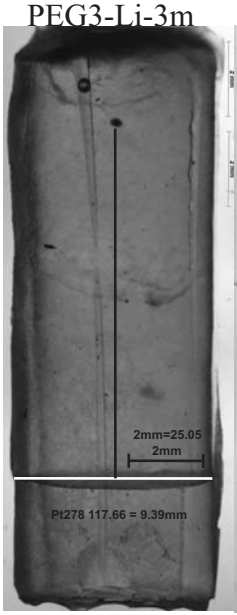

PEG3-Li-3a

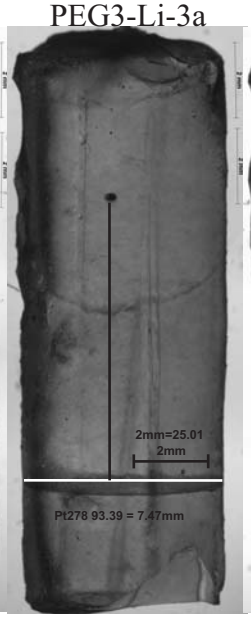

PEG3-Li-3b

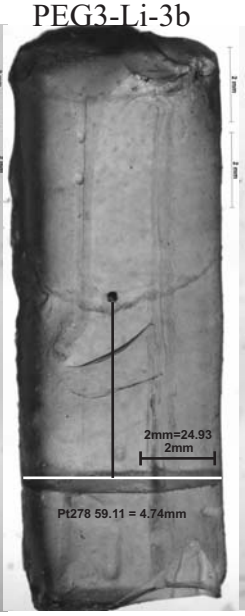

PEG3-Li-3c

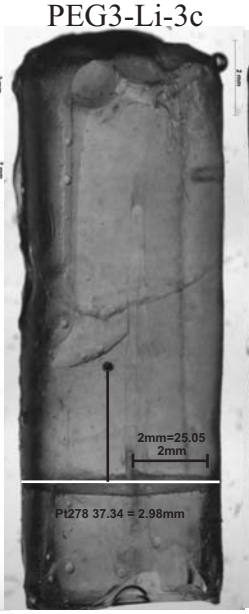

PEG3-Li-3d

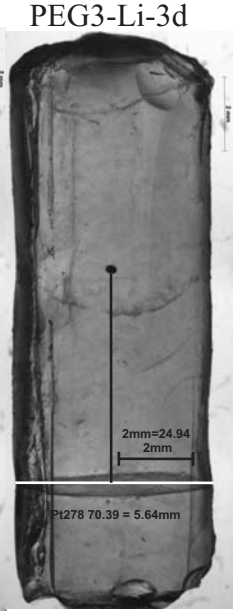

PEG3-Li-6m

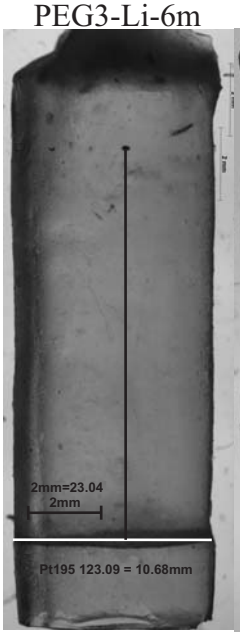

PEG3-Li-6a

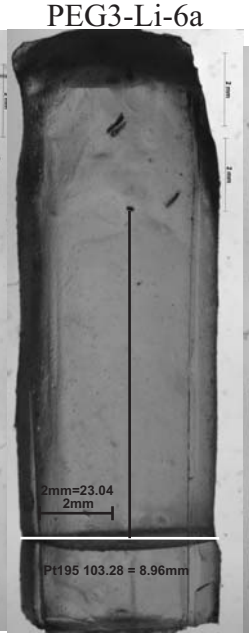

PEG3-Li-6b

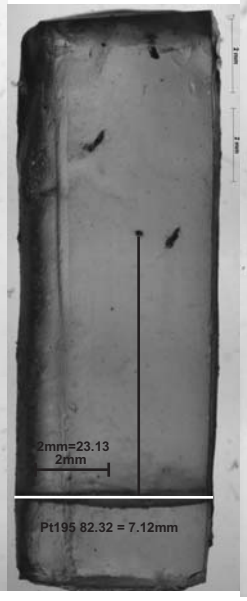

PEG3-Li-6c

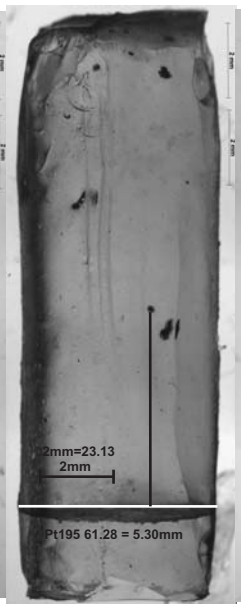

PEG3-Li-6d

PEG3-KLi-1m PEG3-KLi-1a PEG3-KLi-1b PEG3-KLi-1c PEG3-KLi-1d

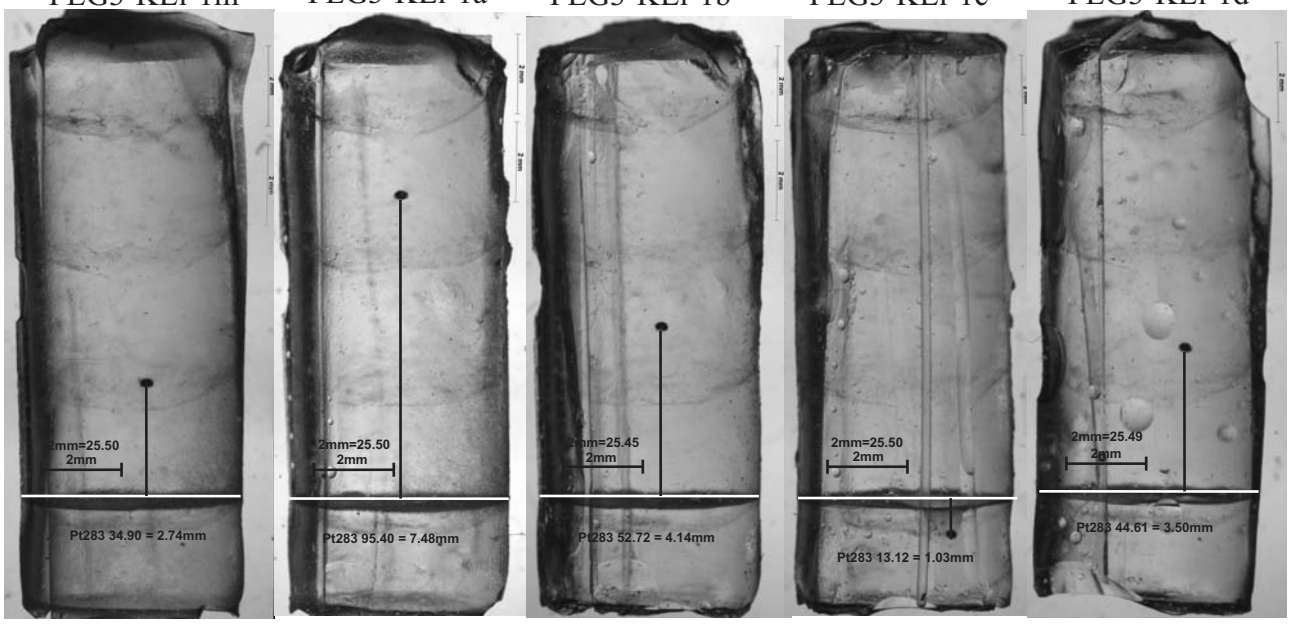

PEG3-KLi-3m PEG3-KLi-3a PEG3-KLi-3m$_2$ PEG3-KLi-3b PEG3-KLi-3c PEG3-KLi-3d

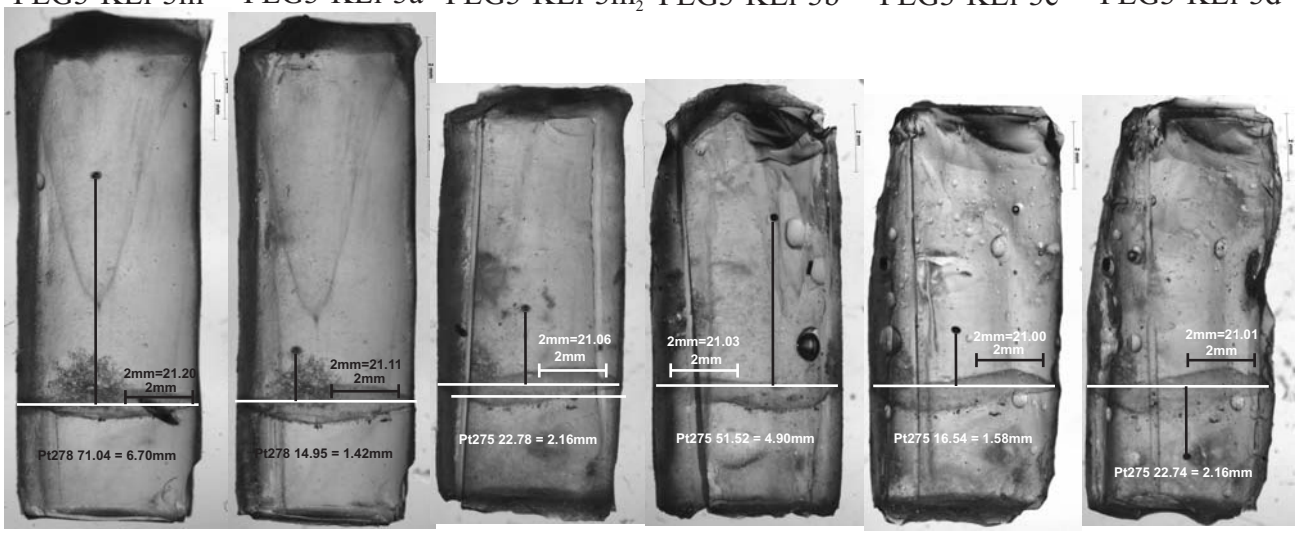

PEG3-KLi-6m PEG3-KLi-6a PEG3-KLi-6b PEG3-KLi-6c PEG3-KLi-6d

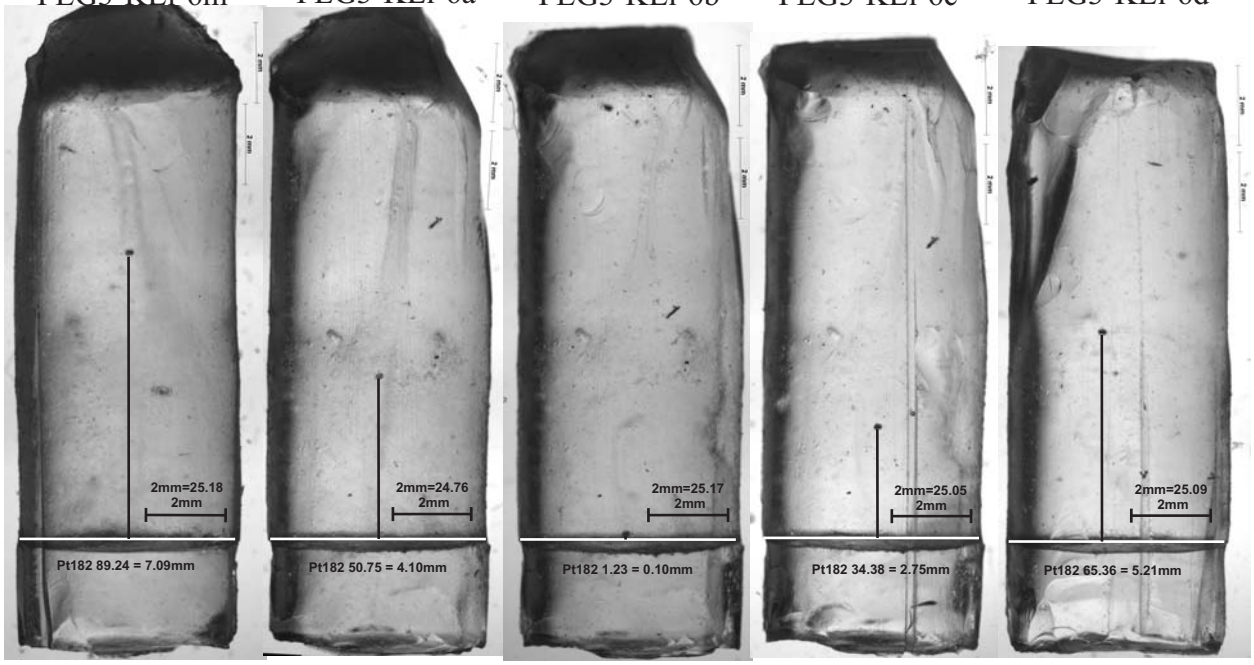

Curriculum Vitae
Alexander Bartels, Dipl.-Geow.

Personal Details

Name and Address	Alexander Bartels Niemeyerstraße 6 30449 Hannover Germany
Telephone (private) (mobile)	0049 (0)511 5683096 0049 (0)177 3388223
E-mail address	a.bartels@mineralogie.uni-hannover.de alex-ewog@web.de
Date of birth	18.05.1982 / Frankfurt/Main, Germany
Marital status	Married
Nationality	German

Education

2010	apprenticeship as first aider
04.2009 – 07.2012	PhD student at the Leibniz University of Hannover (Germany) Title of the doctoral dissertation: The influence of fluorine, boron, phosphorus and lithium on the viscosity of hydrous pegmatite forming melts
2008	Study of earth sciences at the Leibniz University of Hannover (Germany) *(final grade: 1.5, very good)* Title of the diploma thesis: solubility of manganocolumbite and manganotantalite in pegmatitic melts
2005	Bachelor of Science at the Leibniz University of Hannover (Germany)
07.2001 – 05.2002	civilian service at the “german red cross” with apprenticeship as Emergency Medical Technician - Basic
2001	Secondary-school, Gymnasium Großburgwedel, Hannover (Germany) *(final grade: 2.6, satisfactory)*

Work experience

08.2010	Organisation and realization of a 3 week field trip for 30 students to iceland
04.2009 – 06.2012 (expected)	Research assistant (PhD student) at the Leibniz University of Hannover/ Institute for Mineralogy (Germany)
05.2008 – 03.2009	Teacher for special functions at the Leibniz University of Hannover/ Institute for Mineralogy (Germany) *Experiences:* practical courses in geochemistry and microscopy; supervising students in experimental work
09.2008 – 12.2008	Visiting Research Associate, University of Waterloo, Canada Department of Earth and Environmental Sciences
05.2007 - 08.2007	Student research assistant at the Leibniz University of Hannover/ Institute for Mineralogy (Germany)

2004 and 2005	Internship at Federal Institute for Geosciences and Natural Resources (BGR) in Hannover
2004	Internship at “Niedersächsischen Landesmuseum” in Hannover

2007	Field trip to Namibia: Research of highly evolved pegmatite bodies in different areas of namibia
2006	Field trip Vietnam: Field mapping in Tong Xa and Van Trang project: effects of landuse on heavy metal distribution in agricultural soils around handicraft villages, Red River Delta, Vietnam
	Geological excursion to Iceland (2005) and Southern Spain (2004)

Experimental skills

Handling and construction of cold-seal pressure vessels (CSPV) and internal heated pressure vessels (IHPV) for experiments at elevated temperatures and pressures

Handling of high temperature chamber furnaces

Sample preparation for experimental work

Analytical skills

Good knowledge	microscope, microprobe (EMP), infrared spectroscopy (IR), Karl-Fischer-Titration (KFT)
Basic knowledge	Raster Electron Microscopy (REM)

Language skills

German	native	
English	Oral: excellent	Written: excellent
French	Oral: some	Written: some

Computing

Good knowledge	MS Office, Corel DRAW, Adobe Photoshop, SigmaPlot
Basic Knowledge	

Hobbies

Sports (mountainbiking, soccer), photography and travelling

References

Prof. Dr. Harald Behrens, Leibniz University of Hannover – Institute for Mineralogy, h.behrens@mineralogie.uni-hannover.de, telephone: 0049 (0)511 762 8054

Prof. Dr. Francois Holtz, Leibniz University of Hannover – Institute for Mineralogy, f.holtz@mineralogie.uni-hannover.de, telephone: 0049 (0)511 762 8054

Prof. Dr. Robert L. Linnen, Western University, Ontario, Canada – Department of Earth Sciences, rlinnen@uwo.ca, telephone: 001-519-661-2111

Alexander Bartels, Dipl.–Geow.

Niemeyerstraße 6, 30449 Hannover, Germany
Telp.: 0049-511-5683096 mobile phone: 0049-177-3388223
a.bartels@mineralogie.uni-hannover.de / alex-ewog@web.de

LIST OF PUBLICATIONS

PAPER

Bartels A., Behrens H., Holtz F., Schmidt B.C., Fechtelkord M., Knipping J., Crede L., Baasner A., Pukallus N. (2012) The effect of fluorine, boron and phosphorus on the viscosity of pegmatitic liquids. *Chem. Geol.* (submitted)

Backnaes, L., Deubener, J., Behrens, H., Stelling, J., Cichy, S.B. & **Bartels, A** (2011)**:** Diffusion of the 35S isotope in soda-lime-silica and sodium trisilicate glass melts. , *J. Non-Cryst. Solids* 357 (15), pp. 2941-2948

Bartels A., Vetere F., Holtz F., Behrens H., Linnen RL (2011) Viscosity of flux-rich pegmatitic melts. *Contrib. Mineral. Petrol.* 162, 51-60

Bartels A., Holtz F., Linnen R. L. (2010) Solubility of manganotantalite and manganocolumbite in pegmatitic melts. *Am. Mineral.* 95, 537-544

ABSTRACTS

Bartels A., Knipping J., Behrens H., Holtz F., Schmidt B.C.: The influence of F, P and B content on pegmatitic melt viscosity; Goldschmidt 2011, Prag, Czech Republic

Bartels A., Baasner A., Behrens H., Holtz F., Schmidt B.C.: Towards a viscosity model for flux-rich pegmatitic melts: 88. Tagung der Deutschen Mineralogischen Gesellschaft, Münster, Germany

Bartels A., Baasner A., Behrens H., Holtz F., Schmidt B.C.: Viscosity of flux-rich pegmatitic melts; EMPG XIII, Toulouse, France

Bartels, A., Linnen, R.L., and Holtz, F.: Tantalite Associated with Mica Replacement: A Magmatic-Metasomatic Origin?

A. Fiege, C. Kirchner, **A. Bartels**, F. Holtz, R. L. Linnen (2009): Influence of fluorine on the solubility of manganotantalite ($MnTa_2O_6$) and manganocolumbite ($MnNb_2O_6$) in natural rhyolitic, synthetic haplogranitic and pegmatitic melts. 87. Tagung der Deutschen Mineralogischen Gesellschaft, Halle, Germany